FERMI SURFACE OF DONOR AND ACCEPTOR GRAPHITE INTERCALATION COMPOUNDS

by

GUONAN WANG

M.Sc

A Thesis

Submitted to the School of Graduate Studies

in Partial Fulfillment of the Requirements

for the Degree

Doctor of Philosophy

McMaster University

October, 1991

FERMI SURFACE

OF DONOR AND ACCEPTOR

GRAPHITE INTERCALATION COMPOUNDS

DOCTOR OF PHILOSOPHY (1991)
(PHYSICS)

McMaster University
Hamilton, Ontario

Title: Fermi surface of donor and acceptor graphite intercalation compounds

Author: Guonan Wang

M.Sc. (McMaster University, Hamilton, Canada).
M.Sc. (Inst. of Metal Research, Academia Sinica, Shenyang, China).
B.Sc. (Tsinghua University, Beijing, China).

Supervisor: Professor W.R. Datars

Number of pages: xi, 158

ABSTRACT

The Fermi surfaces and the electronic properties of the donor-type stage-1 C_8K and stage-2 $C_{24}K$, as well as the acceptor-type stage-2 $BiCl_3$, stage-3 $HgCl_2$ and stage-3 SbF_5 graphite intercalation compounds were investigated by means of the de Haas-van Alphen effect.

The dHvA spectra of the stage-1 C_8K exhibit two dHvA frequencies, 3126 T and 4250 T. The corresponding effective masses were 0.86 m_0 and 0.92 m_0, respectively. The angular dependence of the dHvA frequencies for a direction within $\pm 18^\circ$ of the c-axis showed that there are both three-dimensional and two dimensional parts of the Fermi surfaces in C_8K. The three-dimensional Fermi surface has a cross-sectional area corresponding to the dHvA frequency of 3126 T. The charge transfer per potassium atom measured from the dHvA effect is 0.97. This implies that the potassium is ionized completely. These dHvA experimental results support both the Tatar and Rabii model and the revised Ohno, Nakao and Kamimura model for C_8K.

Two dominant dHvA frequencies were obtained in stage-2 $C_{24}K$. They are 286 T and 2570 T, respectively. The predictions of Blinowski's model are in agreement with the experimental data. The charge transfer per potassium is found

to be 0.88. This suggests that the potassium s-band is above the Fermi level in $C_{24}K$.

The dHvA measurements for the acceptor compounds show that the stage-2 $BiCl_3$ GIC had two dHvA frequencies, 327T and 1012T, and each stage-3 compound had three dominant frequencies. They are 121T, 523T and 664T for $HgCl_2$, and 172T, 656T and 852T for SbF_5. The cyclotron masses corresponding to the dHvA frequencies for these compounds were measured from the temperature dependence of the dHvA amplitudes. The theoretical predictions of the dHvA frequencies and the cyclotron masses from the Blinowski's band models for stage-2 and stage-3 compounds are in agreement with the experimental results. The angular dependence of the dHvA frequencies show that the Fermi surfaces in these acceptor compounds are cylinders. This proves the two-dimensionality of the band structures of the Blinowski model.

In addition, the charge transfer coefficient per carbon atom is directly determined from the observed sum of the dHvA frequencies for each of the acceptor compounds. The fractional charge distribution along the c axis of the stage-3 compounds is found to be between the uniform charge distribution model and the metallic sandwich model.

ACKNOWLEDGEMENTS

I wish to express my deep appreciation to my supervisor, Dr. W.R. Datars, for his guidance and support during these past years.

I would like to thank Dr. M.F. Collins and Dr. M. McGlinchey for their valuable comments and suggestions.

I am grateful to Dr. P.K. Ummat for his great help with the sample preparation.

I give very special thanks to all members of the Fermi surface group for their helpful hands. In particular I thank Mr. T. Olech for his technical assistance.

Sincere thanks are given to the secretaries: Margaret, Wendy, Jean and Cheryl for their daily help and friendship. I am especially grateful to Wendy for her e-mails during my staying in the United States.

Special thanks are also extended to Bill Scott, Jake Vanderwal, Andy Duncan, Gord Hewitson, Andy Duft and Clarence Verge for their help and friendship. I thank especially Bill Scott for providing liquid Helium for this work.

I would also like to thank the Department of Physics and McMaster University for their financial support.

Finally, with deep gratitude, I express my thanks to my grandmother, my mother and my husband. It was their constant encouragement and support that brought me through every difficult time.

TABLE OF CONTENTS

CHAPTER		PAGE
I	INTRODUCTION	1
II	THEORY	16
	II.1 Fermi surface and structure of graphite	17
	II.2 Band theory for GIC	23
	II.2.1 Blinowski's model	27
	II.2.2 The Fermi surface of C_8K	33
III	EXPERIMENTAL	44
	III.1 Sample preparation	44
	III.2 Intercalation method	45
	III.2.1 Stage-1 C_8K and stage-2 $C_{24}K$	46
	III.2.2 Stage-2 $BiCl_3$-GIC and Stage-3 $HgCL_2$-GIC	48
	III.2.3 Stage-3 SbF_5-GIC	49
	III.3 Sample characterization	49
	III.4 The dHvA measurements	58
	III.4.1 The dHvA effect	58
	III.4.2 dHvA techniques	61
IV	DONOR-TYPE GIC	68
	IV.1 Stage-1 C_8K	69
	IV.1.1 dHvA results and analysis	70
	IV.1.2 Discussion and calculation	77
	IV.1.2.1 The Fermi surface	78
	IV.1.2.2 The charge transfer	81
	IV.1.3 Conclusions for C_8K	87

IV.2 Stage-2 $C_{24}K$ GIC 88
IV.2.1 Experimental results 89
IV.2.2 Calculation and discussion 94
IV.2.2.1 The band structure 95
IV.2.2.2 The charge transfer 100
IV.2.3 Conclusions for $C_{24}K$ 102

V ACCEPTOR-TYPE GIC 103

V.1 Stage-2 $BiCl_3$-GIC 104
V.1.1 Experimental results 105
V.1.2 Calculation and discussion 111
V.1.2.1 Band structure 111
V.1.2.2 Comparison of experimental results for stage-2 acceptor compounds 116
V.1.3 Conclusions for stage-2 $BiCl_3$ 119

V.2 Stage-3 $HgCl_2$-GIC and SbF_5- GIC 120
V.2.1 Experimental results and analysis 121
V.2.2 Discussion 131
V.2.2.1 The energy bands 131
V.2.2.2 The charge distribution 137
V.2.2.3 Data comparison of stage-3 acceptor compounds 138
V.2.3 Conclusions for stage-3 $HgCl_2$ and SbF_5-GIC 141

VI SUMMARY AND CONCLUSIONS 143

REFERENCES 150

LIST OF FIGURES

FIGURE		PAGE
I.1.	Room temperature conductivity along the basal plane as a function of stage for three intercalants, AsF_5, HNO_3 and K	5
II.1.	Crystal structure of graphite	18
II.2.	Electronic energy bands and Fermi surface of graphite	20
II.3.	Graphite π-bands along several high symmetry directions	24
II.4.	Progression of Fermi surface from pure graphite to stage-1 intercalation compounds	26
II.5.	Schematic energy bands of stage-2 GIC	30
II.6.	Band structure near the U(H) point in stage-3 GIC	34
II.7.	The band structure of C_8K from Ohno et al, and the sketches of Fermi surface of C_8K from Inoshita et al	36
II.8.	Energy band structure for C_8K and the Fermi surfaces of C_8K DiVincen and Rabii	38
II.9.	Band structure of C_8K from Tatar and Rabii.....	40
II.10.	Band structure of C_8K from Mizuno et al.....	43
III.1.	Phase diagram of K-GIC	47
III.2.	(001) x-ray diffractogram of C_8K	51
III.3.	(001) x-ray diffractogram of $C_{24}K$	52
III.4.	(001) x-ray diffractogram of stage-2 $BiCl_3$-GIC..	53
III.5.	(001) x-ray diffractogram of stage-3 $HgCl_2$-GIC..	54

III.6. Schematic diagram illustrating the relation $I_c=d_s+(n-1)c_o$ 56

III.7. dHvA coil assembly and holder 62

III.8. Cryogenic system for dHvA experiment 64

III.9. Block diagram of the dHvA detecting system..... 67

IV.1. de Haas-van Alphen oscillations of stage-1 potassium graphite intercalated compound 71

IV.2 Fourier transform of the dHvA signal of stage-1 K-graphite 72

IV.3. Temperature dependence of the 3126 T oscillation of C_8K 73

IV.4. dHvA frequency 3126 T as a function of magnetic field direction from the c-axis of stage-1 K-graphite 75

IV.5. The dHvA amplitude decreases with the angle between the magnetic field and c-axis of the C_8K sample 76

IV.6. The crystal structure of C_8K 82

IV.7. The sketches of the Fermi surfaces of C_8K 84

IV.8. de Haas-van Alphen oscillations of stage-2 K-GIC at 4.2 K 90

IV.9. Fourier transform of the de Haas-van Alphen oscillations in $C_{24}K$ 91

IV.10. de Haas-van Alphen oscillations of stage-2 K-GIC at 1.4 K 92

IV.11. Fourier transform of the de Haas-van Alphen oscillations in $C_{24}K$ at 1.4 K..... 93

IV.12. The band structure of stage-2 K-GIC..... 98

V.1. de Haas-van Alphen oscillations of the stage-2 $BiCl_3$-graphite 106

V.2. Fourier transform of the dHvA signal of stage-2 $BiCl_3$-graphite 107

V.3. Temperature dependence of the dHvA frequencies of stage-2 $BiCl_3$-GIC 109

V.4. dHvA frequencies as a function of magnetic field direction from the c-axis of stage-2 $BiCl_3$-GIC 110

V.5. The dHvA amplitude as a function of the angle between the magnetic field and c-axis of the stage-2 $BiCl_3$-GIC 112

V.6. The band structure of stage-2 $BiCl_3$-GIC..... 117

V.7. de Haas-van Alphen spectrum of the stage-3 $HgCl_2$-GIC.....122

V.8. Temperature dependence of the second dominant frequency of stage-3 $HgCl_2$ GIC 123

V.9. de Haas-van Aphen spectrum of the stage-3 SbF_5-GIC 124

V.10. Temperature dependence of the dHvA oscillation of stage-3 SbF_5-GIC 126

V.11. dHvA frequency of the first dominant oscillation as a function of magnetic field direction from the c-axis of stage-3 SbF_5-GIC 128

V.12. The band structure of stage-3 $HgCl_2$-GIC 135

V.13. The band structure of stage-3 SbF_5-GIC 136

LIST OF TABLES

TABLES		PAGES
I.1.	dHvA frequencies observed in diluted graphite-Br_2 compounds	8
I. 2.	dHvA frequencies observed in donor-graphite compounds	9
I.3.	dHvA frequencies observed in acceptor-graphite compounds.....	10
II.1.	Slonczewski-Weiss-McClure band parameters for graphite.....	22
III.1.	The values of I_c measured from x-ray (001) diffraction.....	50
III.2.	Comparing of measured I_c with eq. III.1.....	57
IV.1	Comparison of experimental data with the BR model for $C_{24}K$.....	96
IV.2	Comparison of experimental data with YE model for $C_{24}K$.....	99
V.1	The experimental data for stage-2 $BiCl_3$-GIC.....	108
V.2	Comparison of the experimental data with Blinowski's model for the stage-2 $BiCl_3$-GIC.....	115
V.3	The comparison of the data for stage-2 BF_4^-, $SbCl_5$ and $BiCl_3$-GIC.....	118
V.4	The experimental data for stage-3 $HgCl_2$ and SbF_5-GIC	125
V.5	The comparison of the experimental data of stage-3 $HgCl_2$ and SbF_5 with Blinowski's model.....	134
V.6	The comparison of the data for stage-3 $HgCl_2$, $SbCl_5$ and SbF_5-GIC.....	139
VI.1	The experimental results obtained from the present work for C_8K, $C_{24}K$, $BiCl_3$-GIC, $HgCl_2$-GIC, and SbF_5-GIC.....	145

CHAPTER I

INTRODUCTION

Intercalation compounds are synthetic materials which have potentially useful properties and novel physical phenomena. During the past decade, both the solid state physics and the materials science communities have paid great attention to this new class of materials.

Intercalation compounds are formed by inserting layers of atoms or molecules of a guest chemical species, called the intercalant, between the layers of a host material which has highly anisotropic layered structure where the intraplaner binding forces are large in comparison with the interplaner binding forces. The intercalation process has been observed in many anisotropic systems like graphite, transition metal dichalcogenides, some silicates and metal chlorides, some clays, and some polymers and gels. (Dresselhaus, 1988).

Of the various type of intercalation compounds, the graphite intercalation compounds (GIC) are of particular physical interest because of their relatively high degree of structural ordering. The distinct ordering property of GIC is that there is a constant number of graphite layers between two intercalate layers. This regular ordering of the intercalate is called the staging phenomenon and the number of graphite layers between two intercalate layers is called the stage index.

Graphite intercalation compounds have been actually synthesized for over 150 years. In 1841, Schafhaustl and Prakt (1841) observed that the immersion of graphite in a mixture of sulfuric and nitric acids caused a dramatic swelling perpendicular to the cleavage plane by as much as a factor of two. In 1932, the crystal structure of intercalation compounds were deduced from x-ray diffractions of graphite intercalated with alkali metals (Schleede and Wellman, 1932). Detailed physical measurements began in the 1940's. But the modern era of research on graphite compounds starts from the preparation of compounds from synthetic near-single-crystal graphite in the 1950's by Henning (1965) and Ubbellohde (1972). In the middle 1970's, the techniques for synthesizing highly oriented pyrolytic graphite (HOPG) were developed (Moore, 1973), many new and exotic phenomena were discovered. Therefore, there was an explosive rebirth of interest in graphite intercalation compounds among physicists, chemists and materials scientists.

A large number of chemicals can be intercalated into graphite. At present, there are several hundred species known to react. They are ranging from such simple substances as Li and Br_2 to such esoteric unstable molecules as IrF_6. These species are divided into two groups, according to whether the electron transfer is from intercalant to carbon or vice versa. Alkali metals, alkaline earths and lanthanides act as electron donors, whereas halogens, acids and other electrophillic molecules remove an electron from the carbon layers, thus

becoming negative ions and called acceptors (Fischer and Thompson, 1978). The formation of donor or acceptor GIC's can be understood from the difference in the electron affinity between the intercalants and the graphite, and the charge transfer in GIC's is essential to stabilize the formation of these compounds.

Because of their unusual staging phenomena, charge transfer effects and large anisotropy, graphite intercalation compounds exhibit quite interesting structural, chemical, electrical, magnetic, optical and thermal properties. One of the most striking properties of GICs is a dramatic change of the basal plane electrical conductivity.

Pure graphite is a semimetal and a moderate conductor which has about 10^{-4} carriers per carbon atom, half of them being electrons and half of them holes. The carrier density of graphite is very small compared with that in typical true metals which is about one electron per atom. However, the in-plane mobilities are high because the carrier effective masses are low, less than 0.04 of the free electron mass (Spain, 1973). Therefore, the conductivity in the graphite planes (in the **a** crystallographic direction) is only 25 times smaller than that of copper at 300 K (Fischer and Thompson, 1978). On the other hand, the conductivity along the c-axis, that is in the direction perpendicular to the graphite planes, is about 10^3 times lower because of the weak interlayer interaction. Thus, the conductivity of graphite is highly anisotropic with

a high value in the graphite planes.

After intercalation of intercalants into graphite, the electron concentration is changed dramatically because of the charge transfer between the intercalants and host, and semimetallic graphite is transformed into metallic compounds because the Fermi level is moved, but the basal-plane mobility is not drastically affected because the carbon layers remain intact. Thus, intercalation results in major changes in the transport properties (Fischer, 1979). The basal plane electrical conductivity increases from that for graphite by an order of magnitude or more for several alkali metal graphite compounds (McRae et al, 1980), and the values of the conductivity comparable to that of copper have been reported for acceptor AsF_5-graphite compounds (Foley et al,, 1977). The magnitude of the increase in the in-plane conductivity depends on the intercalate species and its concentration (stage index). Fig.I.1 shows the dependence of basal-plane conductivity on the intercalation stage for three intercalants, AsF_5, HNO_3 and K. One can see that the conductivity for both the donor and acceptor compounds is increased with different magnitudes, and saturates at different stage indecies. However, the change of the c-axis conductivity (σ_c) after intercalation is different from that of in-plane conductivity (σ_a). It increases for donor compounds and decreases for acceptor compounds. At room temperature, the ratio σ_a/σ_c spans the range from about 30 in

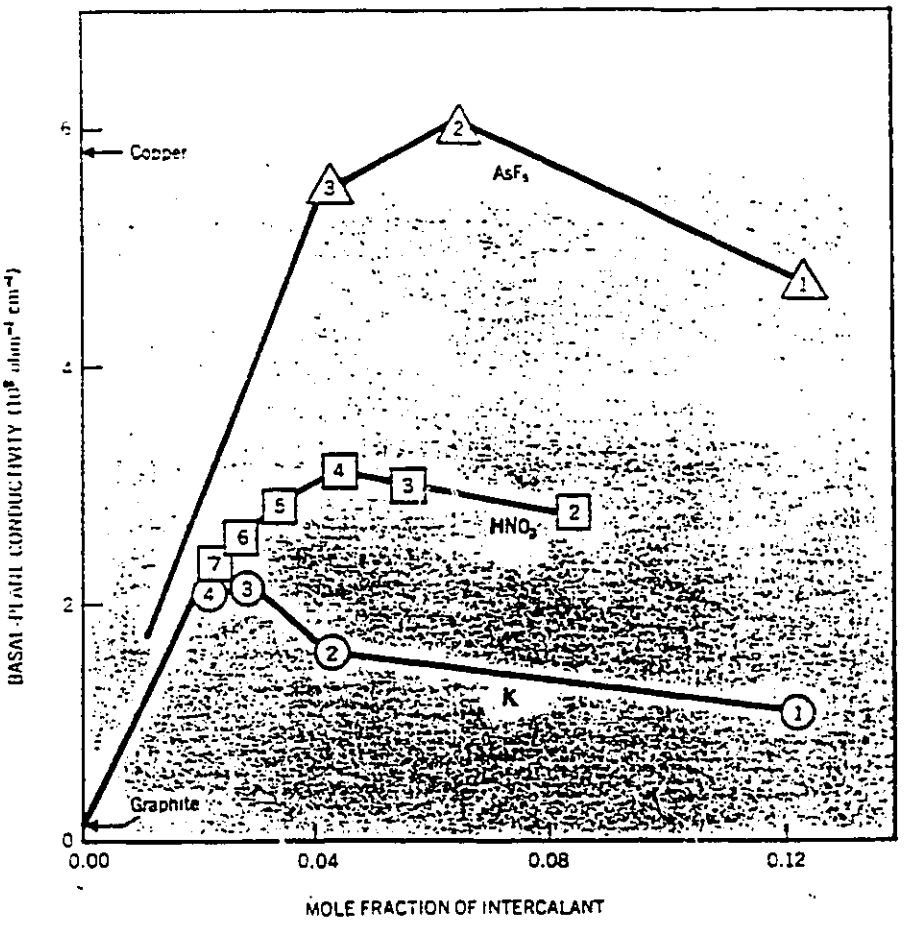

Figure I.1. Room temperature conductivity along the basal plane as a function of stage for three intercalants, AsF_5, HNO_3 and K. The numbers inside the data denote the stage of the compound. (From Fischer and Thompson, 1978).

KC_8 through 10^3 in pure graphite to as high as 10^6 with acceptor intercalants (Fischer and Thompson, 1978). This wide range of behavior in electrical conductivity occurs because intercalation increases the carrier density by a large amount while decreasing the carrier mobility by a smaller amount. The graphite-intercalate interaction varies significantly from one intercalant to another (Dresselhaus, 1984). However, it is the high basal plane conductivity and the two dimensionality which made the graphite intercalation compounds receive special attention for studying two-dimensional physical phenomena and for such possible applications as wires, battery electrodes and hydrogen containers.

A large amount of work has been done studying the chemistry, thermodynamics, structural and electronic properties of the compounds. Among the studies, electronic properties are of central importance since they control all other properties, such as elastic, thermal, optical, and even the mechanical properties. Many experimental methods can be used for probing the electronic properties, such as cyclotron resonance, photoelectron spectroscopy, valence-band x-ray spectroscopy, the de-Haas-van Alphen (dHvA) effect and the Shubnikov-de Haas effect. Different techniques have different advantages for the study of electronic properties. For instance, the cyclotron resonance technique is used especially for probing the effective mass. Magnetoreflection, which probes the transitions between magnetic energy levels in

different bands, has been particularly useful for determining the energy band parameters. Spectroscopic techniques generally probe the energy regions well removed from, as well as near, the electrochemical potential. Full-band spectroscopic techniques usually allow the densities of states to be estimated. The de Haas-van Alphen and Shubnikov-de Haas effects measure the cross-sectional area of the Fermi surfaces. In addition, the conductivity, Hall effect and magnetoresistance, result from an average taken over all carriers near the Fermi energy. Among all the techniques mentioned above, the de Haas-van Alphen and Shubnikov-de Haas effects are precise tools which can probe a particular region of the Fermi surfaces.

The de Haas-van Alphen (dHvA) effect and the Shubnikov-de Haas (SdH) effect are quantum oscillatory phenomena observed in the magnetic susceptibility and in the electrical conductivity, respectively. The quantum oscillatory studies directly yield values for the extremal Fermi surface cross-sectional areas perpendicular to the magnetic field. These techniques have been especially valuable in providing the density of carriers, the shape of Fermi surface, and the effective mass associated with each extremal Fermi surface cross-sectional area.

Measurements using the quantum oscillatory phenomena on graphite intercalation compounds began with Bender and Young's (1973) study of Shubnikov-de Haas oscillations. They pioneered

the application of the Shubnikov-de Haas effect to graphite-bromine compounds and found that the SdH frequencies observed in dilute graphite-Br_2 compounds were stage-independent. Since then, the SdH effect and dHvA effect have been applied to the study of many acceptor and donor graphite intercalation compounds by many research groups over the world. Table I.1 gives the dHvA frequencies reported by several workers for the dilute Br_2-graphite compounds that were not well characterized for stage. A list of the dHvA frequencies for several staged donor graphite compounds is given in Table I.2, and the list for some staged acceptor compounds is given in Table I.3.

Table I.1.

dHvA frequencies observed in dilute graphite-Br_2 compounds

Techniques	dHvA frequencies (T)	Authors
MTO	14.5, 29.3, 61.5, 120, 183, 78.4, 159, 100, 414, 480, 545	Rosenman et al (1979)
SdH	19.1, 61, 79.6, 470	Bender and Young (1972)
dHvA	23, 50, 66, 135, 85, 121	Tanuma et al (1978)

MTO: Magnetothermal oscillations
SdH: Shubnikov-de Haas
dHvA: de Haas-van Alphen

Table I. 2.
dHvA frequencies observed in donor-graphite compounds

Donor intercalant	Stage n	dHvA frequency (T)	Authors
	∞ (HOPG)	0.33, 4.9, 6.5	Soule et al (1964)
K	1 (C_8K)	2870	Higuchi et al (1980)
	2 ($C_{24}K$)	133, 149, 282, 306, 439	Dresselhaus et al (1980)
	3 ($C_{36}K$)	146, 260	Higuchi et al (1980)
	4 ($C_{48}K$)	121, 144, 238, 264, 338	Higuchi et al (1980) and Shayegan et al (1982)
	5	24, 135, 152, 191, 243, 267, 290, 453	Dresselhaus et al (1980)
KHx	1 ($C_4KH_{0.8}$)	30, 106, 647, 4000	Enoki et al (1986)
	2 ($C_8KH_{0.8}$)	41, 283, 763, 1525	
	4	32, 164, 309, 461	
KHg_y	1 ($C_3KHg_{0.77}$)	52, 1090, 2490	Timp et al (1984)
	2 ($C_7KHg_{0.72}$)	50, 221, 901, 1119, 1250, 1490	
	3 ($C_{13}KHg_{0.62}$)	15, 155, 290, 444	
Rb	1 (C_8Rb)	2460, 3130	Tanuma et al (1980)
	2 ($C_{24}Rb$)	28, 213, 255	Dresselhaus et al (1980)
	3 ($C_{36}Rb$)	35, 170, 260, 405	Shayegan et al (1982)
	5	24, 148, 294, 420	

Table I.3.
dHvA frequencies observed in acceptor-graphite compounds

Acceptor	Stage n	dHvA frequency (T)	Authors
--	∞ (HOPG)	0.33, 4.9, 6.5	Soule et al (1964)
AsF_5	1 (C_8AsF_5)	1710, 1840	Markiewitz et al (1980)
	2 ($C_{16}AsF_5$)	580, 1500	
	3 ($C_{24}AsF_5$)	72, 101, 109, 513, 581, 833, 877	Iye et al (1980)
	4 ($C_{32}AsF_5$)	62, 96, 106, 139, 208, 253, 633, 794	
HNO_3	2 ($C_{16}HNO_3$)	235, 470, 570, 805, 1040	Simon et al (1981)
	3 ($C_{24}HNO_3$)	40, 80, 240, 421, 662	
	4 ($C_{32}HNO_3$)	109, 219, 300, 351, 411, 460, 521, 630	
	5	56, 101, 168, 195, 238, 429	Tanuma et al (1980)
	6	28, 31, 52, 58, 97, 104, 237, 249	
$PdCl_2$	3 ($C_{12}PdCl_2$)	7, 39, 66, 91, 360	Oshima et al (1980)
$CuCl_2$	2	21, 46, 85, 106, 160, 178	Yosida (1989)
$SbCl_5$	1 ($C_{12}SbCl_5$)	1211	Zaleski et al (1984), (1987)
	2 ($C_{24}SbCl_5$)	422, 1190	
	3 ($C_{36}SbCl_5$)	152, 654, 811	Wang et al (1988)
SbF_6^-	1	1627	Zaleski et al (1985)
BF_4^-	2	523, 1377	Zaleski et al (1985)
$SbCl_4F$	1	480, 1250	Zaleski et al (1989)
	2	450	

From the tables, one can see that most of the observed dHvA frequencies in both donor and acceptor compounds are intercalant-dependent and stage-dependent. Many of the observed dHvA frequencies are greater by several orders of magnitude than those in pristine graphite. This is interpreted as a large increase in the Fermi surface cross-sectional areas resulting from the charge transfer effect. On the other hand, the observed dHvA frequencies are very many for a given sample in most cases, but usually some of them can be identified as harmonics, sum and differences or the splitting of a few fundamental frequencies. People have tried to explain both the numbers and magnitudes of the observed dHvA frequencies in those graphite intercalation compounds by using some electronic energy bands models proposed, for instance, for acceptor compounds by Blinowski and Rigaux (1980), Blinowski et al (1980), Dresselhaus and Leung (1980), Holzworth (1980) and Bok et al (1978) and for donor compounds by Inoshita et al (1977), Ohno et al (1979), Tatar and Rabii (1984), Koma et al (1986), Dresselhaus et al (1980), Saito and Kamimura (1985) and Yang and Eklund (1988).

This work presents the results of the investigations of the electronic bands and Fermi surfaces for several acceptor and donor graphite intercalation compounds by the dHvA effect. The compounds studied are donor-type potassium-graphite stage-1 C_8K and stage-2 $C_{24}K$, acceptor-type bismuth-trichloride-

graphite stage-2 $C_{17}BiCl_3$, mercury-chloride-graphite stage-3 $C_{17}HgCl_2$, and antimony-pentafluoride-graphite stage-3 $C_{27}SbF_5$. These compounds were chosen as the subjects of this thesis work for the following reasons.

For the donor-type potassium-graphite intercalation compounds (K-GIC), one of the interesting properties is the occurrence of superconductivity in the stage-1 compound (Tc=0.128-0.198 K). Since Hannay et al (1965) found that the first stage compounds C_8M (where M is a heavy alkali metal: K, Rb) show superconductivity, the compounds have attracted great interest because of the low dimensionality of the crystal structure, and also because neither of the starting constituents (graphite or the alkali metal) is a superconductor. However, superconductivity above 11 mK has not yet been observed in the higher stage compounds $C_{12n}M$ ($N \geq 2$) (Koike et al, 1980). Therefore, many theoretical and experimental groups all over the world have been attracted to the studies of the electronic properties for these compounds. The first electronic band calculations for C_8K by Inoshita et al (1977) showed the existence of Fermi surface pieces of two distinct types: one consisting of three-dimensional (3D) warped spheres centered at the middle and the top center of the Brillouin zone, the other consisting of two-dimensional (2D) cylinders along the Brillouin zone edges. This raises the question of which kind of carriers, 2D or 3D, contribute to superconductivity. The analysis of Kamimura (1987) gives the

point out that the net electron-electron interaction between 3D electrons is attractive in C_8M compounds and results in superconductivity. However, the dHvA experiment in C_8K by Tanuma et al. (1978) only found the cross-section of the 2D cylindrical Fermi surface and no 3D Fermi surfaces have been reported. In addition, despite a large amount of experimental effort and theoretical modeling, the charge transfer issue ($f=1$ or $f<1$) for the donor compounds (C_8M) continued to be debated hotly (Kamimura, 1984; Divincenzo and Rabii, 1982). Therefore, there is a need for careful dHvA experiment on well-characterized and high stage-fidelity alkali metal GIC samples.

Metal chlorides-graphite intercalation compounds constitute the largest group of acceptor-type GICs (Stumpp, 1977). However, the intercalation of all metal chloride-graphite compounds only takes place in the presence of chlorine (Behrens et al, 1988). This makes the staging fidelity of samples depend on not only the temperature of graphite (T_g) and metal chloride (T_i) but also the pressure of chlorine (P_{Cl2}) in the conventional "two-zone oven method". In 1988, Behrens et al (1988) found the conditions (T_g, T_i, P_{Cl2}) for the intercalation of $BiCl_3$ into graphite flakes, and pure stage $BiCl_3$-GICs with stage indexes 2, 3 and 4 are easily obtained with a high pressure of chlorine (600 mbar). In 1989, Datars and Ummat (1989) reported the conditions for intercalating large pieces of highly oriented pyrolytic

graphite (HOPG) with $HgCl_2$ and pure stage-3 $HgCl_2$-GIC is obtained with the sample in chlorine gas with a pressure of 800 mbar. Because of their high staging fidelity, both $BiCl_3$-GIC and $HgCl_2$-GIC are expected to be the new "favorite" compounds in the group of metal-chloride GICs for the investigation of the electronic properties by the dHvA technique.

The acceptor-type SbF_5-intercalated graphite compounds are similar to the AsF_5-GICs and $SbCl_5$-GICs. All of the compounds have high electrical conductivity among other GICs (Vogel, 1977; Wortmamn et al, 1988). However, both AsF_5-GICs and $SbCl_5$-GICs have been studied extensively with respect to structure, electrical properties and chemical composition while the SbF_5-GICs have received considerably less attention. Therefore, SbF_5-GIC was chosen as one of the research subjects.

This thesis work focusses on the measurements of the Fermi surface properties for these donor and acceptor compounds by using the dHvA technique. An introduction to the dHvA effect and the experimental techniques are provided in Chapter III. The details of the sample preparation and x-ray characterization are given in Chapter III also. Chapter II is concerned with the background theories which discuss the energy band structure of pure graphite and describe the theoretical models for both donor and acceptor GICs. In Chapter IV, the experimental results from the donor compounds

are presented and the theoretical predictions from each model for the donor compounds are compared with the dHvA results. The Fermi surface is also mapped and the charge transfer is derived based on the experimental data. In Chapter V, the dHvA experimental results from the acceptor compounds are presented. The energy band structures of these compounds are studied by using Blinowski's band models. The charge transfer and charge distribution along the c-axis are determined. These experimental data are also compared with those of other acceptor GICs reported previously. Finally in Chapter VI, all the results for both donor and acceptor compounds are summarized and the conclusions are presented.

CHAPTER II

THEORY

Graphite intercalation compounds have many similarities in structure and electronic properties to those of their parent constitutive materials: the graphite host and the intercalant. For example, the intralayer bonding is strong and the interlayer bonding is relatively weak in both graphite and graphite intercalated compounds (Dresselhaus and Dresselhaus 1981), the spacing between carbon atoms within layers remains essentially unchanged during the intercalation process (Nixon and Parry, 1969), the in-plane mechanical strength of the intercalated compound is similar to that of pristine graphite (Herinckx et al, 1972) and a high basal plane mobility of the carriers is observed in both graphite and its intercalation compounds (Zaleski, 1985).

The similarity between the pristine graphite and the intercalation compounds is a basis for developing the theoretical models of the electronic structure of intercalation compounds from the band structure of graphite. Especially, because the intralayer bonding of carbon atoms remains essentially unchanged during intercalation, one expects that the electronic structure of intercalation compounds is closely related to that of pristine graphite.

II.1 Fermi surface and band structure of graphite

The three-dimensional crystal of graphite consists of layers spaced by c_0 = 3.35 Å, as shown in Fig. II.1. The graphite layers are stacked in abab order with every second layer rotated by 60 degrees around an A atom. In a graphite layer, carbon atoms are arranged in a honeycomb array which gives a three-fold symmetry of the nearest neighbors with a distance of 1.42 Å. Therefore, there are four carbon atoms per unit cell in graphite crystal, which are denoted by A, B, A' and B' in Fig. II.1. The c-axis lattice vector is $\mathbf{a}_3 = 2c_0$ and the in-plane primitive lattice translation vectors are $\mathbf{a}_1$ and $\mathbf{a}_2$ with a magnitude of a=2.46 Å. The reciprocal lattice is also hexagonal, with vectors $\mathbf{b}_1$ and $\mathbf{b}_2$ of magnitudes $4\pi/(\sqrt{3}a)$ and $\mathbf{b}_3$ is equal to π/c_0.

Each carbon atom has four valence electrons which occupy 2s and 2p states. In the graphite crystal, the basis states are 2 P_z and three hybrid states made of 2s, $2p_x$ and $2p_y$ orbitals (sp^2 hybridization). The crystalline $2sp^2$ states give rise to six bonding σ and six antibonding σ^* bands. Between the σ and σ^* bands, there are two π and two π^* bands from the $2p_z$ states. The twelve σ-bands and the four π-bands are in the three-dimensional graphite unit cell containing four carbon atoms. Three of the four electrons from each carbon atom completely fill the σ bands and the remaining electron goes to the π bands. One can see that the two π bands can be fully

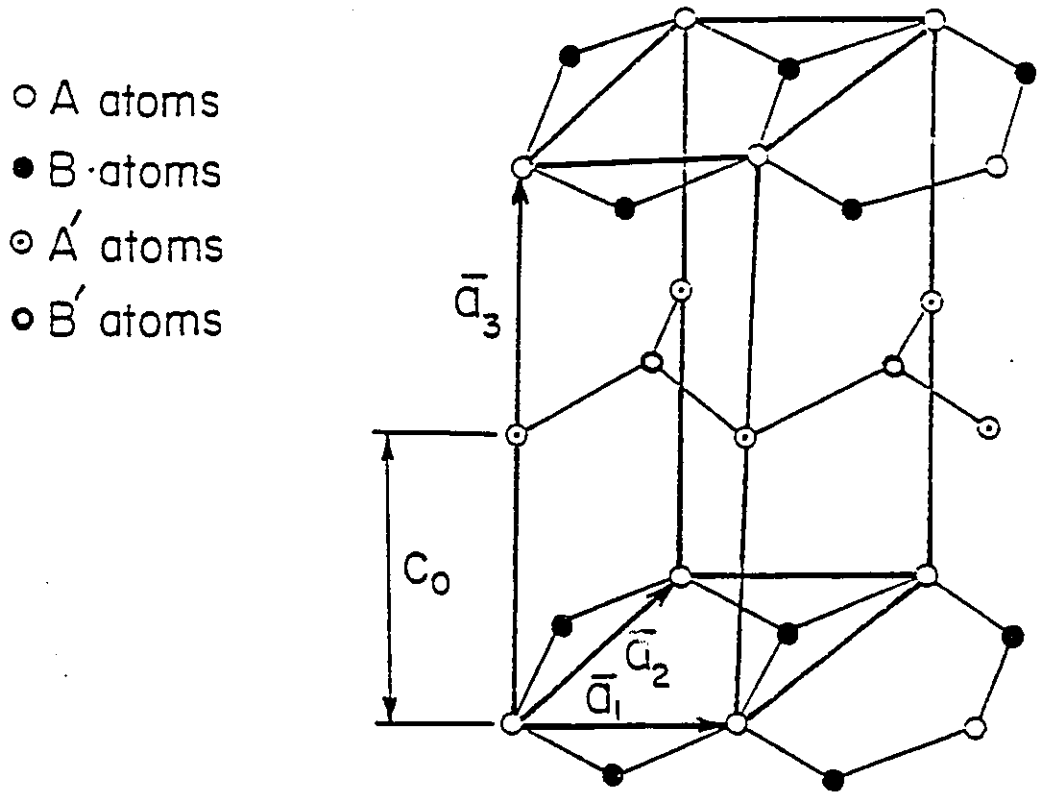

Figure II.1. Crystal structure of graphite.

filled. However, graphite is a compensated semimetal with a total carrier concentration of about 10^{-4} carriers per carbon atom at room temperature for both electrons and holes (Fischer and Thompson, 1978). This means that there exists a small overlap between the π and π^* bands. Therefore, a theoretical model describing the band structure of graphite should predict the semimetallic properties.

A widely used model for the dispersion relation for the four π bands of graphite was developed by Slonezewski and Weiss (1958) and McClure (1957, 1960) (SWMcC). The basic idea of the SWMcC model is to use the fact that the region occupied by carriers (the extent of the Fermi surface) is small compared with the in-plane reciprocal lattice vector (Brillouin zone dimension), and a **k•p** expansion is made in the k_{xy} plane. In the k_z direction, a Fourier expansion is used for the dispersion with k_z.

The energy dispersion relations for the four π bands are schematically shown in Fig. II.2 (a). A simple expression for the four π-bands from the SWMcC model when γ_3 is neglected are as follows:

$$E = (E_1+E_3)/2 \pm [(E_1-E_3)^2/4 + (\gamma_0-\gamma_4\Gamma)^2\sigma^2]^{1/2} \qquad \text{(II.1a)}$$

$$E = (E_2+E_3)/2 \pm [(E_2-E_3)^2/4 + (\gamma_0+\gamma_4\Gamma)^2\sigma^2]^{1/2} \qquad \text{(II.1b)}$$

where $E_1 = \Delta + \gamma_1\Gamma + \gamma_5\Gamma^2/2$

$E_2 = \Delta - \gamma_1\Gamma + \gamma_5\Gamma^2/2$

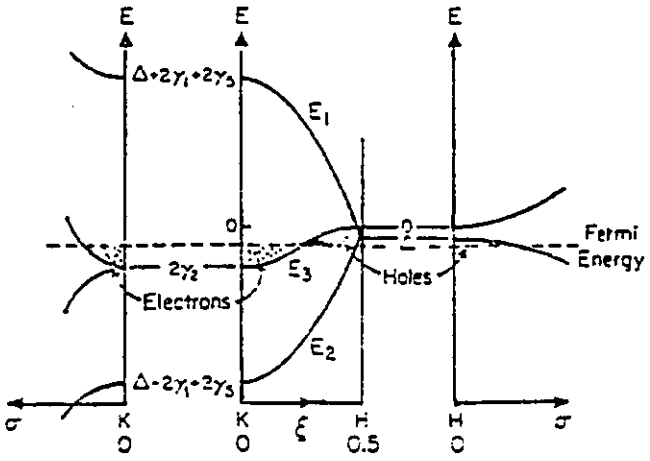

(a)

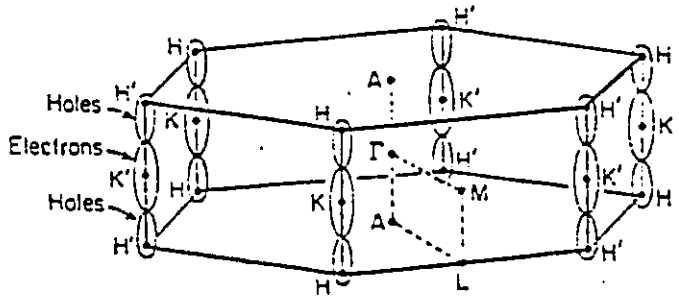

(b)

Figure II.2. (a) Electronic energy bands near the HK axis of Brillouin zone in graphite (SWMcC band model)
(b) Brillouin zone and Fermi surface of graphite.

$$E_3 = \gamma_2\Gamma^2/2$$

and $\Gamma = 2\cos(k_z c_0)$, $\sigma=\sqrt{3}ak/2$, $\mathbf{k}$ is the k_{xy}-plane wave vector measured from the Brillouin zone edges. The values of the band parameters (γ_0, ..., γ_5, Δ) and their physical meanings are given in Table II.1.

From Fig. II.2(a), one can see that three-dimensional graphite has a band overlap of $2\gamma_2$ (~0.04 eV) according to the SWMcC model. This prediction is consistent with the semimetallic properties of graphite. Therefore, the SWMcC model is widely used to interpret many experiments relevant to the electronic structure and Fermi surface of graphite (Spain, 1973; McClure, 1971).

The Brillouin zone and Fermi surface of graphite is shown in Fig. II.2 (b). Along each HKH edge of the Brillouin zone, there are three elongated trigonally warped pockets which have three-fold symmetry with respect to the edge. The central pocket contains electrons and the outer pockets contain holes. The Brillouin zone boundary cuts hole pockets into two pieces which are referred to as majority and minority holes. The dHvA frequencies are 6.5, 4.9, and 0.33 T for the majority electron, majority hole and minority hole respectively, when the magnetic field is parallel to the c axis (Soule et al 1964, Williamson et al 1965, Woollam 1970, Cooper et al 1970, Toy et al 1977). The Fermi surface is highly anisotropic, the length along the c axis is about 13 times the width perpendicular to the direction (Dresselhaus and Dresselhaus

Table II.1. Slonczewski-Weiss-McClure band parameters for graphite (from Dresselhaus and Dresselhaus 1980)

Band Parameter	Order of Magnitude (eV)	Physical origin
γ_0	3.16 ± 0.05	Overlap of neighboring atoms in a single layer plane.
γ_1	0.39 ± 0.01	Overlap of orbitals associated with carbon atoms located one above the other in adjacent planes. Width of π bands at point K is $4\gamma_1$.
γ_2	-0.020 ± 0.002	Interaction between atoms in next nearest layers and from coupling between π and σ bands. Band overlap is $2\gamma_2$. Majority de Haas-van Alphen frequencies determined by γ_2.
γ_3	0.315 ± 0.015	Coupling of the two E_3 bands by a momentum matrix element. Trigonal warping of the Fermi surface determined by γ_3.
γ_4	0.044 ± 0.024	Coupling of E_3 bands to E_1 and E_2 bands by a momentum matrix element. Determines inequality of K-point effective masses in valence and conduction bands.
γ_5	-0.038 ± 0.005	Interaction between second nearest layer planes. Introduced in E_1 and E_2 to be consistent in the order of the Fourier expansion.
Δ	-0.008 ± 0.002	Difference in crystalline fields experienced by inequivalent carbon sites in layer planes. Volume of minority hole carrier pocket sensitive to Δ.

1981) Therefore, the Fermi surface of graphite is almost cylindrical and thus graphite is often called a two-dimensional material.

Although the SWMcC model is widely used, it is based on a first order expansion of the bands in the region of the Brillouin zone around the HKH edge. Therefore, it is only valid for the description of the band structure of graphite around the edge. In fact, the carriers in graphite only occupy the small region around the edge, as shown in Fig. II.2 (b). So, the SWMcC model is suitable for the electron structure of graphite. However, if one wants to use the band structure of graphite far away from the HKH edge to analyze other physical properties of graphite, for instance, the optical properties, the SWMcC is not good enough. A full band structure calculation throughout the Brillouin zone of graphite was proposed by Johnson and Dresselhaus (1973) to account for the optical properties of graphite. This model uses a three-dimensional Fourier expansion for the basis functions. The dispersion relation for the π bands along several high symmetry directions is shown in Fig. II.3.

II.2 Band theory for GIC

In graphite intercalation compounds, the intercalated species are either fully or partially ionized. A charge of equal magnitude and opposite sign on carbon atoms maintains

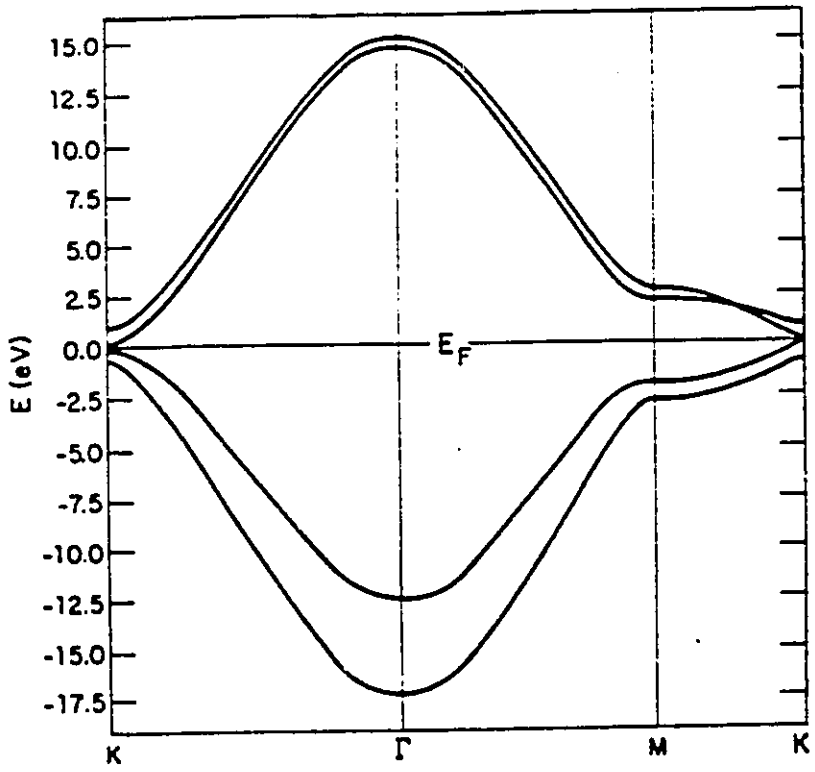

Figure II.3. Graphite π-bands along several high symmetry directions (Johnson and Dresselhaus, 1973).

the neutrality of the graphite intercalation compounds. If the band structure of GICs is assumed to be described by the SWMcC model (this is the idea of a rigid band model), the effect of the intercalant is primarily to increase the number of carriers by either removing electrons from the top of the valence bands (acceptor type) or by filling the bottom of the conduction bands (donor type) with carriers, that is, by changing the Fermi level. The shifting of the Fermi level causes the electron ellipsoid of the FS to grow while the hole ellipsoids shrink and finally disappear for donor-type intercalation. The opposite process with acceptor-type intercalation leads to a merging of the hole surfaces, as shown in Fig. II.4.

Based on the π bands of graphite, models of the band structure of GICs have to consider some major modifications which result from the change of the c-axis spacing for different stage indecies n. The charge distribution between graphite layers for $n \geq 3$, the possible interaction between carbon and intercalate orbitals and the in-plane intercalate structure have to be considered also. However, in general, the parameters describing these modifications need to be determined experimentally. Therefore, some assumptions have to be made for special cases to eliminate the modifications and simplify the theoretical calculation.

The rigid band models of graphite intercalation compounds are based mainly on the following assumptions: The band

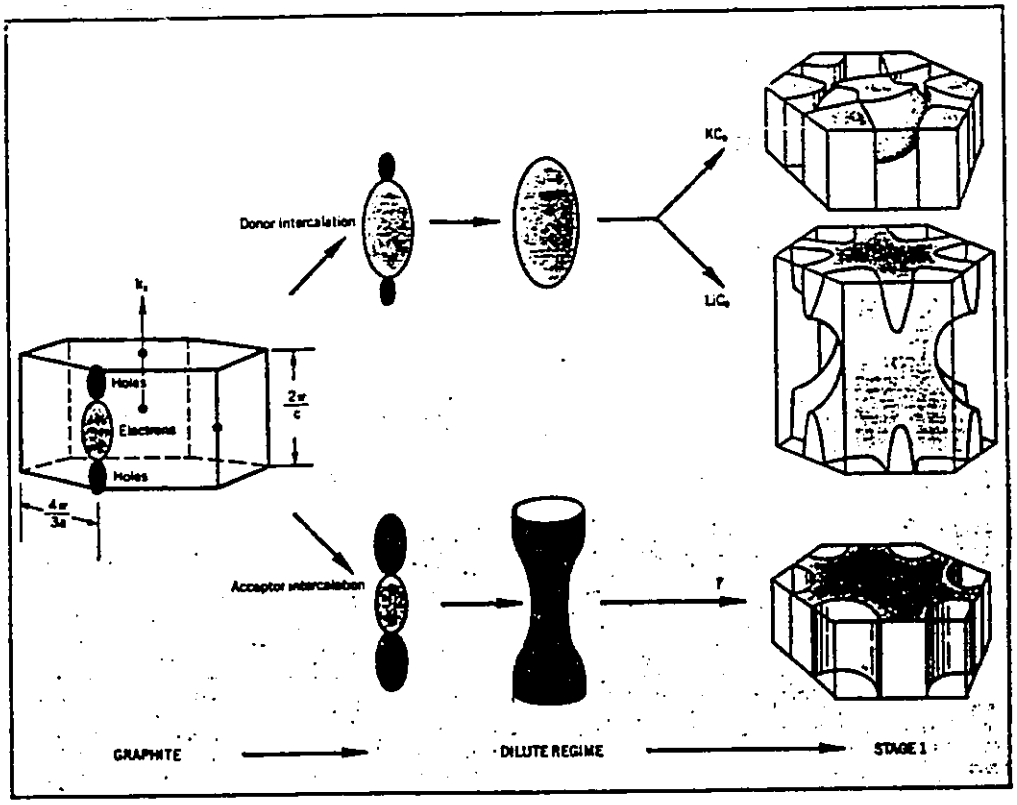

Figure II.4. Progression of Fermi surface from pure graphite to stage-1 intercalation compounds (from Fisher and Thompson, 1978).

structure of an nth stage compound is the same as the structure of n graphite layers. All interactions with the intercalant are ignored. The interaction between carbon atoms separated by the intercalate layer is zero while the remaining interactions between carbon atoms are the same as in the pristine graphite, and the in-plane lattice vectors are also as same as those in pristine graphite.

For donor compounds with n=1, the rigid band model with these assumptions is not valid if the hybridization between graphite and the intercalate happens. In this case, first principle calculations or special band structure calculations are needed.

II.2.1 Blinowski's model

Blinowski's model (Blinowski and Rigaux, 1980, Blinowski et al 1980) is the simplest model of the electronic structure of GICs. It is also one of the rigid band models because it treats the nth stage graphite compound as a set of equivalent, independent subsystems of n graphite layers limited by intercalated layers. This model is based on the tight binding approximation and includes the intralayer and interlayer nearest neighbor interactions.

For a stage-1 intercalation compound, there are two carbon atoms per unit cell, and only the interactions between the intralayer nearest neighbor are included. This gives the

energy solution (Blinowski et al 1980)

$$E=\pm\sqrt{3}\gamma_0 a|\boldsymbol{k}|/2 \qquad \text{(II.2)}$$

It is clear that this result can be obtained from the SWMcC model by setting all band parameters other than γ_0 equal to zero in eq. (II.1), that is, neglecting all interactions other than the nearest-neighbor in-plane overlap energy γ_0. However, the value of γ_0 in Blinowski's model is not fixed as it is in the SWMcC model. It is a modified parameter and could have different values for different intercalates due to the excess charge of carbon atoms obtained from the intercalate.

For a stage-2 intercalation compound, there are two graphite layers in each subsystem, and the arrangement of carbon atoms between successive intercalated layers is the same as in pure graphite. There are four carbon atoms per unit cell. Both the intralayer and interlayer nearest neighbors interactions are included. The energy bands are given by (Blinowski et al 1980)

$$E_1^{c.v}=\pm\left(\sqrt{\gamma_1^2+3\gamma_0^2a^2k^2}-\gamma_1\right)/2 \qquad \text{(II.3a)}$$

$$E_2^{c.v}=\pm\left(\sqrt{\gamma_1^2+3\gamma_0^2a^2k^2}+\gamma_1\right)/2 \qquad \text{(II.3b)}$$

This result can be obtained from eq. (II.1) by setting all band parameters other than γ_0 and γ_1 equal to zero at $k_z=0$. Again, the values of the band parameters (γ_0, γ_1) are not the same as the ones in the SWMcC model. They depend on the charge transfer coefficient per carbon atom f/l (f is the charge transfer per intercalated atom or molecular in compounds C_lX) the number of carriers per carbon atom) and on the spatial distribution of the excess charge. The relation which connects γ_0 with the Fermi energy E_F and the charge transfer coefficient f/l for the stage-2 compound is given by (Blinowski et al 1980):

$$E_F=\gamma_0\sqrt{\pi\sqrt{3}f/l} \qquad \text{(II.4)}$$

It should be noted that eq. (II.4) is the corrected one by Zhang and Eklund (1987). The one in the reference (Blinowski et al 1980) is in an error (with an extra $1/\sqrt{2}$).

The dispersion relation near the Brillouin zone corner for stage-2 compounds is shown in Fig. II.5. There are two valence and two conduction bands. The valence and conduction bands meet at the point U, the corner of the Brillouin zone, and there is no overlap between them.

For a stage-3 compound, there are electrostatic effects due to the presence of the excess charge on the graphite layers. These effects are not important in first and second stage compounds in which all graphite layers are equivalent

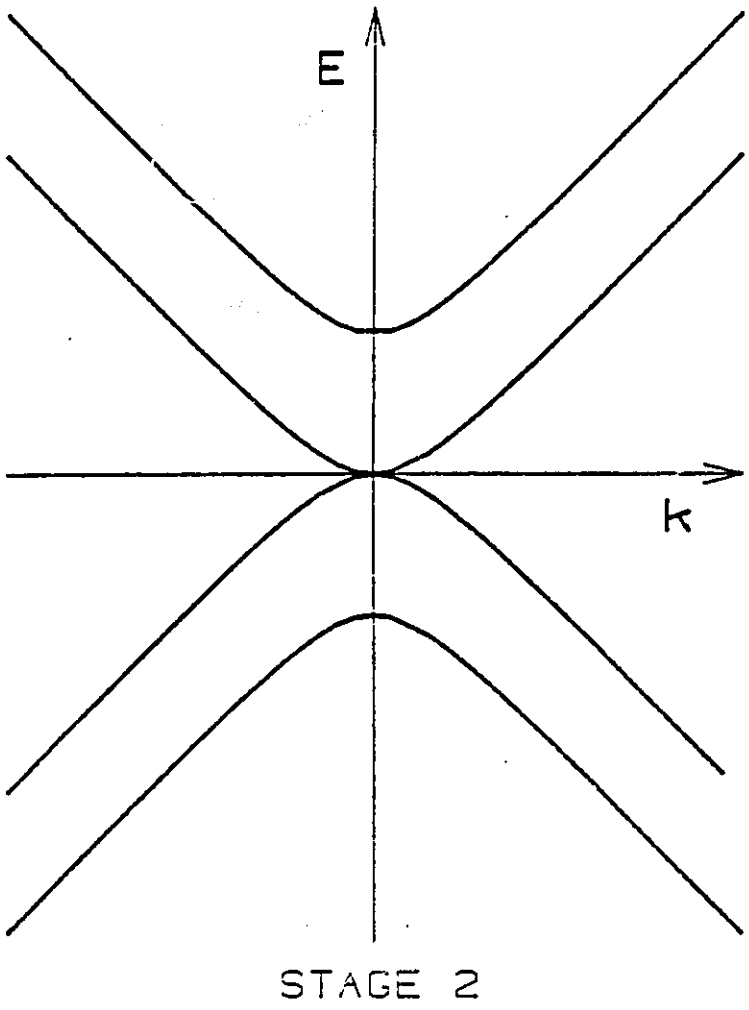

Figure II.5. Schematic energy bands of stage-2 GIC near the U(H) point according to the model of Blinowski et al.

and the same excess charge is accumulated on each layer. The situation is quite different however in GICs of stage $n \geq 3$. The layers are no longer electrostatically equivalent and the electrostatic forces affect the equilibrium excess charge distribution of the system.

In Blinowski's model (Blinowski and Rigaux, 1980), the electrostatic effects have been taken into account. For stage-3 compounds, the basic tight-binding functions constructed from six atomic $\psi_z(\mathbf{r})$ functions localized at the atomic sites ρ_i are

$$U_{ik}(\boldsymbol{\gamma}) = \sqrt{\Omega/\Sigma} \sum_{\rho_m} e^{ik\rho_i} \psi_z(\boldsymbol{\gamma}-\boldsymbol{\rho}_i), \; i=1,\ldots,2n. \; (n=3),$$

where $\Omega = \sqrt{3}a^2/2$ is the area of the 2D elementary crystal cell and Σ is the area of the system in the xy plane. The 2D wavevector $\mathbf{k}$ is restricted to the first Brillouin zone. By a straight forward generalization of the approximation procedure used for a stage-2 compound (Blinowski et al 1980), they get the corresponding secular equation as follows:

$$\begin{pmatrix}
\delta+\delta_1 - E & -X & \gamma_1 & 0 & 0 & 0 \\
-X^* & \delta-\delta_1 - E & 0 & 0 & 0 & 0 \\
\gamma_1 & 0 & -\delta+\delta_2 - E & -X^* & \gamma_1 & 0 \\
0 & 0 & -X & -\delta-\delta_2 - E & 0 & 0 \\
0 & 0 & \gamma_1 & 0 & \delta+\delta_1 - E & -X \\
0 & 0 & 0 & 0 & -X^* & \delta-\delta_1 - E
\end{pmatrix} = 0$$

where, in the vicinity of the U points of the 2D Brillouin zone, $|X| = (\sqrt{3}/2)\gamma_0 ak$, k being the distance from **k** to the U point. γ_0 and γ_1 are the resonance integrals for the nearest atoms in the intralayer and interlayer directions, respectively. The parameter 2δ, is the potential energy difference between the external and internal layers, $2\delta_1$ is that between two nearest neighbors in the same external layer, and $2\delta_2$ is that between two nearest neighbor atoms in the same internal layer. They all depend on the excess charge distribution. The 2δ turns out to be (see Blinowski and Rigaux, 1980 appendix)

$$2\delta = 0.1 \text{ eV} + (f/l)(Z\ 57.6 \text{ eV} - 2.7 \text{ eV}) \qquad \text{(II.5)}$$

where Z denotes the fraction of the excess charge accumulated on internal layers.

If δ_1 and δ_2 are approximated to be zero, the secular equation can be solved analytically. The band energies in the vicinity of the U point are:

$$E_1^{C.V.} = \delta \pm |X| \qquad \text{(II.6a)}$$

$$E_2^{C.V.} = \pm\sqrt{\delta^2 + \gamma_1^2 + |X|^2 - \sqrt{\gamma_1^4 + (4\delta^2 + 2\gamma_1^2)\,|X|^2}} \qquad \text{(II.6b)}$$

$$E_3^{C.V.} = \pm\sqrt{\delta^2+\gamma_1^2+|X|^2+\sqrt{\gamma_1^4+(4\delta^2+2\gamma_1^2)\,|X|^2}} \qquad \text{(II.6c)}$$

From these formula, we see that the electrostatic potential energy difference between the external and internal layers, δ, is included in the band structure. In other words, it affects the band structure. Fig.II.6 shows these energy bands for arbitrary values of δ=0, $\gamma_1/3$ and $2\gamma_1/3$. One can see that there are three valence and conduction bands in each case. For the valence bands, with increasing δ, the band 1V is pushed up, the band 2V acquires the camelback shape at small k, and crosses the band 1V at $|X| = 2\delta$ and becomes practically linear for larger k, the band 3V is slightly pushed down.

The Blinowski model has been extended to stage-4 compound (Blinowski and Rigaux, 1980) in which case four valence bands and four conduction bands are obtained.

Since the Blinowski model treats an n stage compound as a collection of independent graphite subsystems consisting of n graphite layers, the band structures are two-dimensional and the Fermi surfaces are cylindrical.

II.2.2 The Fermi surface of C_8K

The stage-one potassium graphite intercalation compound (GIC) C_8K is considered to be a prototype for the understanding of the electronic properties of the large family of GIC synthetic metals. However, the rigid band models of

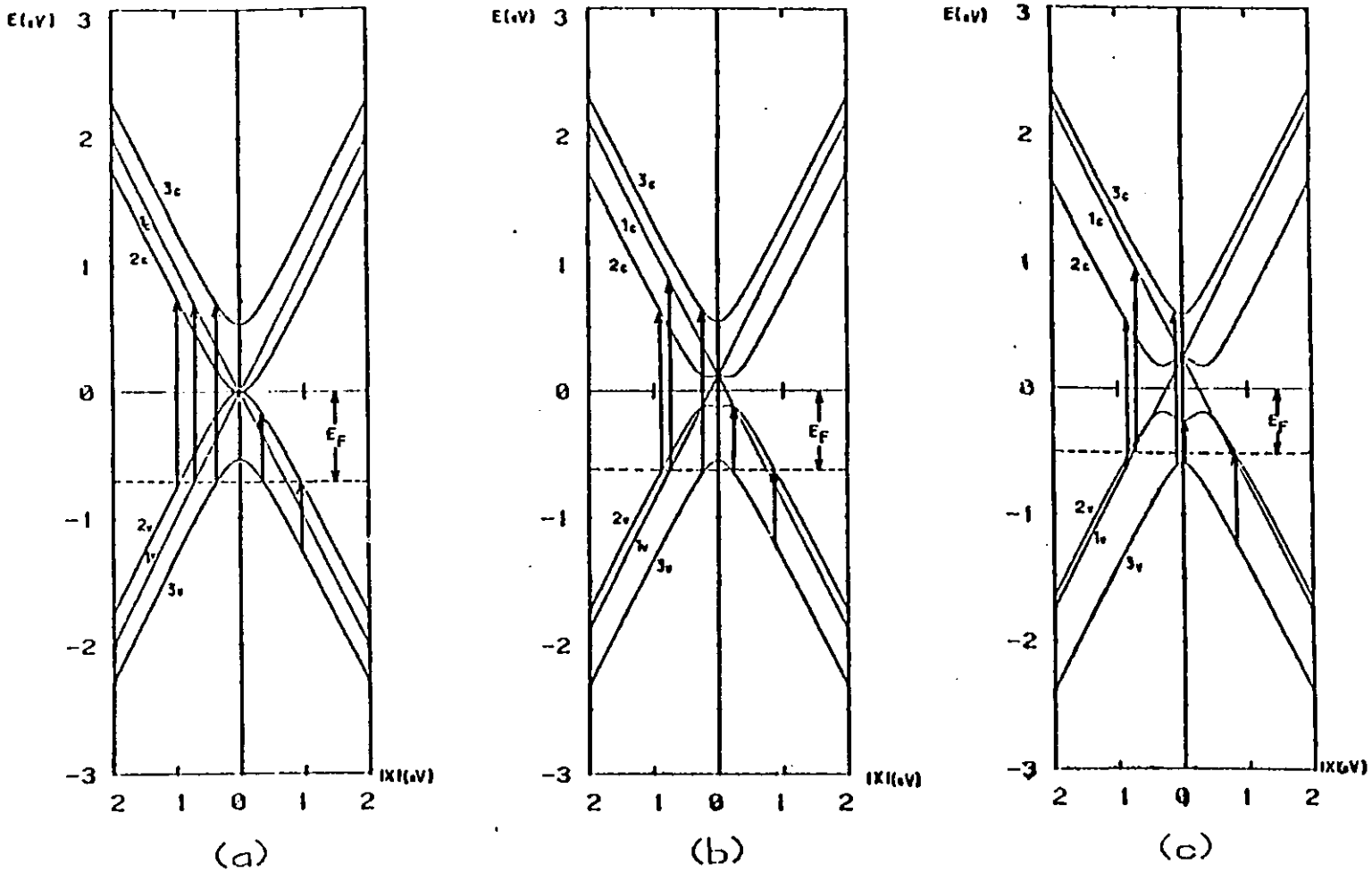

Figure II.6. Band structure near the U(H) point in stage-3 GIC ($|X| = (\sqrt{3}/2)\gamma_0 ak$). (a) $\delta=0$, (b) $\delta=\gamma_1/3$, (c) $\delta=2\gamma_1/3$ (from Blinowski and Rigaux, 1980).

GICs can not be used to describe the electronic structure of this compound because of the hybridization between K-atoms and C-atoms. Therefore, many special models for C_8K have been proposed, and the electronic structure as well as the Fermi surface of this first stage compound has been controversial both theoretically and experimentally for more than a decade. In this section, all the theoretical models for C_8K are discussed and some experiments used to support these models are also noted.

The first band structure calculation of C_8K was proposed by Inoshita et al (1977) using a tight binding method and was followed by the first principles, self-consistent calculation of Ohno, Nakao and Kamimura (ONK) (Ohno et al, 1979). In the ONK model, the potassium s-band in C_8K is partially filled and the charge transfer from the potassium atoms to the graphite layers is incomplete with a charge transfer per potassium atom (f) of 0.6. The band structure and the Fermi surface calculation from the model are shown in Fig. II.7, which are very similar to those calculated previously by Inoshita et al. (1977). One can see that one of the potassium 4s-bands (lower conduction band) crosses the Fermi level, forming a nearly-spherical three-dimensional (3D) Fermi surface in the center of the Brillouin Zone (BZ). Another potassium 4s band (higher conduction band) only crosses the Fermi level when the wave vector k is close to $k_z/2$ along the z direction, forming a small 3D Fermi surface at the top center of the BZ. Near the

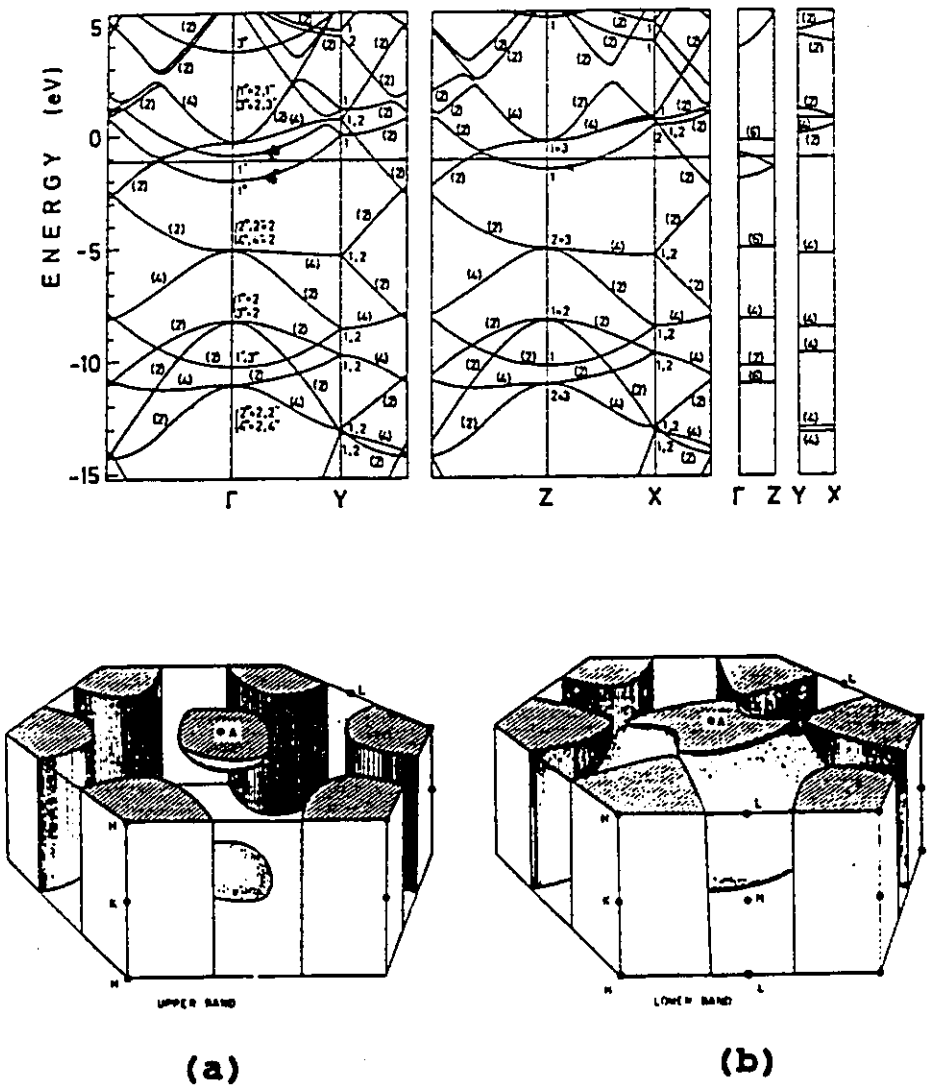

Figure II.7. The band structure of C_8K (from Ohno et al, 1979) and the sketches of Fermi surface of C_8K for (a) upper conduction band and (b) lower conduction band (from Inoshita et al, 1977).

Brillouin zone boundary, the Fermi surface is primarily of graphite π-band character: it is generally cylindrical, and gives rise to 2D properties. Many experiments have been reported to test the model. Some of them (Oelhafen et al, 1980; Cartier et al, 1980; Higuchi et al, 1980; Gubler et al, 1982; Koma et al, 1986) have supported the band structure. Moreover, the experimental results from the angle-resolved ultraviolet photoelectron spectroscopy by Takahashi et al. (1986) give a value of f=0.6 for the charge transfer in C_8K, which is the same as that predicted by the ONK model.

However, in 1982, DiVincenzo and Rabii (DR) (1982) found, using a non-self-consistent Korringa-Kohn-Rostoker (KKR) method, that the K 4s-band minimum in C_8K is located 1.8 eV above the Fermi level, the charge transfer is complete (f=1) and the 3D Fermi surface does not exist. Fig. II.8 shows the band structure and the Fermi surface calculated from the DR model. One can see that the metal band is completely empty and the Fermi surface only consists of the electron sheets centered at each of the six corners of the Brilloin zone. The experimental results of both high energy electron transmission and x-ray photoelectron spectroscopy by Ritsko and Brucher (1982) supported the band structure of DR.

In 1984, a new calculation using the density functional approximation for the band structure of C_8K was presented by Tatar and Rabii (TR) (1984). Their calculations were made self consistent by using the norm-conserving pseudopotentials. This

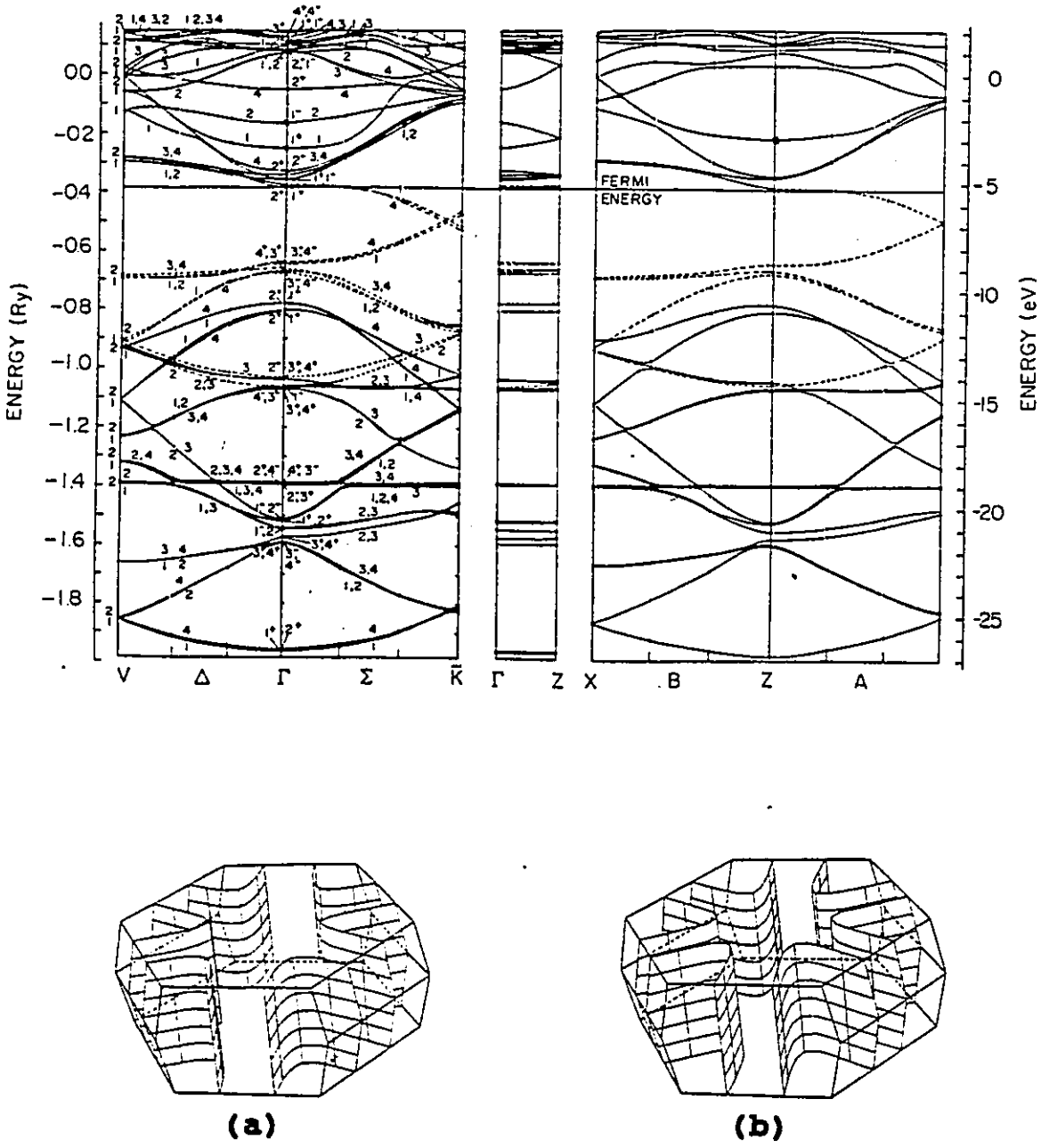

Figure II.8. Energy band structure for C_8K and the Fermi surfaces of C_8K for (a) lower band and (b) upper band (from DiVincenze and Rabii, 1982).

model showed complete charge transfer from the alkali atoms and the s levels 1.5 eV and 3.4 eV well above the Fermi-level. The FS consisted of large 2D trigonal prisms centered along the corners of the BZ and a small 3D elongated pocket at the center of the zone which was related to the graphite π-band and not to the alkali metal. Fig.II.9 shows the band structure of the TR calculation. This TR model agrees with ONK's model with respect to the existence of a 3D FS in the center of the BZ, but the character of the 3D FS is very different; it has potassium character in the ONK model and graphite character in the TR model. Preil and Fisher (1984) measured the x-ray photoelectron spectra of the valence bands of C_8K and found that the K-4s character at the Fermi level is very low (less than 0.04 electron/K-atom). This experimental result strongly favors that the FS of C_8K is of graphite character, and therefore supports both the TR and DR models.

In 1986, Koma et al (1986) and Kamimura (1986) gave a new interpretation of the K-4s like band in the ONK model by calculating the charge density distribution of the lowest occupied K-4s like conduction band states at k=0. They found the charge density is very different from the K-4s charge density and has the features of an interlayer state (Posternak et al, 1983). Therefore, they explained that the lowest occupied K-like conduction band is a kind of interlayer state with graphite character at the center of the BZ (instead of a K 4s-like band), and the K-4s band is shifted to an energy

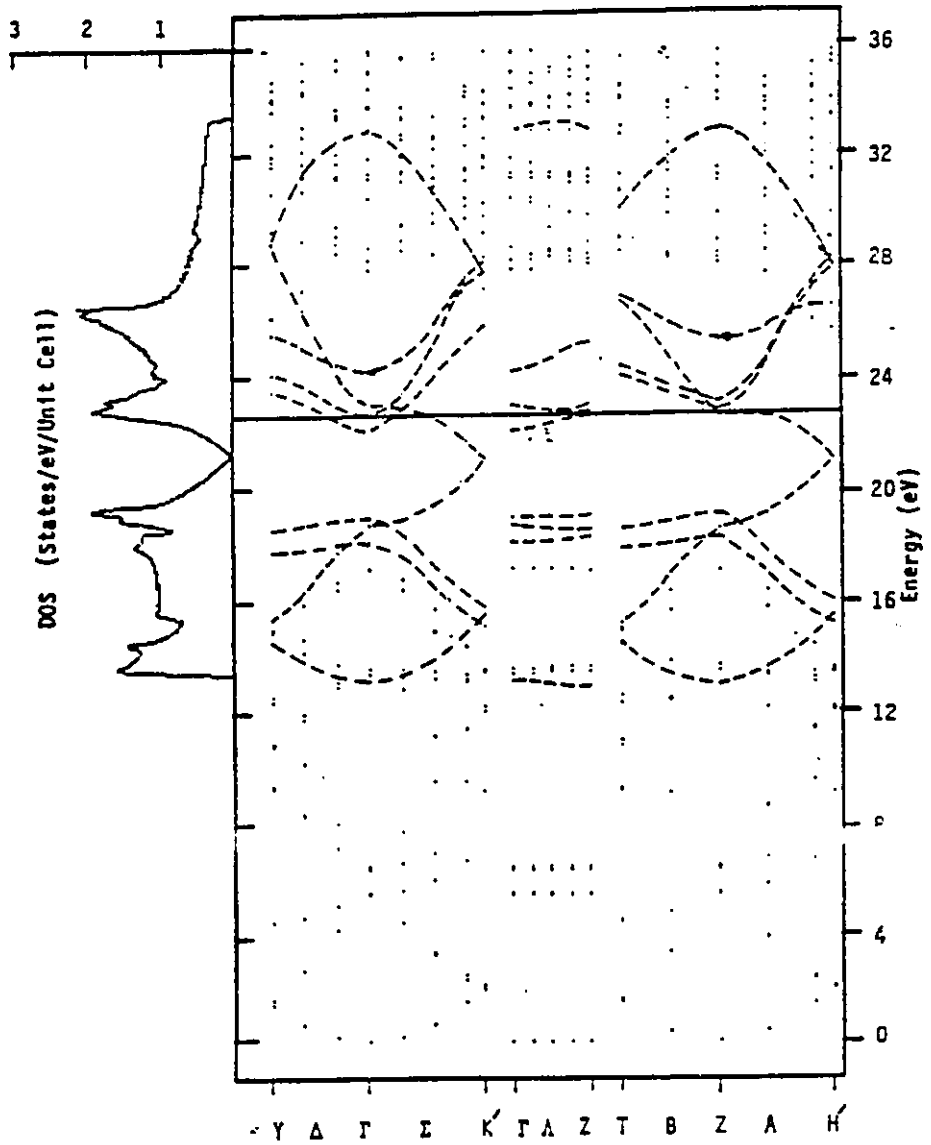

Figure II.9. Band structure of C_8K (from Tatar and Rabii, 1984).

that is higher than the interlayer band by more than 7 eV at k=0 (Koma et al, 1986). According to this interpretation, the alkali atom also yields a unit charge transfer and the 3D FS at the BZ center should be related mainly to the interlayer band. Now, both the revised ONK (rONK) and the TR models agree on the full ionization of the alkali atoms, and on the graphite origin of the central Fermi pocket (Marchand et al, 1988). However, the character of the central 3D FS is still different in the two models in the sense that it is from an interlayer band extending along the K-layers in the rONK model and it has carbon character extending along the graphite layer in the TR model (Koma et al, 1986).

In 1987, Mizuno, Hiramoto and Nakao (MHN) (Mizuno et al, 1987) performed another type of band structure calculation for C_8K by using the self-consistent numerical basis set LCAO method within the local-density-functional scheme. They found that there exist 3D FS (convex cylinders) in the center of the BZ which originate from the graphite bands and that this is due to the charge unbalance between environmentally non-equivalent carbon atoms in a graphite layer produced by the potassium atoms. From the final atomic configuration obtained by the self-consistent calculation, the amount of the charge transfer from a K atom to eight C atoms is 0.6 per K atom (Kamimura et al, 1988). However, the K-4s bands located at 2.9 eV above the Fermi level in the MHN model should result in a unit charge transfer. The experimental results from the

angle-resolved ultra-violet photoelectron spectroscopy by Takahaski et al. (1986) support the MHN band structure (Fig. II.10) except that non-dispersive conduction bands were observed instead of the 3D-conduction band around the center of the BZ.

In summarizing all the band structure calculations mentioned above, three questions arise from their discrepancies. Firstly, is there a 3D FS in the center of the BZ for C_8K? Secondly, is the charge transfer per K-atom complete or incomplete? Thirdly, what is the character of the 3D FS, i.e., is it from a K-4s like band, a graphite π-band or an interlayer band? In order to clearly resolve these questions and clarify these models, more definitive experiments, for instance, the dHvA measurements, are needed although many previous experiments (Dresselhaus and Sugihara, 1984) have been interpreted to support one or another of these models.

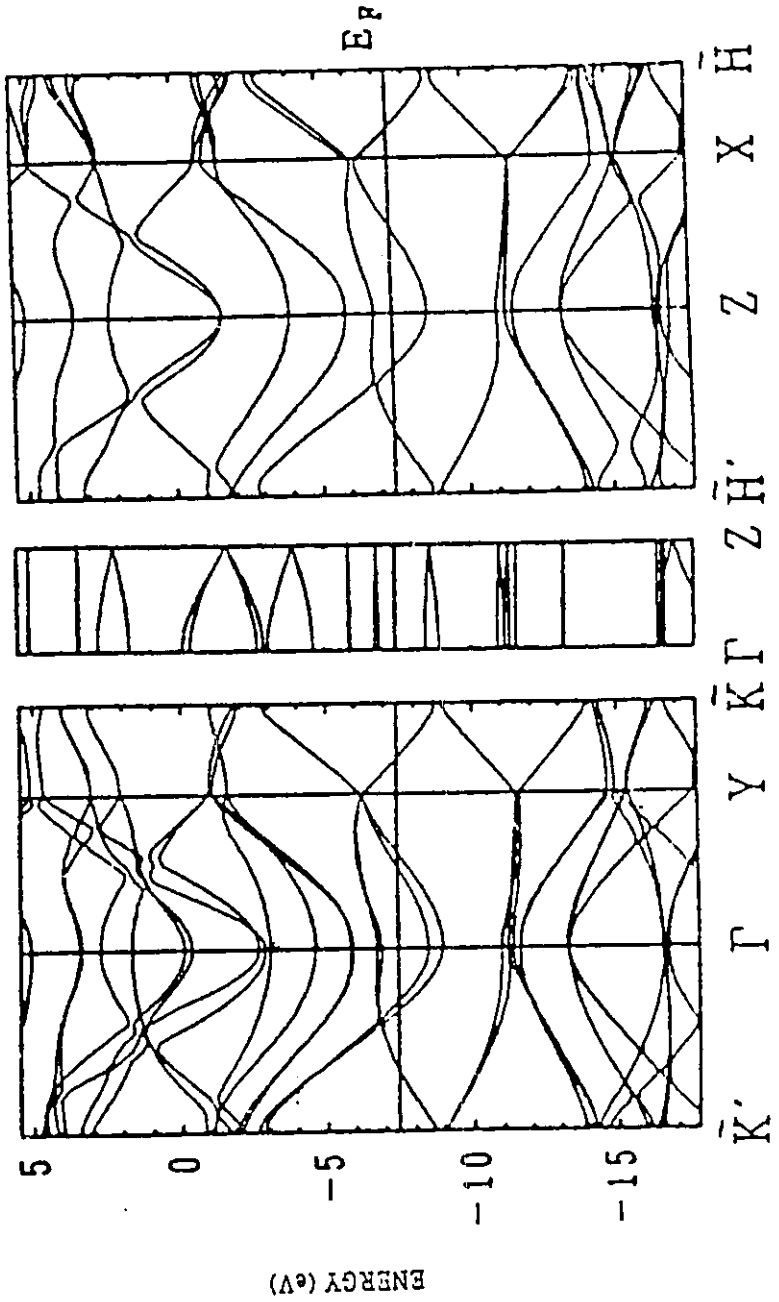

Figure II.10. Band structure of C_8K (from Mizuno et al, 1987).

CHAPTER III

EXPERIMENTAL

The experiments during this study consist of sample preparation and intercalation, sample characterization and measurements of the dHvA effect.

III.1 Sample preparation

For making a sample of intercalation compounds of graphite with pure stage index, great attention had to be given to each step of preparation.

The high reactivity of materials used for intercalation required handling in an atmosphere free of water vapor and oxygen. Thus, most of the handling was done in a glove box filled with dry nitrogen. The content of water vapor inside the dry box was less than 1 ppm.

The starting materials was highly oriented pyrolytic graphite (HOPG). Slabs of HOPG were cut into pieces of about 2.5x3.5 mm^2. The pieces were cleaved to about 0.7 mm thickness. The outer layer was removed by peeling. The pieces were then washed in acetone in an ultrasonic cleaner. Cleaned HOPG pieces were put into a glass container and dried under vacuum at an elevated temperature.

III.2 Intercalation method

A number of general methods (reviewed by Dresselhaus and Dresselhaus, 1981) have been developed for the preparation of graphite intercalation compounds (Ebert 1976, Herold 1977, 1979) including the two-zone vapor transport technique, the liquid intercalation method, the electrochemical method and the cointercalation technique. For the various techniques employed, the parameters of significance are temperature, vapor pressure, the chemical and physical properties of the intercalant and the characteristics of the graphite host materials. (Dresselhaus and Dresselhaus 1981).

The most common for the preparation of well-staged specimens is the two-zone vapor transport method in which the intercalant is typically heated to some temperature T_i, and the graphite, which is some distance away, is heated to a higher temperature T_g to prevent intercalant condensation on the sample. The stage of the compound, or the weight uptake of the intercalant, is practically controlled by the temperature difference T_g-T_i. Smaller values of T_g-T_i produced compounds with lower stage.

The samples presented here were prepared by using a two-zone furnace. First, a piece of graphite was put into a pyrex glass tube. Then the tube was connected to a vacuum line and evacuated for a few hours at an elevated temperature. After that, it was transferred into a dry box where the intercalant

was added to the tube. The nitrogen dissolved in the intercalant was removed after taking it out of the dry box by pumping. Then, the tube was sealed and put into the two-zone furnace.

III.2.1 Stage-1 C_8K and stage-2 $C_{24}K$

With the use of the phase diagram of K-GIC as shown in Fig. III.1, obtained by Nixon and Parry (1968), the temperatures of the HOPG and potassium metal were chosen as 297 °C and 263 °C, respectively, for stage-1 C_8K. The temperature difference, 34 °C was less than 100 °C. The period of reaction was about 8 days.

For stage-2 $C_{24}K$, the potassium metal at one end of the pyrex tube was heated at a temperature of about 245 °C and the HOPG at the other end was heated to about 355 °C. The temperature difference, 110 °C, was between 100 °C to 200 °C. The period of the reaction was from 4 hours to one day, depending on the size of the HOPG, the size of the ampoules, the amount of potassium metal and the distance between the HOPG and the potassium.

The color of stage-1 C_8K is golden-yellow and stage-2 $C_{24}K$ is rich bluish-green. The color disappears when the samples are exposed to air for just a few seconds. This is due to the instability of alkali metal samples in the presence of air and moisture. Therefore, after the reactions were completed, the

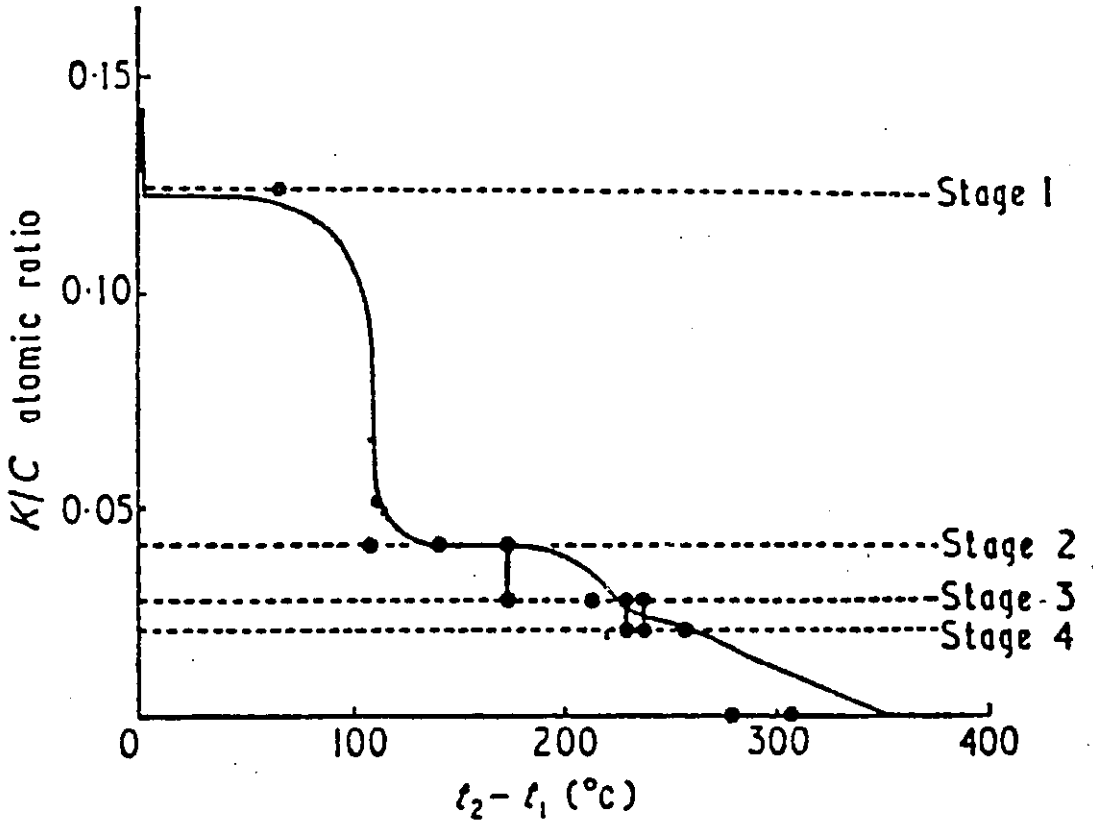

Figure III.1. Phase diagram of K-GIC. t_2-t_1 is the temperature difference between the sample (t_2) and the potassium (t_1). t_1=250 °C in all cases. Mixtures of two stages are represented by a line linking the stages involved (from Nixon and Parry, 1968).

tubes were transferred into the dry box and the samples were sealed in sample holders for both x-ray examination and dHvA measurements.

III.2.2 Stage-2 $BiCl_3$-GIC and Stage-3 $HgCL_2$-GIC

For the preparation of all metal chloride-graphite compounds, the addition of chlorine is necessary, except when the metal chloride itself generates Cl_2 by decomposition (Behrens et al, 1988). Therefore, for the conventional "two-zone oven method", the intercalation of metal chloride into graphite via the vapor phase is controlled by not only the temperature of HOPG (Tg) and the vapor pressure of the metal chloride (controlled by its temperature T_i), but also the pressure of chlorine (P_{Cl2}).

For the stage-2 $BiCl_3$-GIC, by referring to the report of Behrens et al. (1988), the HOPG and $BiCl_3$ were heated in a sealed reaction tube to a temperature of 253 °C with $T_i=T_g$, and the pressure of Cl_2 in the tub was 800 mbar. The intercalation time was extended to 14 days.

The stage-3 $HgCl_2$-GIC was made with the method of Datars and Ummat(1989). The HOPG and $HgCl_2$, in chlorine gas with a pressure of 800 mbar, were heated to a temperature of 250 °C with $T_i=T_g$. An intercalation time of 432 h (18 days) was required to form a fully developed, stage-3 $HgCl_2$-GIC.

After the intercalation reactions were completed, the

samples were washed with dilute HCl, deionized water and acetone, and then were dried in vacuum. Both the $BiCl_3$-GIC and the $HgCl_2$-GIC are stable in air.

III.2.3 Stage-3 SbF_5-GIC

The stage-3 SbF_5-GIC was made with the method of Wu et al (1981). The HOPG and SbF_5 were loaded into an H-shaped tube. The SbF_5 side was placed in a constant-temperature bath at 20 °C (T_i) and the other side containing the sample was put into a tube furnace at a temperature of 100 °C. The reaction time was about 7 days. The SbF_5-GIC was not stable in air, and therefore, when the reaction was completed, the tube was transferred into the dry box and the sample was sealed in a sample holder.

III.3 Sample characterization

A number of techniques (reviewed by Dresselhaus and Dresselhaus, 1981) are exploited for sample characterization of GICs, including visual inspection, weight uptake, chemical analysis, c-axis dilatation, diffraction measurements and electron microscopy.

Since many properties of measurements for GICs strongly depend on the stage index, the x-ray (001) diffraction method, which yields the stage index and information on staging

fidelity, is widely used to characterize GIC samples.

The stage index of most of the samples in the present work was determined with x-ray diffraction measurements using a powder diffractometer and CuKα radiation. The x-rays were incident at an angle θ to the xy-plane of the sample and were detected at the angle of 2θ to the direction of incidence. The intensity of the reflected radiation was recorded as a function of the angle 2θ. Figures III.2-III.5 shows the x-ray spectra for each sample. The position of the (00l) reflection peaks θ_l were read off the recorder chart and values of $d_l = I_c/l$, where I_c is the identity period along the c-axis, or repeat distance, were calculated from the Bragg formula

$$d_l = \lambda \; / \; 2\sin(\theta_l)$$

A straight line was fit to the reflection of order l versus $1/d_l$ and the value of I_c was calculated from the slope of the line. Table III.1 shows the results for I_c.

Table III.1

The values of I_c measured from x-ray (00l) diffraction.

	n	I_c (Å)
C_8K	1	5.35
$C_{24}K$	2	8.67
$BiCl_3$	2	13.06
$HgCl_2$	3	16.40

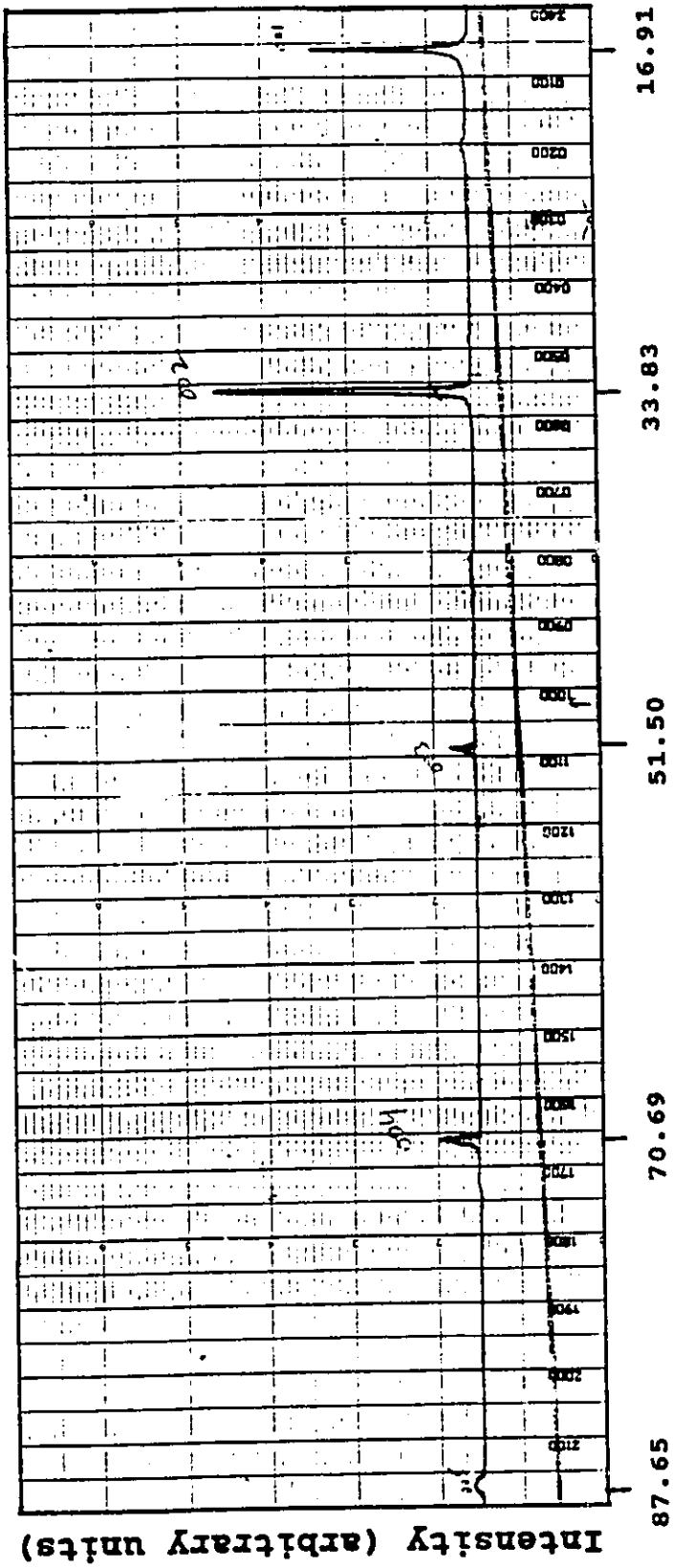

Figure III.2. (001) x-ray diffractogram of C_8K.

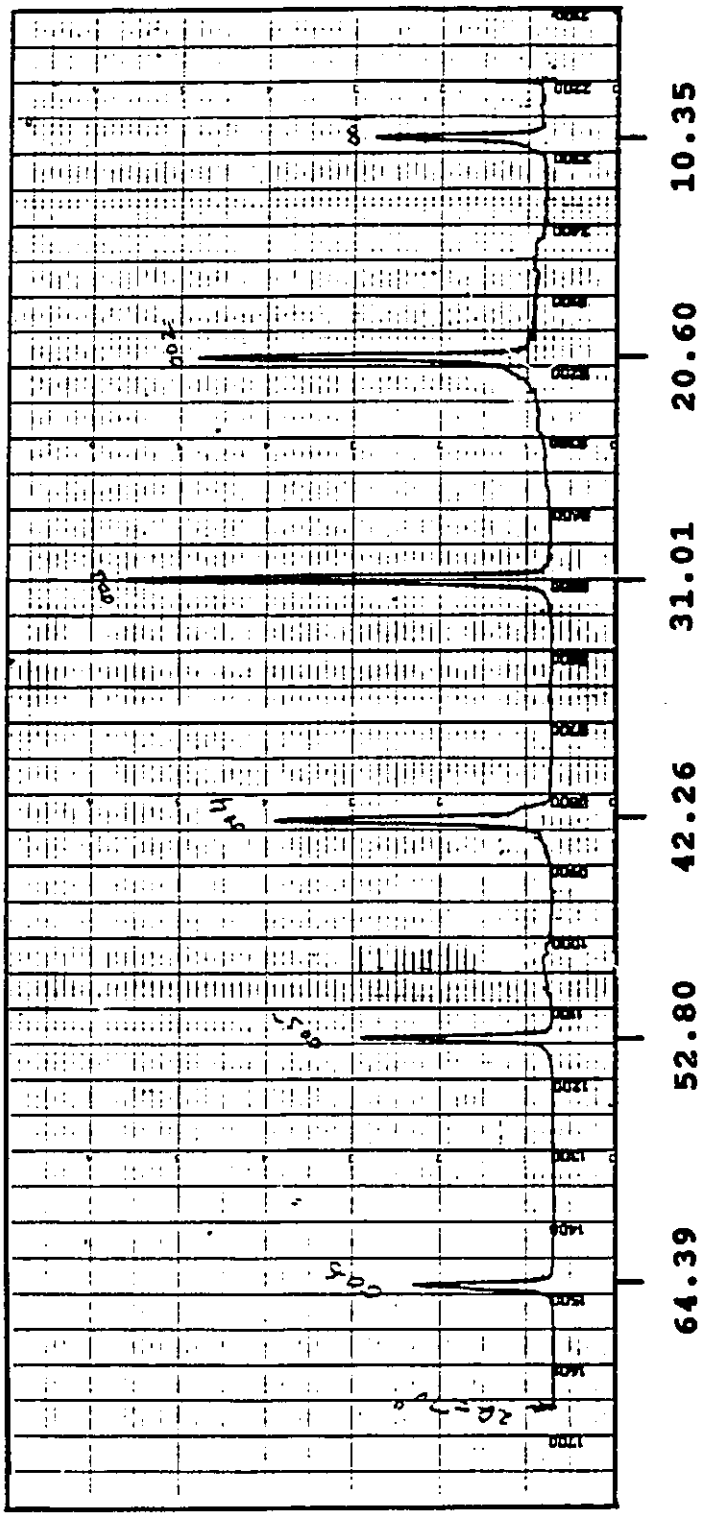

Figure III.3. (001) x-ray diffractogram of $C_{24}K$.

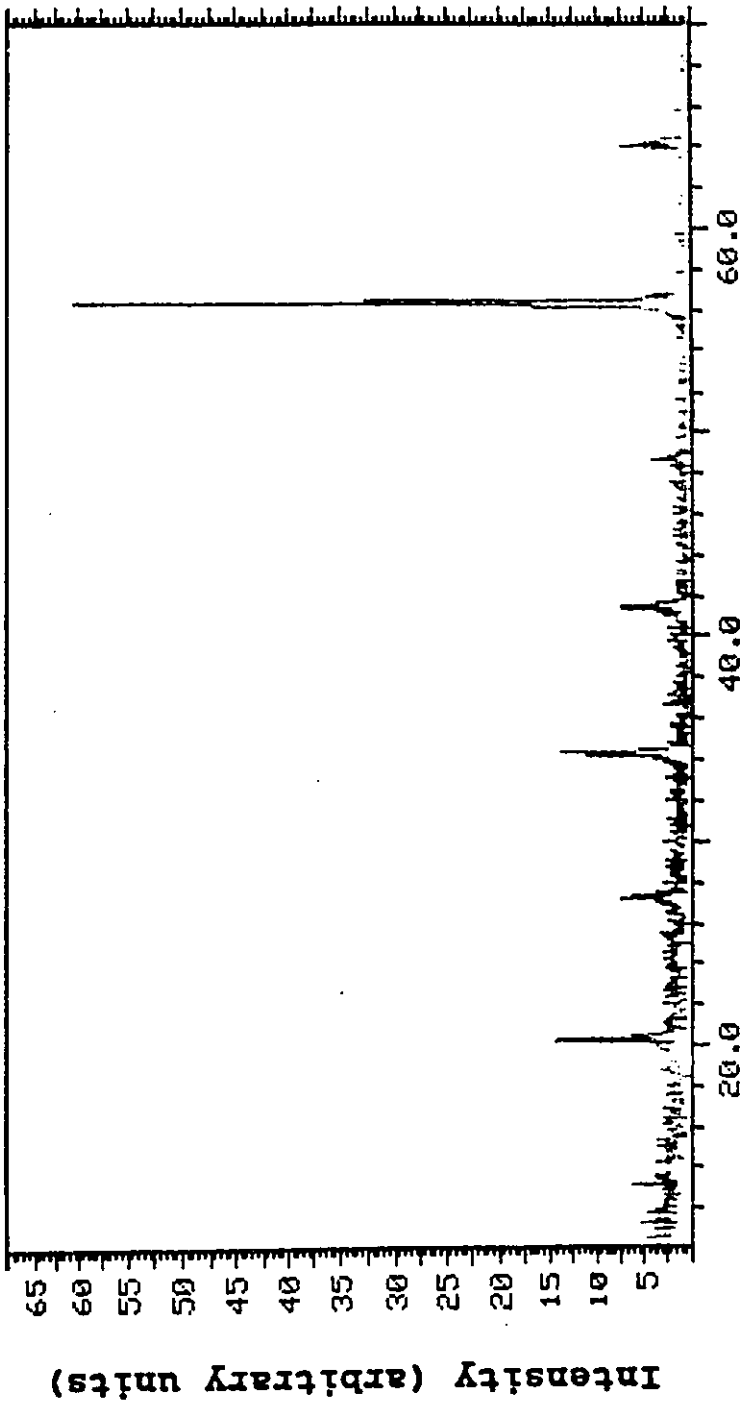

Figure III.4. (001) x-ray diffractogram of stage-2 $BiCl_3$-GIC.

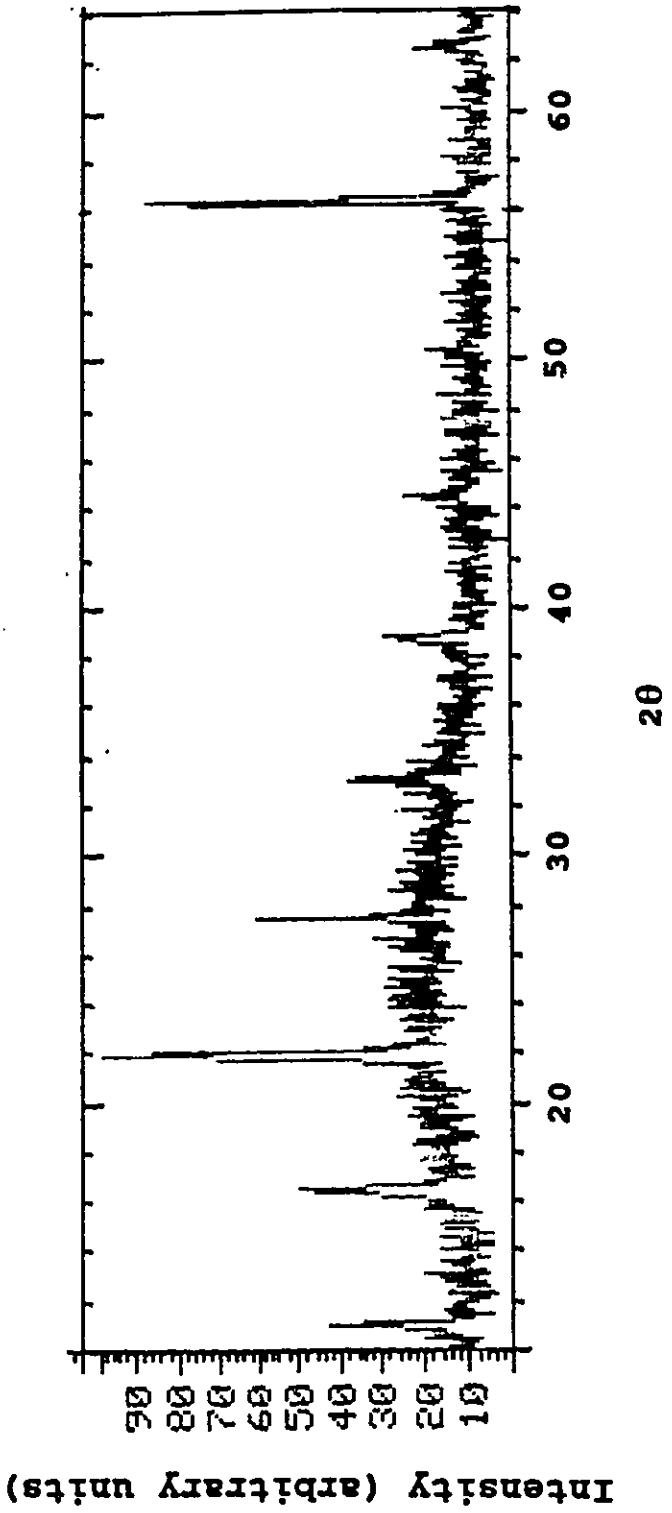

Figure III.5. (00l) x-ray diffractogram of stage-3 $HgCl_2$-GIC.

After knowing the repeat distance I_c, one can find the stage index n from the relation: (Dresselhaus and Dresselhaus 1981)

$$I_c = d_s + (n-1)c_o \qquad \text{(III.1)}$$

where c_o is the distance between adjacent graphite layers. (Since the basic symmetry within the graphite interior layers remains unaffected by intercalation, the spacing between adjacent graphite layers in intercalation compounds is essentially the same as in pristine graphite, c_o = 3.35 Å). The d_s, called the intercalate sandwich thickness, is the distance between two graphite layers between which an intercalate layer is sandwiched, as shown in Fig. III.6. d_s is usually determined from the measurement of extended x-ray absorption fine structure (EXAFS), the calculation of close-packed arrangement of carbon and intercalant balls, or the observation of x-ray (001) diffractions.

The results of the repeat distance I_c obtained from eq. (III.1) are compared in table III.2 with the measured I_c for the donor and accepter compounds in the present work.

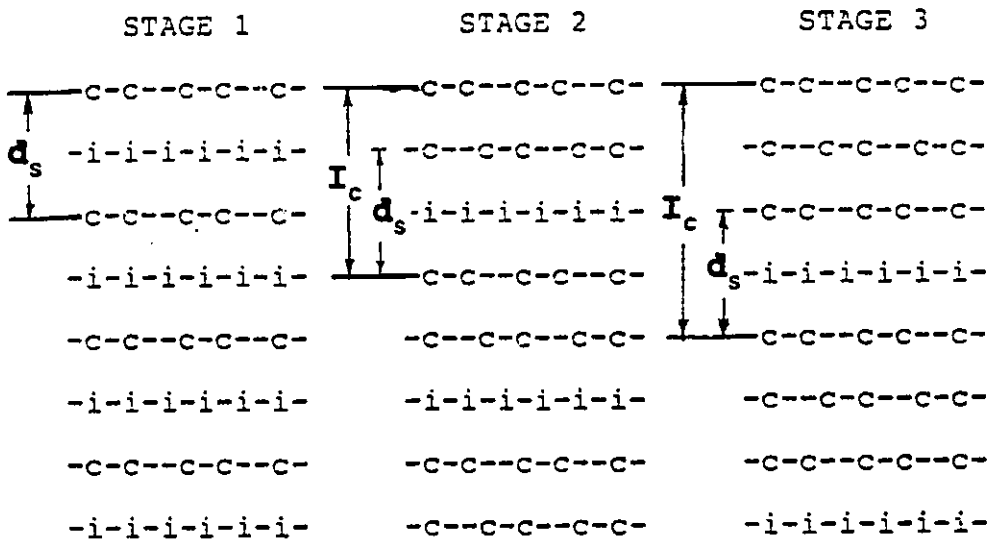

Figure III.6. Schematic diagram illustrating the relation $I_c=d_s+(n-1)c_o$.

Table III.2

Comparing of measured I_c with eq. III.1.

	n	d_s (Å)	I_c (Cal.)	I_c (Exp.)
C_8K	1	5.35	5.35	5.35
$C_{24}K$	2	5.38	8.73	8.67
$BiCl_3$	2	9.65	13.00	13.06
$HgCl_2$	3	9.75	16.45	16.40

The values of d_s in Table III.2 are taken from the work of Parry (1971) for C_8K, of Nixon and Parry (1968) for $C_{24}K$, of Behren et al (1988) for $BiCl_3$, and of Stumpp (1977) for $HgCl_2$. One can see that the measured values of I_c in the present work are close to the expected values of I_c from the stage formula (III.1) for each kind of compound. Therefore, well staged samples for each compounds were obtained for dHvA experiments.

The stage index of stage-3 SbF_5 was examined by the weight uptake method. The chemical composition $C_{27}SbF_5$ was obtained from the ratio:

$$M_g/M_c : \Delta M/M_{SbF5}$$

where M_g is the mass of HOPG before the intercalation. ΔM is the mass uptake after the intercalation. M_c is the atomic weight of carbon and M_{SbF5} is the molecular weight of the SbF_5

intercalant. The composition of $C_{27}SbF_5$ is consistent with the result of Wu et al(1981) for stage-3 SbF_5-GIC, which has the value of 15.10 Å for I_c.

III.4 The dHvA measurements

The de Haas-van Alphen effect (dHvA) results from quantum oscillations of the electronic magnetic moment. It is a very precise tool that is widely used to measure the size of a Fermi surface. It also gives other information about the Fermi surface. The major tool of this study of the electronic properties of the GIC is the dHvA effect. The introduction for the dHvA effect is given as follows, and the dHvA experimental apparatus are described as well.

III.4.1 The dHvA effect

When a magnetic field is present, the motion of an electron in the field is described by the Lorentz force equation

$$\hbar\dot{\boldsymbol{k}}=e(\boldsymbol{v}\times\boldsymbol{B}) \qquad \text{(III.2)}$$

where **k** is the wave vector, and **B** is the magnetic field vector. **v** is the electron velocity expressed by

$$v=\frac{1}{\hbar}\nabla_k E(k) \qquad \text{(III.3)}$$

When the orbit is a closed curve, the allowed states of the electron are obtained by using the Bohr-Sommerfeld quantization rule

$$\oint p\cdot d\gamma=2\pi\hbar(n+\gamma)=\oint(\hbar k-eA)\cdot d\gamma \qquad \text{(III.4)}$$

and become quantized, where **A** is the magnetic vector potential, n is an integer and γ is a phase factor. By using Stokes theorem, one gets:

$$\oint(\hbar k-eA)\cdot d\gamma=e\Phi \qquad \text{(III.5)}$$

where Φ is the flux through allowed orbits. Comparing eq.(III.5) with eq.(III.4), it can be shown that the flux becomes quantized too. Furthermore, by considering the relationship between real space and reciprocal space in scale, the reciprocal space areas of orbits are given by Onsager's condition

$$A_n=2\pi\frac{eB}{\hbar}(n+\gamma) \qquad \text{(III.6)}$$

which means that the area of allowed orbits in the plane normal to the magnetic field is quantized. In reciprocal space, the allowed states form tubes whose axes are parallel

to the magnetic field direction. These states are called Landau levels. The quantization of the allowed states leads to the quantization of the energy spectrum. The energy difference between two subsequent Landau levels is

$$\Delta E=\left(\frac{\partial A}{\partial E}\right)^{-1}\Delta A=eB\hbar\left(\frac{\hbar^2}{2\pi}\frac{\partial A}{\partial E}\right)^{-1} \qquad \text{(III.7)}$$

where

$$\frac{\hbar^2}{2\pi}\frac{\partial A}{\partial E}=m_c$$

The quantity m_c is called the cyclotron mass by analogy with the case for free electrons in a magnetic field.

The quantization of the energy spectrum leads to a periodic variation of the number of electrons at the Fermi energy as the magnetic field changes. The period of oscillation is determined by the condition that a Landau level is tangent to the Fermi surface which occurs whenever the area of an orbit A_n is equal to the extremal cross sectional area of the Fermi surface A_F. The frequency of the oscillation is given by

$$F=\frac{1}{\Delta(1/B)}=\frac{\hbar}{2\pi e}A_F \qquad \text{(III.8)}$$

and F is also called the dHvA frequency. According to this formula, one can imagine the shape of the Fermi surface by measuring dHvA frequencies with different angles between the

c-axis of the sample and the magnetic field direction.

The dHvA amplitude is proportional to $T/\sinh(bm_cT/Bm_o)$, (Lifshitz and Kosevich, 1956), where T is temperature, m_c is the cyclotron mass, B is the magnetic field, m_o is the free electron mass and b is a constant (14.69 TK^{-1}). Thus, the cyclotron mass can be determined by measuring the temperature dependence of the dHvA amplitude.

III.4.2 dHvA techniques

The dHvA measurements were performed with the low frequency field modulation technique. In this method, a sample was placed into a sample holder, the holder was put inside a set of coils which consisted of a modulation coil, a pick up coil and a balance coil. Fig. III.7 shows the set of coils used in the present work. The set of coils was placed inside a 5.5 Tesla superconducting solenoid. When doing the dHvA experiment, an alternating current with an audio frequency (about 50-150 mA and around 517 Hz in the present work) was fed to the modulation coil which produced modulation of the magnetic field. The signal which was proportional to the rate of change of the sample magnetization was detected by the pick-up coil placed around sample. The balance coil was connected antiparallel to the pick up coil to offset the steady component of the induced voltage.

All the measurements were done with the temperature below

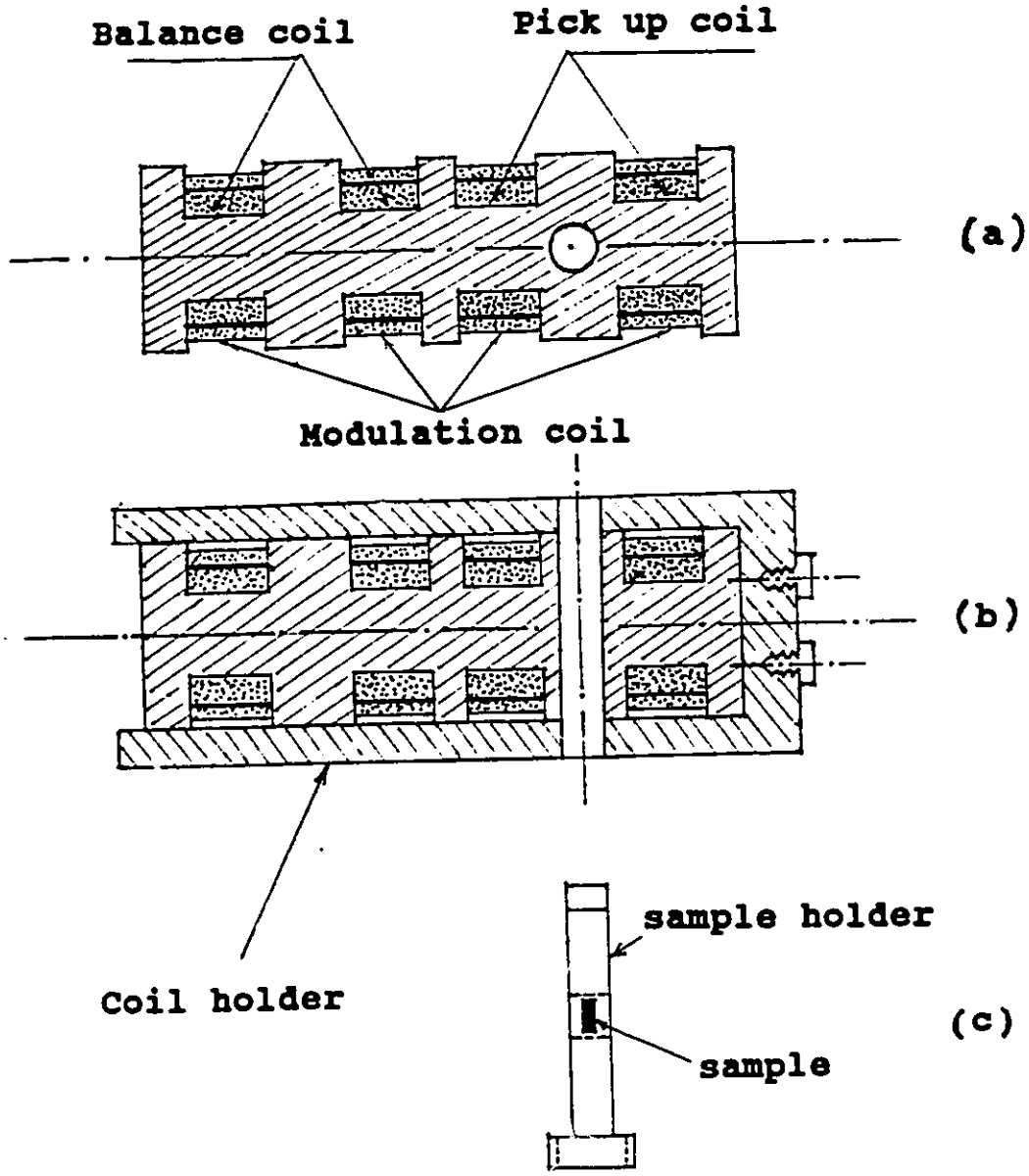

Figure III.7. (a) dHvA coil assembly and (b) holder (c) sample holder.

4.2 K. Fig. III.8 shows the cryogenic system in the experiment. Three dewars were assembled. The set of detecting coils with the sample inside was put in the inner dewar which was in the second dewar and in the center of the superconducting solenoid. Before cooling the system, the vacuum jackets of the three dewars were connected to a vacuum pump by opening the valves of 1, 2 and 3, as shown in Fig. III.8. Liquid-N_2 was transferred into the outer dewar through the line 4 to cool the system first. It usually took 4-6 days to cool it from room temperature to 77 K with a slow cooling rate. Liquid He was first transferred into the middle dewar slowly through line 5 to cool the magnet down. It took about 2 hours from 77 K to 4.2 K. After the magnet was cooled to 4.2 K, about 10 liters L-He was needed to fill the middle dewar to make sure that the magnet was covered with liquid He during about the 10 hours of the experiment. The inner dewar also had to be filled with liquid He through line 6 to keep the temperature of the sample below 4.2 K; usually it took a half hour to cool and about 3 liters liquid He to fill. After finishing the transfer of liquid He, all valves and lines were closed except the gas return lines which took the He gas boiled out from the dewars back to He-gas system. To obtain the temperature of the sample below 4.2 K, the pump which was connected to the gas return line of the inner dewar was used to reduce the pressure of the He gas in the inner dewar and meanwhile the temperature of the sample went down according to the phase diagram of liquid He.

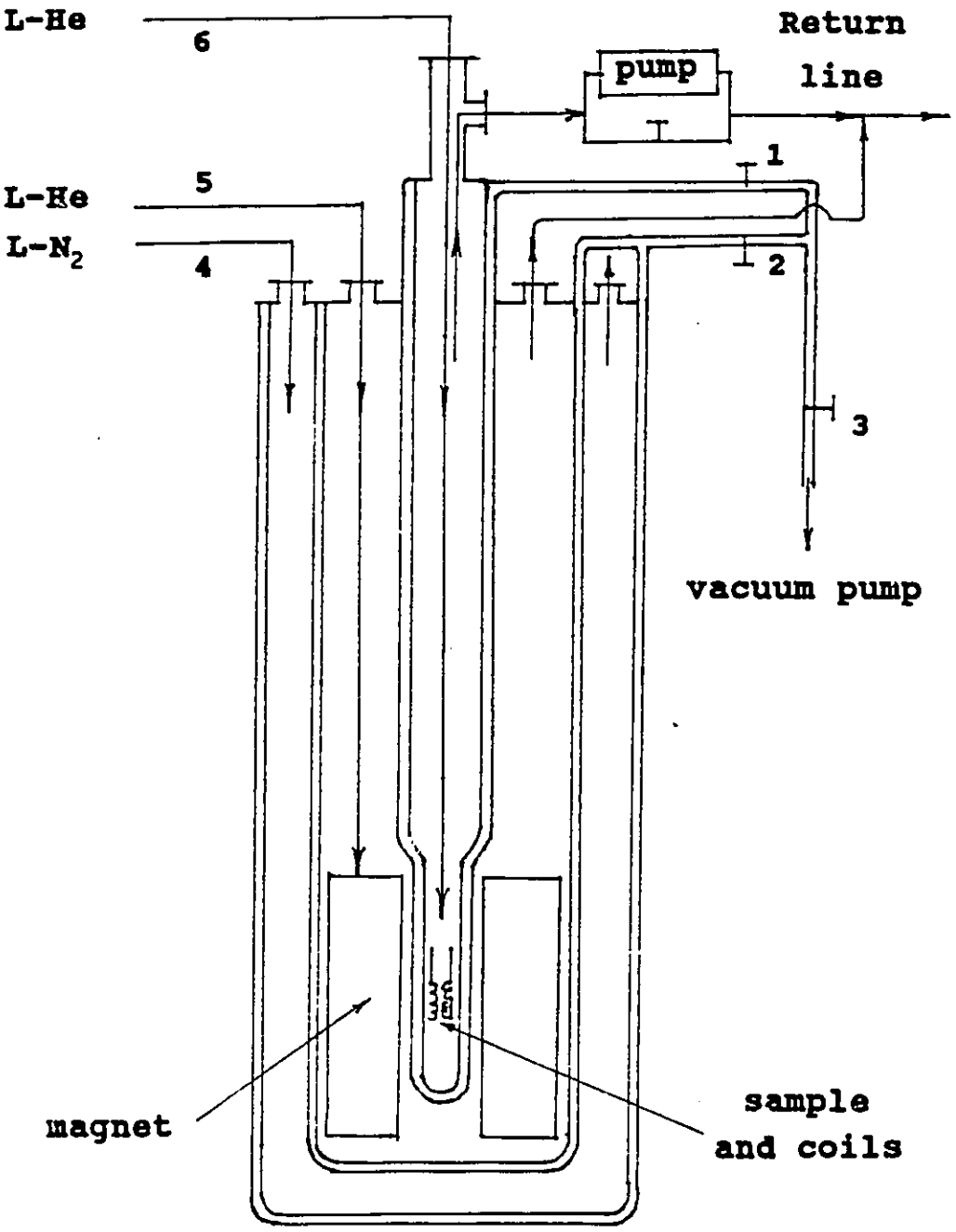

Figure III.8. Cryogenic system for dHvA experiment.

The pressure of liquid He in the inner dewar was measured with a high precision pressure meter.

Fig. III.9 shows a simplified block diagram of the detection system. Modulation current was supplied by a low distortion amplifier driven by a precision sine wave oscillator. The value of the magnetic field was obtained by measuring the current of the superconducting magnet. The signal from the pickup coil was fed into a lock-in amplifier set to operate at the second harmonic of the modulation frequency. The dHvA signal was measured at the output of the lock-in amplifier. The voltage for the signal amplitude and magnetic field were simultaneously recorded in a computer after which the Fourier transform was calculated. The output of the lock-in amplifier was also recorded on a chart which recorded the dHvA oscillations with magnetic field.

For measuring the temperature dependence, all the measurements were done with the c axis of the sample parallel to the direction of the magnetic field. The cyclotron mass value was determined from the temperature dependence of the dHvA amplitudes between 1.3 and 4.2 K. Two methods of measuring amplitudes were used in the experiments. In the case where one dominant oscillation was observed, the amplitudes were read off the recorder chart. The second method used was to fit the amplitude of oscillations to the small magnetic field range of the recorded data. The results of both methods were consistent within the limit of error.

For measuring the angular dependence, a toothed wheel was glued to the end of the sample holder to allow the rotation of the sample with a small screw at the end of a rod that extended to the top of the dewar. By rotating the sample holder, the angle between the magnetic field direction and the c axis of the sample was changed. Each quarter turn of rotation of the rod changed the sample position by 3 degrees.

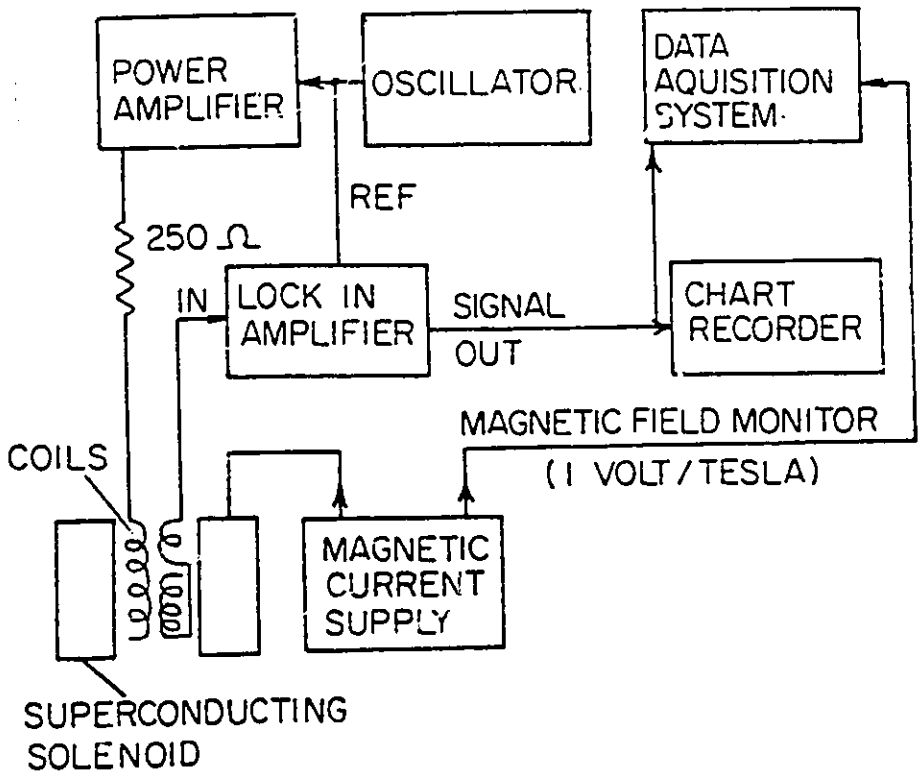

Figure III.9. Block diagram of the dHvA detecting system.

CHAPTER IV

DONOR-TYPE GIC

Graphite intercalation compounds (GIC) are classified into donor and acceptor types, depending on whether the graphite layers in the GIC acquire positive or negative charge, upon intercalation. The electronic properties and Fermi surface parameters of both donor and acceptor graphite intercalation compounds can be determined by the experimental techniques that involve the oscillatory Shubnikov-de Haas (SdH) effect of the magneto conductivity and the de Haas-van Alphen (dHvA) effect of the magnetic susceptibility. In these experiments, donor-GIC's cause much more experimental difficulties than acceptor-GIC's because they usually have larger Fermi surface (FS) pieces, heavier cyclotron masses and sample instability.

The potassium-graphite intercalation compounds are donor-type GICs because the electrons are transferred from the potassium atoms to the graphite layers. The present work is to investigate the electronic structures and the Fermi surfaces of both stage-1 and stage-2 potassium-graphite compounds from dHvA experiments by using a set of high sensitively detecting coils and well staged samples.

IV.1 Stage-1 C_8K

From the theories discussed in II.2.2, one can see that there are three questions about the 3D F.S. and the charge transfer in C_8K to be answered by definitive experiments.

A very definitive experiment for providing unambiguous answers to the first two questions uses the de Haas-van Alphen (dHvA) effect. This is because the frequency of the dHvA oscillations directly measures the FS cross section, the angular-dependence of the dHvA frequency gives insight into the actual shape (3D or 2D) of the FS and the dHvA frequencies are related to the charge transfer. In addition, the temperature dependence of the dHvA amplitude directly determines the electron effective mass which is related to the energy bands. However, dHvA experiments in C_8K are very difficult because of the high effective mass of the electrons (Wang et al, 1988), imperfection in the samples (Higuchi et al, 1980) and other effects (Dresselhaus, 1988). In 1980, Higuchi et al (1980) reported a single dHvA frequency, 2870 T, in C_8K for $\mathbf{H} \| \mathbf{c}$, and in 1988 Wang et al (1988) observed a strong dHvA frequency, 3070 T, in C_8K for $\mathbf{H} \| \mathbf{c}$. The reason for the discrepancy between the two reported frequencies was not clear since they were probably from the same piece of Fermi surface. Also, the angular-dependence of the dHvA frequencies is needed to determine whether the frequency is from a 2D FS or a 3D FS.

This section presents the results of the investigation by the dHvA effect of the FS, charge transfer and the angular dependence for C_8K. The experimental data are compared with the theoretical models, the Fermi surface is constructed and the charge transfer is derived based on the dHvA data.

IV.1.1 dHvA results and analysis

The dHvA signal was detected at temperatures below 2.4 K and magnetic fields above 3.2 T. Fig. IV.1 shows a typical trace of the dHvA oscillations in C_8K which was obtained at T=2.2K and with fields from 5.1 T to 5.6 T with the c-axis of the sample parallel to the direction of the magnetic field ($\mathbf{H} \| \mathbf{c}$).

Fig. IV.2 shows the Fourier transform spectrum of the data taken from 4.9 T to 5.1 T at T=1.4 K, also with $\mathbf{H} \| \mathbf{c}$. One can see that there are two frequencies in this spectrum. The stronger one is 3126 T and the second one is 4250 T. The frequencies are reproducible from sample to sample. Totally five C_8K samples were measured. The first frequency changes between 3070 T and 3126 T, depending on the range of the magnetic field chosen to take the data. The second frequency only appears at temperatures below 1.7 K.

The cyclotron masses corresponding to the two frequencies were determined from the temperature dependence of the dHvA amplitudes between 1.3 K and 2.2 K with $\mathbf{H} \| \mathbf{c}$. Fig. IV.3 shows

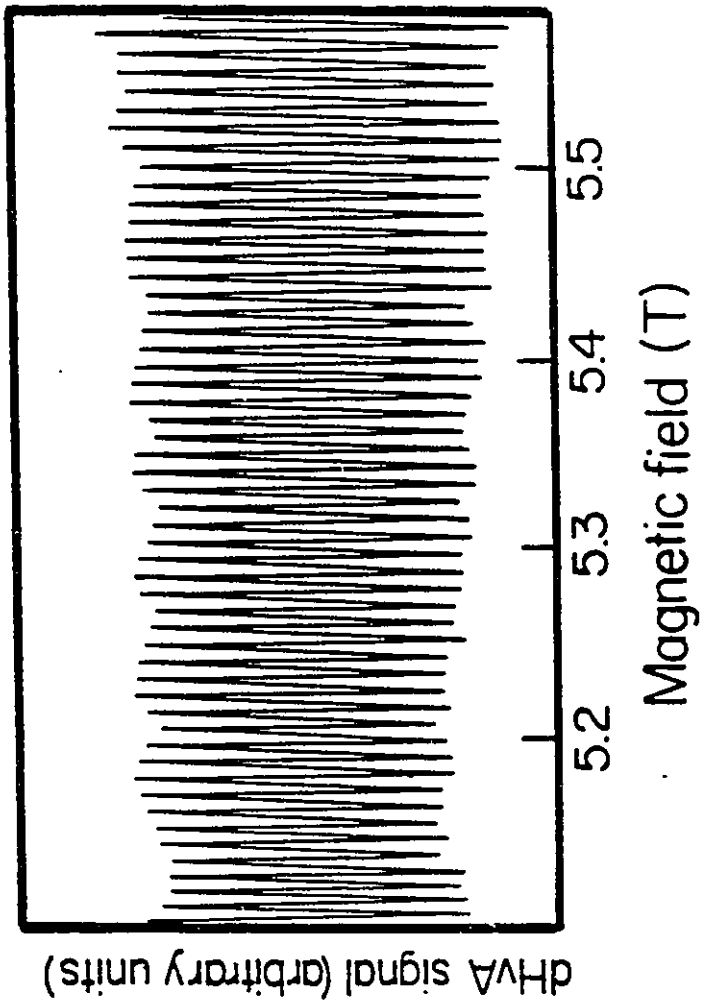

Figure IV.1. de Haas-van Alphen oscillations of stage-1 potassium graphite intercalated compound.

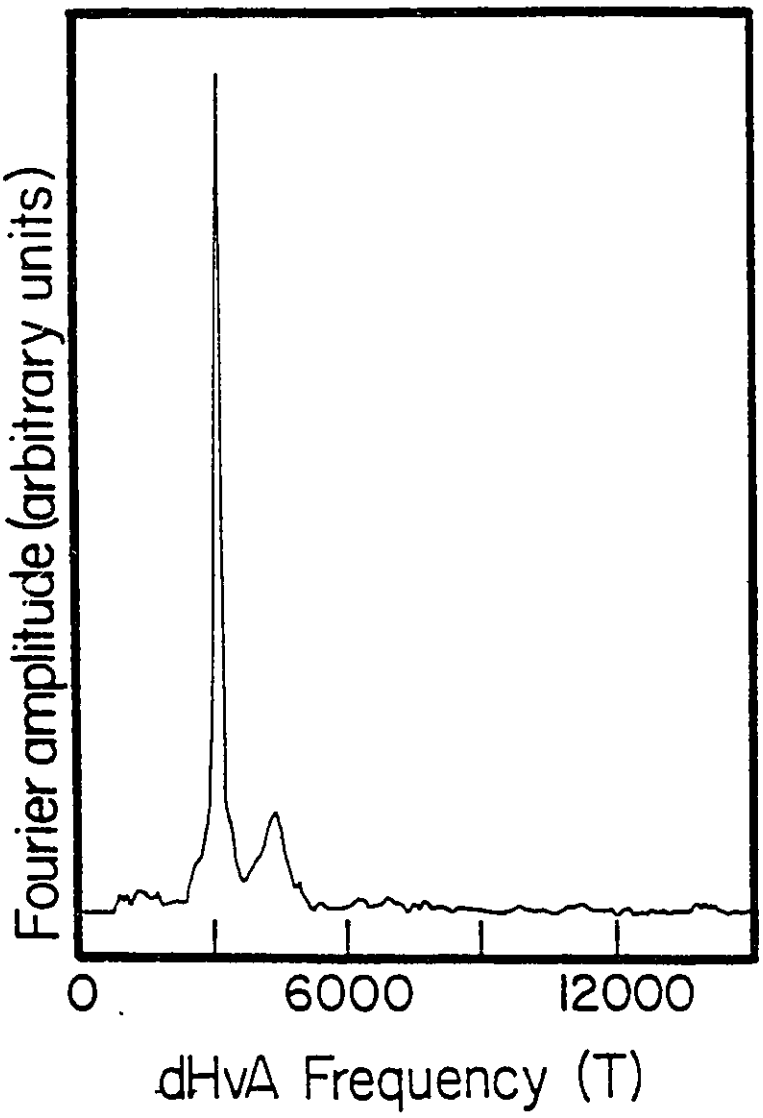

Figure IV.2 Fourier transform of the dHvA signal of stage-1 K-graphite.

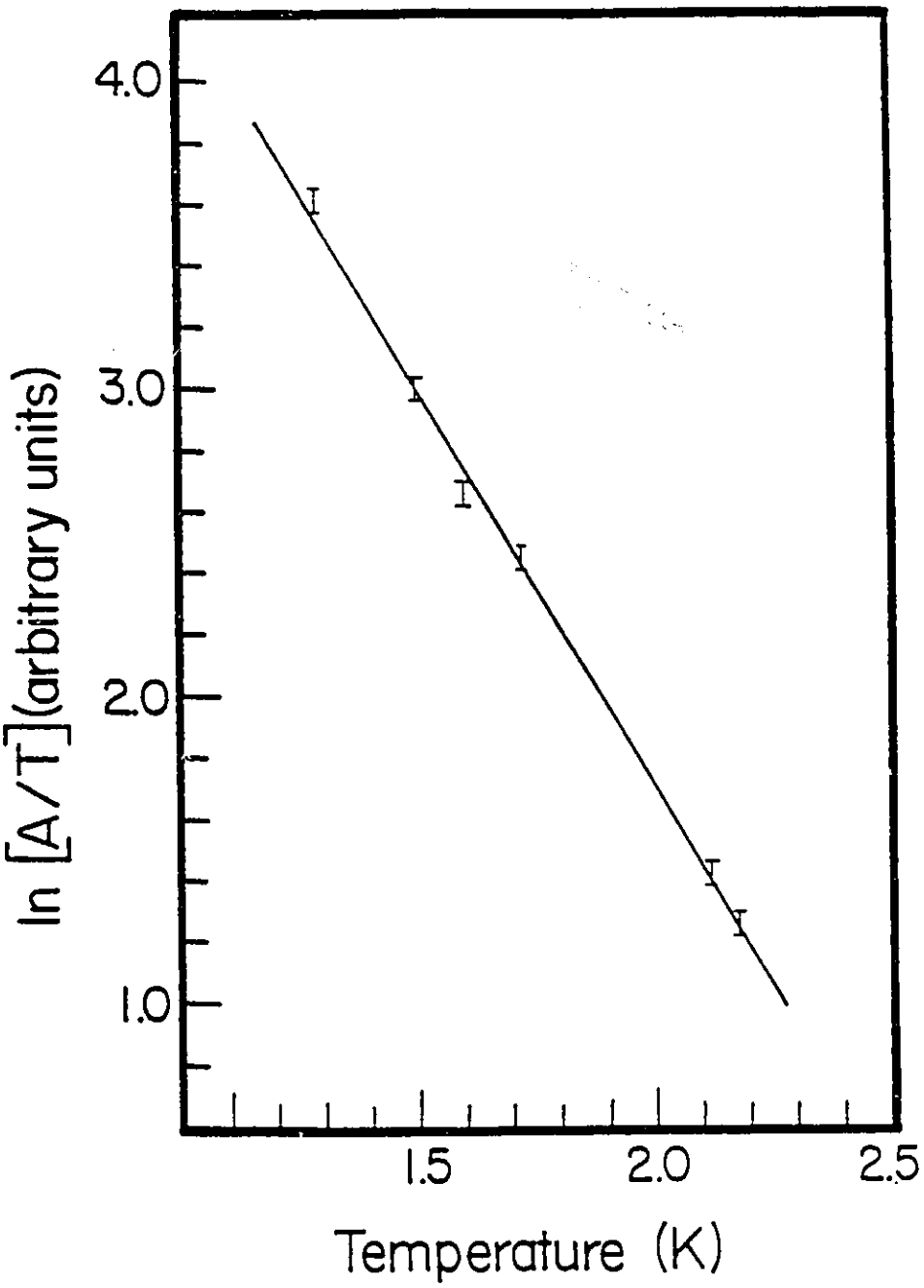

Figure IV.3. Temperature dependence of A/T, where A is the amplitude of the 3126 T oscillation of C_8K. The data are fitted to $A \propto T/\sinh(bm_cT/Bm_0)$ (solid line).

a plot of ln(A/T) verses T for the first frequency, where A is the dHvA amplitude at temperature T. The results are $m_1^*=0.86$ m_0 and $m_2^*=0.92$ m_0. The high value of the effective masses is one of the factors which make it very difficult to detect the dHvA signal.

In order to investigate the actual shape of the FS for this compound, the angular dependence of the dHvA frequency was measured from $\theta=0^0$ to $\theta=-21^0$ for one side and $\theta=0^0$ to $\theta=90^0$ for the other side of the c-axis. Here θ is the angle between the direction of the magnetic field and the c-axis of the sample. The data were measured at 3^0 intervals. Fig. IV.4 shows the experimental results and the theoretical predictions for the first frequency as a function of the angle θ. The solid curve represents the prediction for a 2D straight cylinder of the FS given by $f_\theta = f_0 /\cos\theta$, where f is the dHvA frequency. The dashed line parallel to the axis of the field direction represents the prediction for a 3D spherical FS given by $f_\theta = f_0$. The circles are the experimental data. One can see, from Fig.IV.4, that the first dHvA frequency follows a 3D spherical behavior very well for angles up to 18^0 for both sides of the c-axis. Therefore, the existence of the 3D FS in C_8K is proven experimentally.

The amplitude of the dHvA frequency decreased dramatically with increasing θ, as shown in Fig. IV.5 and the dHvA signal disappeared after $\theta=21^0$. This limited the angular dependence measurements of the frequency to the region $\theta <$

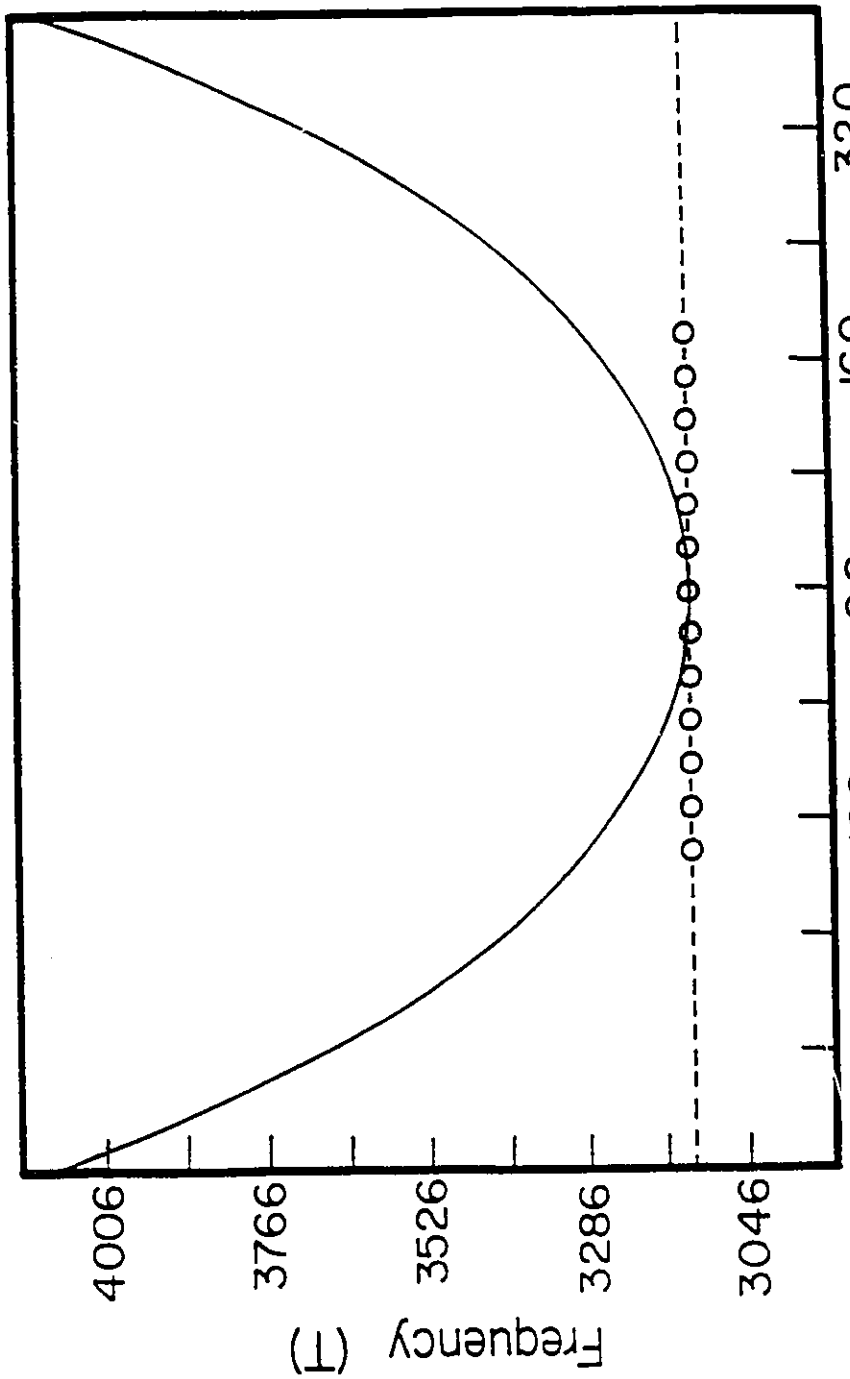

Figure IV.4. dHvA frequency 3126 T as a function of magnetic field direction from the c-axis of stage-1 K-graphite. The solid line is cylindrical fit, and the dashed line is spherical fit.

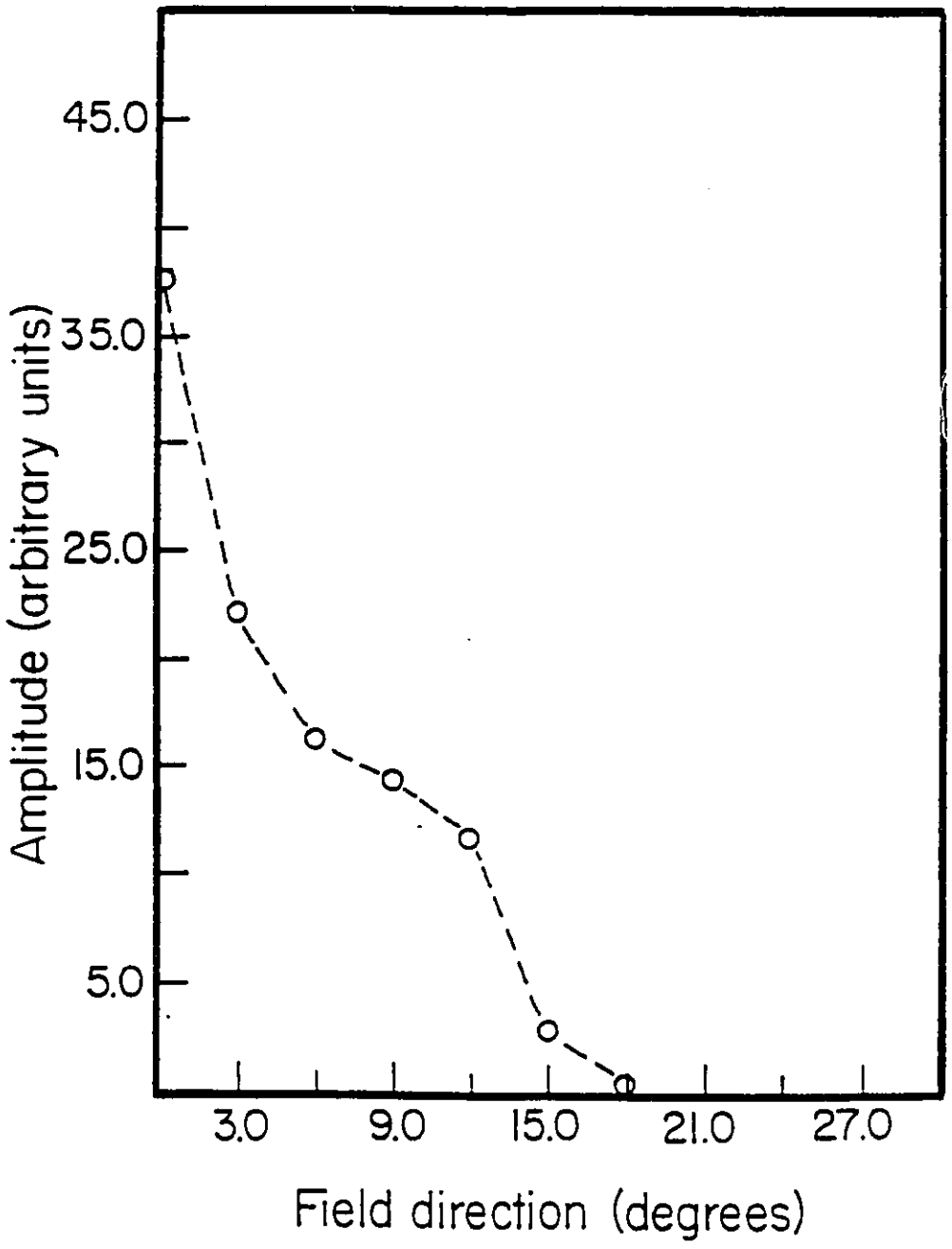

Figure IV.5. The dHvA amplitude decreases with the angle between the magnetic field and c-axis of the C_8K sample.

21^0.

The decrease of the dHvA amplitude with angle occurs in many other GICs but with different rates and different maximum angles at which the dHvA signal disappears. The maximum angle is stage dependent: it increases with stage index. For instance, it is greater than 70^0 for pure graphite (Higuchi et al, 1980), 57^0 and 61^0 for stage-3 SbF_5 (Wang et al, 1991), and $SbCl_5$ (Wang et al, 1988), respectively, 30^0 for stage-2 $BiCl_3$ (Chapter V of this thesis), and only 21^0 for stage-1 C_8K. Therefore, it is reasonable to expect that, in addition to the increasing of the cross-section area with angle, the electron-carbon and the electron-intercalant scattering also limits the electron orbits with increasing θ, especially for the 3D FS in C_8K which has no change in cross-sectional area with angle.

The second dHvA frequency 4250 T, is considered to be from the major 2D FS in C_8K because a 2D behavior is expected for one Fermi surface piece as in other GICs. This frequency is very weak even at $\theta=0^0$ due to the high value of the cyclotron mass. It disappears when the angle is changed from $\theta=0^0$ to $\theta=3^0$.

IV.1.2 Discussion and calculation

Based on the dHvA experimental results, the comparison of all the theoretical models for C_8K with the experimental data are made in this section. Both the 3D and 2D FS are

constructed in the Brillouin zone and the charge transfer coefficient is derived from the Fermi structure and the dHvA experimental data.

IV.1.2.1 The Fermi surface

In principle, it seems that the experimental proof for the existence of both 3D and 2D FS pieces in C_8K supports all models which predict both a 3D and 2D FS for C_8K. However, different models have different discrepancies from the experimental results. The comparison of the dHvA results with each theoretical model is made as follows.

A. ONK and rONK models

The model ONK and rONK predict a rather spherical 3D FS centered at the center of the BZ for the lower band and at the top center of the BZ for the upper band, in addition to the triangular prismatic 2D FS sections along the zone edges which have nearly equal sizes for the upper and lower bands. The 3D FS and the 2D FS are separated by a small amount. This prediction for the FS in C_8K is in agreement with the experimental results qualitatively except for the following two aspects.

Firstly, two additional smaller extremal cross-section areas are predicted at the hexagonal BZ planes for the upper

and lower bands. Therefore there should be four dHvA frequencies appearing in C_8K, according to the model. However, only two dVHA frequencies were observed. One may say that the two experimental frequencies could be from the two smaller areas and the two larger areas were missed due to the difficulties of the experiments. However, the answer is clear when the high values of the experimental frequencies and the fixed size of the BZ are considered. Moreover, the smaller areas should be observed more easily than the larger areas, but they did not show up. It therefore seems that the two smaller FS areas in C_8K do not exist.

Secondly, in the theory, the calculated dHvA frequency from the 2D triangular FS is 3030 T (Higuchi et al, 1980). Compared with the experimental value of 4250 T, the difference can not be ignored.

Although differences between the experiment and the theory do exist, the main results are consistent. In fact, the band structure of the ONK model can be changed by adjusting parameters to fit the experimental data. Therefore, the experiment actually gives qualitative support for the band calculations of ONK and rONK model.

B. MHN model

MHN's model also predicts both 3D FS and 2D FS parts for C_8K with the energy bands similar to these of the ONK model.

But the shape of the 3D FS from both the lower and upper conduction bands is a convex cylinder in the center of the BZ instead of a rather spherical FS as predicted by ONK or a quite spherical FS as observed in the experiment. So, in this theory, not only the number of the dHvA frequency but also the shape of the 3D FS are contrary to the experimental results. However, the correct prediction for the existence of both the 3D FS and 2D FS indicates that this theory is partly supported by this experiment.

C. DR and TR models

In the DR model, the Fermi surface of C_8K contains only cylindrical parts with at most a very small isolated pocket at the center of BZ. There is no 3D Fermi surface appearing in C_8K. The dHvA frequency corresponding to the cross-section of the 2D cylindrical parts for both upper and lower bands are 4700 T and 3700 T, respectively. These calculation values are close to the 2D dHvA frequency, 4250 T, observed from the experiment. Therefore, although this theory failed to predict the existence of the 3D FS, the calculation for the 2D FS is in good agreement with the experimental results.

In the TR model, there also exist both 3D and 2D FS pieces. However, the cross-section of the 3D FS is smaller than that of the 2D FS and, in particular, shrinks to zero at the top face of the BZ. According to this model, there should

be just two dHvA frequencies in C_8K, and the frequency from the 3D FS should be smaller than the one from the 2D FS. This prediction is in agreement with the experimental results and is supported by the experiment.

IV.1.2.2 The charge transfer

The charge transfer is obtained from the dHvA data in the following way. The number of carriers per unit cell is equal to $2V_F/V_B$, where V_F is the total volume of reciprocal space enclosed by the FS, V_B is the volume of the BZ. The factor of 2 comes from the spin degeneracy.

The total charge per carbon atom, x, is equal to the ratio of $2V_F/V_B$ divided by m, the number of carbon atoms in the unit cell of the compound, that is

$$x = 2V_F/(V_B m) \quad . \qquad \text{(IV.1)}$$

The volume V_F is related directly to the extremal Fermi surface area A_F which is perpendicular to the k_z direction and

$$A_F = (2\pi e/\hbar)F \qquad \text{(IV.2)}$$

where F is the dHvA frequency. Thus, the dHvA effect is connected with the charge transfer.

The crystal structure of C_8K has a $P(2x2)R0^0$ in-plane superlattice (Rudoff and Schulze, 1954), as Fig. IV.6 (a)

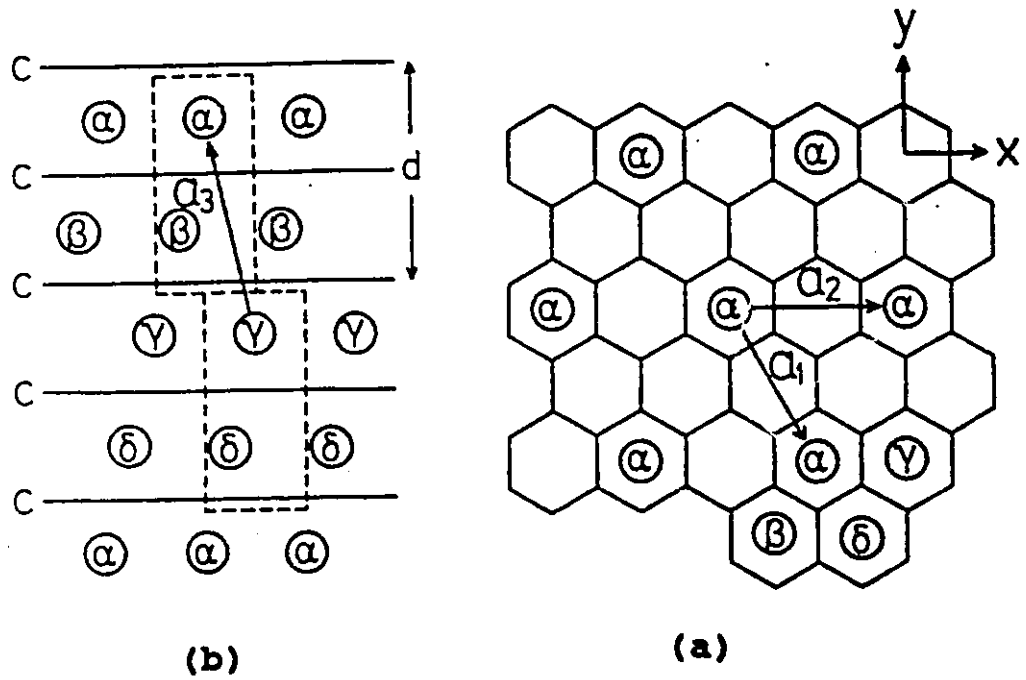

Figure IV.6. The crystal structure of C_8K as seen from above (a) and as seen from side (b). Here α, β, γ and δ denote potassium atoms in non-equivalent staggered layers. The in-plane structure of these metal sheets is the same (from Inoshita et al, 1977).

shows. The layer stacking sequence is $c\alpha c\beta c\gamma c\delta c\alpha...$, where c denotes a carbon layer, and α, β, γ, δ stand for potassium layers (Rudoff, 1959) as shown in Fig. IV.6(b). In each metal sheet, potassium atoms form a two-dimensional triangular lattice with a side of 4.91 Å. The in-plane structure of the carbon layer remains the same as a hexagonal net with a nearest neighbor carbon-carbon distance of 1.42 Å, while the distance between adjacent carbon layers increases from 3.35 to 5.35 Å upon intercalation.

The planar unit cell for the C_8K compound is four times larger in area than the graphite unit cell, so that the corresponding planar unit cell for the compound in reciprocal space is one-fourth as large as that for graphite. The length of the BZ edge k_B, as shown in Fig. IV.7(a), is one half of that in graphite, i. e. $k_B=(4\pi/3a)/2= 0.85$ Å^{-1}, where a = 2.46 Å is the length of the primitive lattice translation vector in graphite.

According to eq. (IV.2) and the observed dHvA frequencies F1=3126 T and F2 = 4250 T, the Fermi radii of the Fermi surface with the approximation of a circular cross-section are $k_{F1}=0.31$ Å^{-1} and $k_{F2}=0.36$ Å^{-1}. Both the 3D and 2D FS are constructed in the Brillouin zone plane at $k_z = 0$ as shown in Fig. IV.7(a). One can see that in the k_x-k_y plane at $k_z =0$ $2k_{F2}$ is less than k_B along the line from corner to corner, and $k_{F1}+k_{F2}$ is less than k_B along the line from the corner to the center of the BZ. Thus, the 3D FS is well separated from the

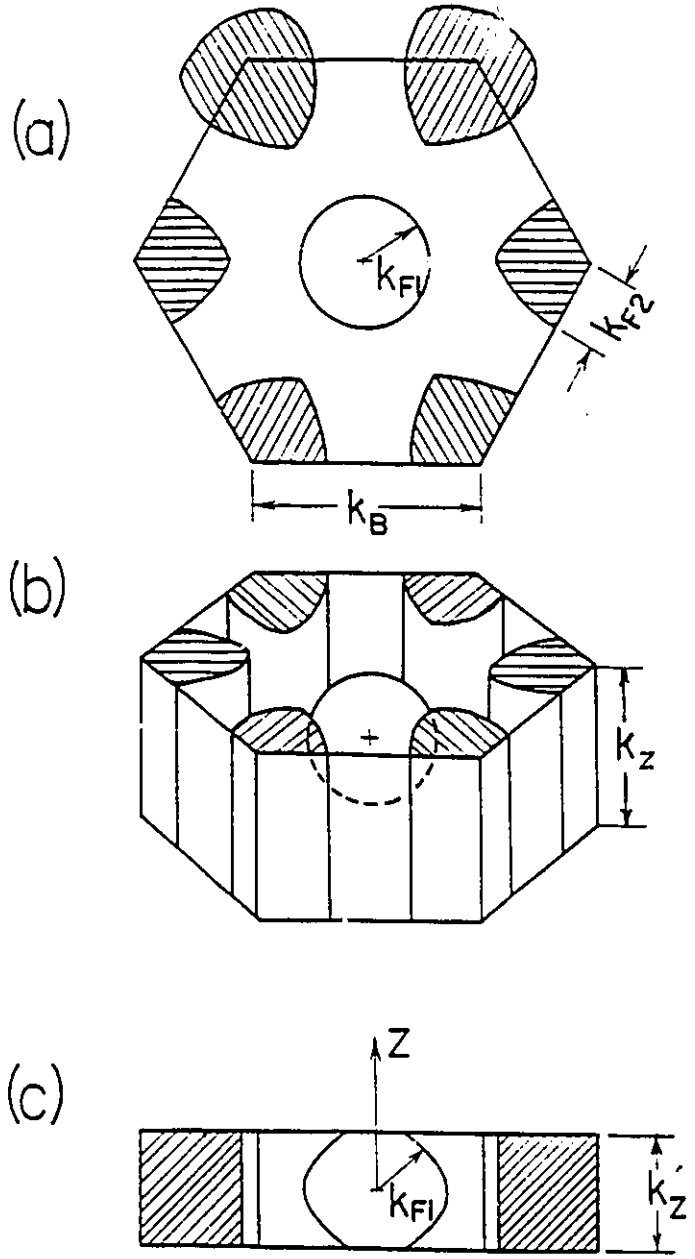

Figure IV.7. (a) The horizontal cross section of the Fermi surfaces of C_8K at $k_z = 0$.
(b) The sketch of the Fermi surfaces of C_8K for $I_c = 5.35$ Å.
(c) The perpendicular cross section of the Fermi surfaces of C_8K for $I_c' = 10.7$ Å.

2D FS and the charge transfer can be calculated easily.

The volume of the BZ of C_8K is given by

$$V_B = 4\pi^3/(a^2 I_c/3) \qquad \text{(IV.3)}$$

where I_c is the c-axis component of the unit cell, or c-axis repeat distance for C_8K. Because the I_c was chosen in different ways by different models, the charge transfer has to be calculated for each case.

For the unit cell which contains one potassium atom and eight carbon atoms, as chosen by TR, the I_c is equal to 5.35 Å. It is the distance between the adjacent carbon layers.

Therefore, $k_z=2\pi/I_c$ is 1.1744 $Å^{-1}$. The 3D FS is totally inside the BZ, because $2k_{F1}$ = 0.62 $Å^{-1}$ is less than k_z. When the approximation of a perfect spherical 3D FS as shown in Fig. IV.7(b) is applied, the total volume enclosed by the 3D and 2D FS in the Brillouin zone is

$$V_F = 4\pi k_{F1}^3/3 + 2(A_{F2}2\pi/I_c) \qquad \text{(IV.4)}$$

Combining eqs. (IV.1)-(IV.4), the charge per carbon atom x in the unit cell with eight carbon atoms is x=0.1215. Thus the charge per potassium atom is 0.972.

For a unit cell which contains two potassium atoms and 16 carbon atoms, as chosen by ONK, the I_c' is twice the distance between the adjacent carbon layers, that is 10.70 Å. In this

case, $2k_{F1}$ is a little larger than $k_z' = 0.5872$ Å^{-1}. So, the top and bottom of the 3D FS are cut a little by the BZ planes, as shown in Fig. IV.7(c). Therefore, the volume of the 3D FS is

$$V_{F1}=2\int_0^{k_z'/2}\pi\,(k_{F1}^2-Z^2)\,dZ \qquad \text{(IV.5)}$$

and the volume of the 2D FS is

$$V_{F2} = 2\ (A_{F2}4\pi/I_c') \qquad \text{(IV.6)}$$

The factor of 2 in eq. (IV.6) comes from the fact that the energy band of the 2D FS is doubly degenerated for this unit cell (Inoshita et al, 1977).

For the total volume $V_F' = V_{F1}+V_{F2}$, the charge per carbon atom with this unit cell is $x'=0.121$ and the charge per potassium atom is 0.968.

Comparing the values of the charge transfer from the two kinds of unit cells, one can see that there is no difference between them and the charge transfer is almost unity. This result for the charge transfer is consistent with many other experiments. The recent measurement for the near-edge photo absorption spectra by Loupias et al. (1990) gives the charge transfer to be 0.85. From the same experiments done in 1988, Loupias et al (1988) concluded that the charge transfer in C_8K is nearly total. Other experiments, electron-energy-loss

spectra (Ritsko and Brucker, 1982), x-ray photoelectron spectroscopy (Preil and Fischer, 1984), and soft-x-ray emission spectroscopy (SXES) carbon K emission band measurements (Mansour et al, 1987) also imply a complete charge transfer for C_8K.

The nearly complete charge transfer in C_8K means that there is full ionization of the potassium atoms and an almost empty potassium band exist. Therefore, the theory which has the 3D FS from the K 4s band is not acceptable by the present experiment. The models which predict incomplete charge transfer are also not consistent with the experimental results. Both the revised ONK and TR descriptions agree with the unit charge transfer and on the graphite origin of the 3D FS. They are supported by the dHvA experimental work. But the difference between the two models, that is whether the character of the 3D FS is from interlayer bands or graphite π band, can not be clarified by the dHvA effect.

IV.1.3 Conclusions for C_8K

The dHvA experiments for C_8K shows two dHvA frequencies, 3126 T and 4250 T, with the magnetic field parallel to the c-axis. The effective masses corresponding to the two frequencies obtained from the temperature dependence of the dHvA amplitude are 0.86 m_0 and 0.92 m_0, respectively. The angular dependence of the dHvA frequency shows that there

exist both 3D FS and 2D FS sections in C_8K. The 3D FS, which has the cross sectional area corresponding to 3126 T, is spherical for the field within $\pm 18^0$ of the c-axis. The Fermi structure constructed from the experimental data are reasonable with respect to the size of the BZ. The charge transfer per potassium atom is measured directly by the dHvA frequencies. It is 0.97 for the different unit cells chosen by the different models. This value of the charge transfer is consistent with many other experiments results. The almost complete charge transfer implies that the K 4s band is almost empty and the 3D FS does not arise from the K 4s band. By comparing the experimental results with the predictions of each theoretical model, the TR model is supported completely by the experiment. The revised ONK model is basically supported and could be supported strongly by the dHvA experiment if the sizes of the Fermi surfaces, especially the 3D FS, could be adjusted to fit the experimental data.

IV.2 Stage-2 $C_{24}K$ GIC

The first SdH measurement in $C_{24}K$ was done by Dresselhaus et al (1980). They found five SdH frequencies in $C_{24}K$. The dominant frequency is about 150 T, others range from 133 T to 439 T. No higher frequencies were reported.

Since the charge transfer in $C_{24}K$ has been estimated to be nearly complete from the experiments of the specific heat

(Mizutani et al, 1978; Dresselhaus and Dresselhaus, 1981) and the Knight shift of ^{13}C nuclear magnetic resonance (NMR) line (Conard et al, 1980; Dresselhaus and Dresselhaus, 1981), one expects that larger pieces of the FS should exist in $C_{24}K$. The absence of a high-frequency orbit in the SdH measurements may be due to the experimental difficulties with the donor-GIC's. The purpose of this work was to measure all the dHvA frequencies and to investigate the electronic structure as well as the charge transfer in $C_{24}K$.

IV.2.1 Experimental results

The dHvA signal in stage-2 $C_{24}K$ obtained at a temperature 4.2 K is shown in Fig.IV.8. The Fourier-transform of the oscillation from 1.55 T to 3.25 T gives only one dHvA frequency, 286 T, as shown in Fig.IV.9. This frequency is the same as one of the SdH frequencies, 282 T, observed by Dresselhaus et al (1980).

When the temperature was decreased to 1.4 K, the dHvA signal became much stronger and different. Fig.IV.10 is the part of the dHvA oscillation obtained at 1.4 K from 4.50 T to 5.41 T. This oscillation shows that there is more than one dHvA frequency. From the Fourier transform, as shown in Fig. IV.11, one can see two dominant dHvA frequencies in this spectrum, one is the low frequency 286 T, another one is 2570 T. These measurements were repeated two weeks later, and all

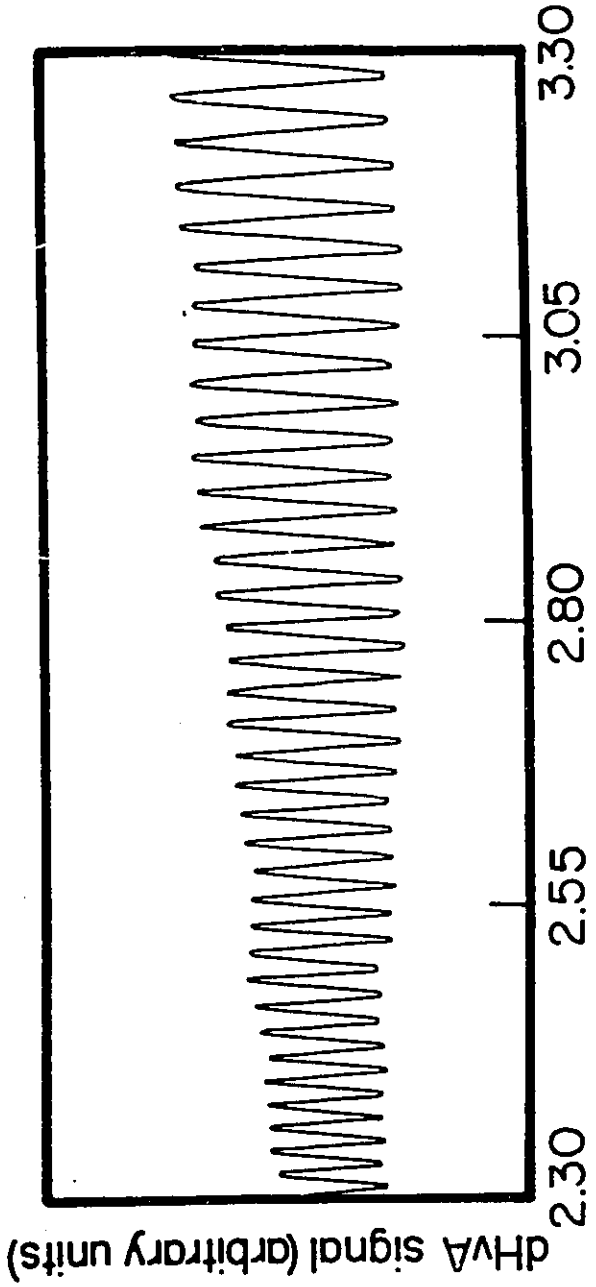

Figure IV.8. de Haas-van Alphen oscillations of stage-2 K-GIC at 4.2 K.

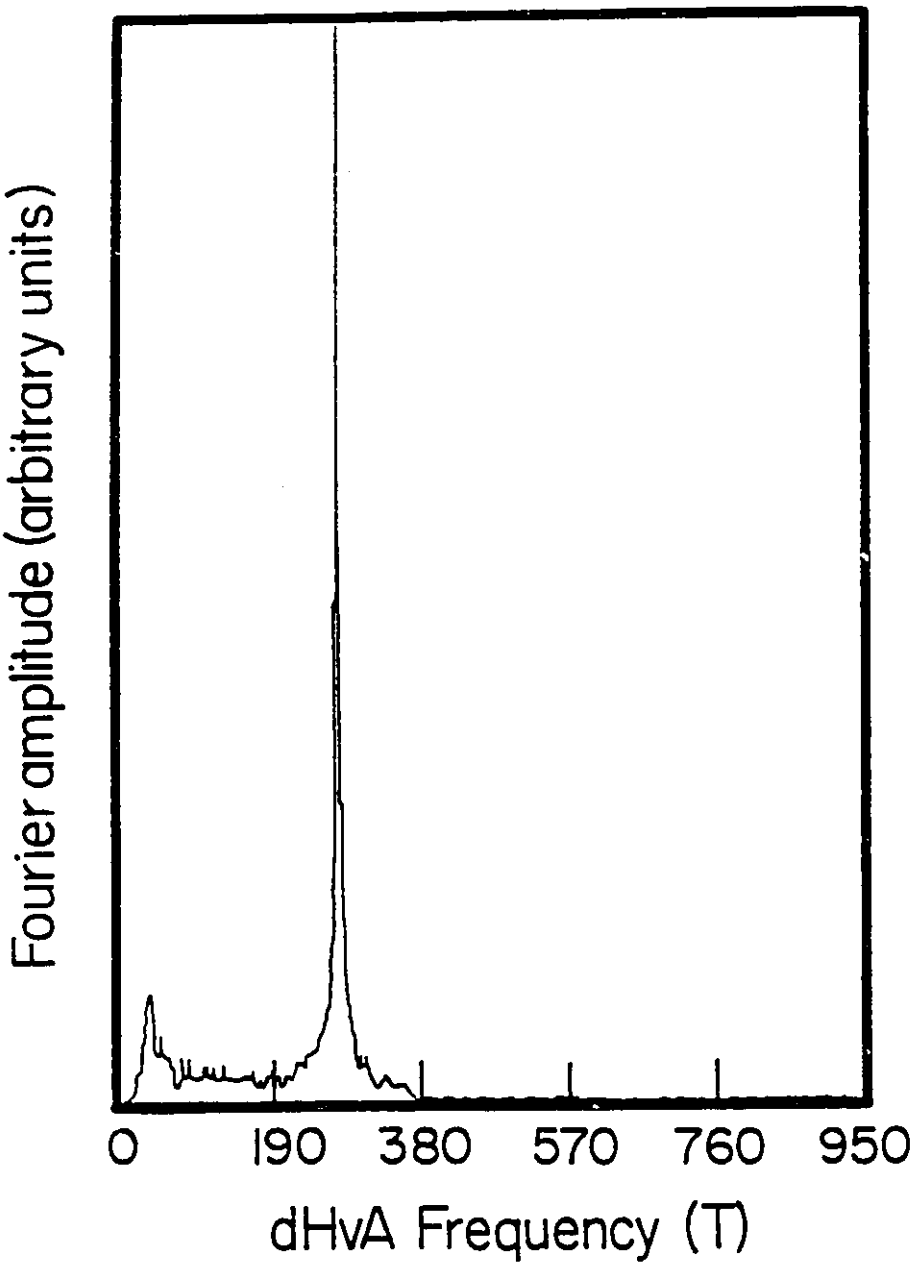

Figure IV.9. Fourier transform of the de Haas-van Alphen oscillations in $C_{24}K$ from 1.55 T to 3.25 T at 4.2 K.

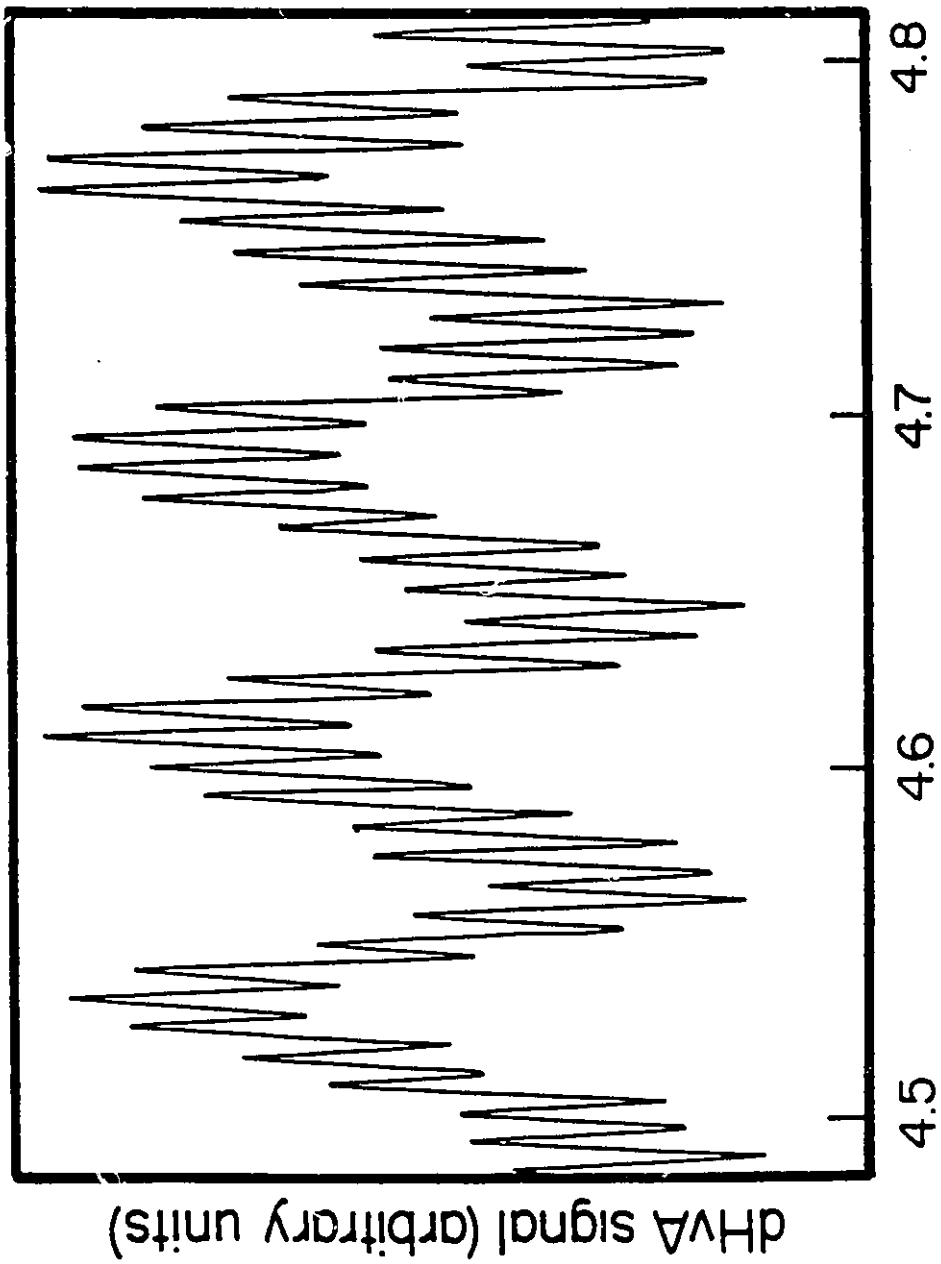

Figure IV.10. de Haas-van Alphen oscillations of stage-2 K-GIC at 1.4 K.

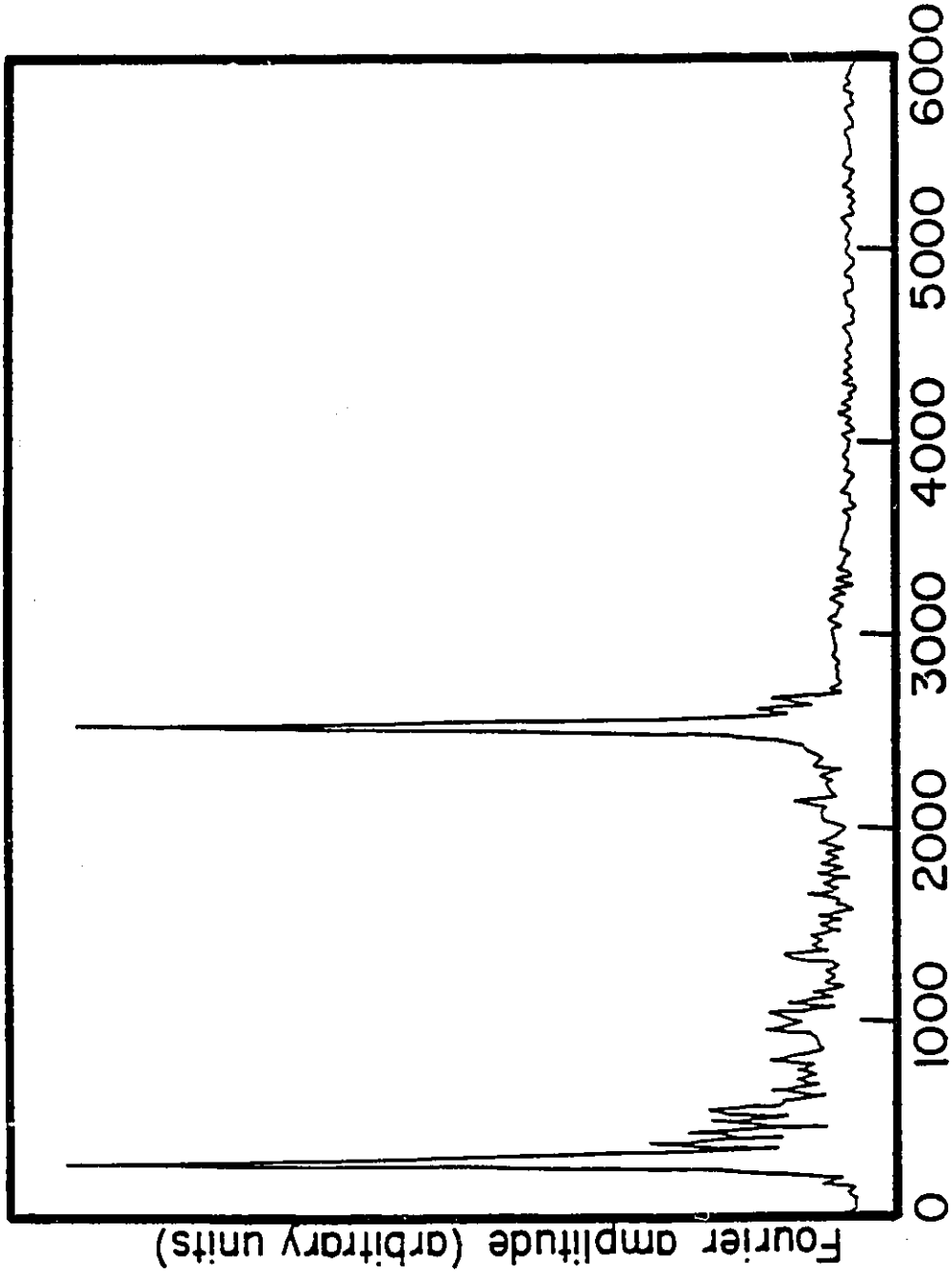

Figure IV.11. Fourier transform of the de Haas-van Alphen oscillations in $C_{24}K$ from 4.5 T to 5.41 T at 1.4 K.

results were reproducible. For different ranges of magnetic field chosen to take data, the low frequency was between 270 T and 286 T, and the high frequency was between 2540 T and 2570 T.

IV.2.2 Calculation and discussion

The theoretical band model proposed by Blinowski et al. (1980) discussed in Chapter II is used to analyze the dHvA experimental data. This model has been used to explain successfully the reflectance data in $C_{24}K$ below the threshold for interband absorption involving the K (4s) states and the charge transfer to the carbon band is about one electron per K atom (Eklund et al, 1986; Doll et al, 1987; Zhang and Eklund, 1987). It also explains the optical density for $C_{24}K$ reasonably well below the inter π-band absorption threshold (Zhang and Eklund, 1987). Therefore, this model is expected to provide a good description of the band structure of $C_{24}K$.

Another theoretical calculation for the band structure of $C_{24}K$ by Yang and Eklund (YE) (1988) is based on the phenomenological 2D tight binding model of Saito and Kamimura (1985). The calculated dHvA frequencies from this band structure are 1399 T and 1820 T. These theoretical values will be compared with the experimental results in this section.

In addition, the charge transfer per potassium atom is determined from both the experimental results and Blinowski's

model.

IV.2.2.1 The band structure

As presented in Chapter II, Blinowski's model predicts two valence-conduction pairs of bands for a stage-2 compound. The electron dispersion (i.e., the band equation) is assumed to be independent of the intercalated species and the number of electrons transferred to or from the graphite. The band parameters in this model can be adjusted for different intercalated species, and the Fermi level depends on the number of electrons when the band parameters are fixed.

For a stage-2 donor-GIC, the two conduction bands are given as

$$E_1^C = [(\gamma_1^2 + 3\gamma_0^2 a^2 k^2)^{1/2} - \gamma_1]/2 \qquad \text{(IV.7a)}$$

$$E_2^C = [(\gamma_1^2 + 3\gamma_0^2 a^2 k^2)^{1/2} + \gamma_1]/2 \qquad \text{(IV.7b)}$$

where k is the wavevector measured from the corner of the Brillouin zone. γ_0 is the in-plane nearest-neighbor interaction and γ_1 is the interaction energy of nearest atoms between two adjacent layers. The Fermi areas of the bands are given by

$$A_{F1} = 4\pi(E^2 - E\gamma_1)(3\gamma_0^2 a^2)^{-1} \qquad \text{(IV.8a)}$$

$$A_{F2} = 4\pi(E^2 + E\gamma_1)(3\gamma_0^2 a^2)^{-1} \qquad \text{(IV.8b)}$$

The model is used in the following way. First, the band parameters, γ_0 and γ_1, are assumed to be 2.4 eV and 0.38 eV, respectively, because these values were used for other stage-2 GIC's (Zaleski et al., 1987, 1989). Then the value of the Fermi energy is adjusted to fit the sum of the experiment Fermi areas obtained from eq. (IV.2): $A_F = (2\pi e/\hbar)F$

by $$E_F = (3/8\pi)^{1/2}\ \gamma_0 a (A_{F1} + A_{F2})^{1/2} \qquad \text{(IV.9)}$$

The Fermi energy and the band parameters (γ_0, γ_1) are then used to calculate the Fermi areas and dHvA frequencies, which are compared with the experimental values.

This procedure was repeated several times and the band parameters, γ_0 and γ_1, were determined to be 1.12eV and 0.39 eV, respectively, for the stage-2 $C_{24}K$. The Fermi energy was then calculated to be 0.5 eV. The comparison of the experimental data with the model is shown in Table IV.1

TABLE IV.1

Comparison of experimental data with the Blinowski model for $C_{24}K$.

AREA ($Å^{-2}$)		FREQUENCY (T)	
EXP.	CAL.	EXP.	CAL.
0.0273	0.0301	286	316
0.2453	0.2455	2570	2572

The value of γ_0, 1.12 eV, for stage-2 $C_{24}K$ is less than 2.4 eV, the value of γ_0 for stage-2 $SbCl_5$-GIC (Zaleski et al., 1987). This deviation is consistent with the model which predicts that the larger the Fermi surface the lower the value of γ_0. In fact, the largest Fermi area is 0.1136 $Å^{-2}$ for stage-2 $SbCl_5$-GIC, it is much less than the area, 0.2453 $Å^{-2}$, for stage-2 $C_{24}K$. Therefore, it is reasonable that $C_{24}K$ has a smaller value of γ_0 than $SbCl_5$-GIC. In addition, one can see from Table IV.1, that the predicted area and frequency for the higher freqency are perfectly matched with the observations, and the lower one is within 10%.

Fig. IV.12 shows the energy bands for the stage-2 $C_{24}K$ according to eq. (IV.7) with γ_0=1.12 eV and γ_1=0.39 eV. The two conduction bands are partially filled with electrons which are transferred to graphite from the donor intercalate species. The Fermi energy is positive with a value of 0.5eV and is shown by the broken line in Fig. IV.12.

Now, we compare the calculation for $C_{24}K$ by Yang and Eklund (YE) (1988) with the dHvA experimental results. Their calculation for $C_{24}K$ is based on the 2D tight-binding model of Saito and Kamimura (SK) (1985), but the parameters in the model of SK are adjusted by comparison with the calculated interband dielectric function with YE's experimental optical data. A simple k dependence of the nearest-neighbor carbon transfer integral parameter γ_0 is introduced to the model as well.

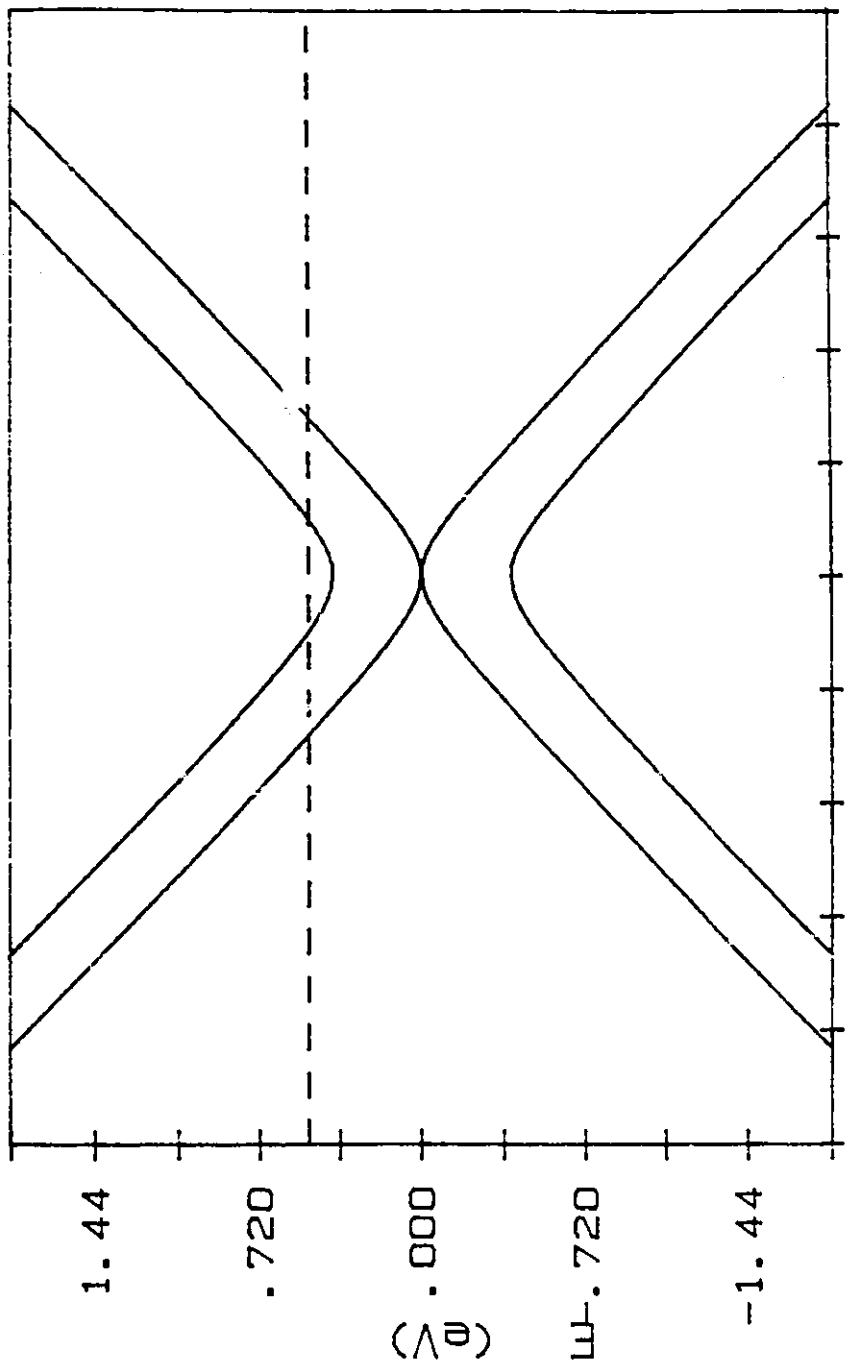

Figure IV.12. The band structure of stage-2 K-GIC with the band parameters γ_0 = 1.12 eV, and γ_1 = 0.39 eV. The dashed line is the Fermi level of 0.5 eV.

The energy band structure of YE also has two conduction and two valence bands for $C_{24}K$ and both conduction bands are partially filled with electrons. Therefore, this theory predicts two dHvA frequencies for $C_{24}K$ as Blinowski's model predicted.

The calculated Fermi areas and dHvA frequencies by Yang and Eklund (1988) for $C_{24}K$ are compared with the dHvA experimental data in Table IV.2. One can see that the theory predicts the right number of dHvA frequencies for $C_{24}K$ but the values of the frequencies, 1399 and 1820 T, do not match the experimental data very well. One is too high and the other one is too low. However, this theory is in good agreement with YE's optical data. Therefore, the theory could be improved for $C_{24}K$, if the right parameters in the energy bands could be obtained to describe both the optical data and the dHvA data.

TABLE IV.2

Comparison of experimental data with YE model for $C_{24}K$.

AREA ($Å^{-2}$)		FREQUENCY (T)	
EXP.	CAL.	EXP.	CAL.
0.0273	0.1335	286	1399
0.2453	0.1735	2570	1820

IV.2.2.2 The charge transfer

As discussed in Sec. (IV.1.2.2), the charge transfer per carbon atom is expressed by eq. (IV.1): $x=2V_F/(V_B m)$.

For the graphite intercalation compounds with the same in-plane unit cell as pure graphite, the volume of the Brillouin zone is

$$V_B=\frac{(2\pi)^3}{(\sqrt{3}a^2 I_c/2)} \qquad \text{(IV.10)}$$

For 2D energy bands, the volume enclosed by all pieces of cylindrical Fermi surface in the Brillouin zone is

$$V_F=2\frac{(2\pi)}{I_c}(\sum_i A_{Fi}) \qquad \text{(IV.11)}$$

where A_{Fi} is the Fermi surface cross-section area perpendicular to the k_z-direction, and it is directly proportional to the dHvA frequency F_i.

For a stage-n compound, there are 2n carbon atoms in the unit cell: it gives

$$m=2n \quad . \qquad \text{(IV.12)}$$

Therefore, by combining eq. (IV.1) and eqs. (IV.10)-(IV.12), the charge transfer per carbon atom for a stage-n GIC with 2D energy bands is directly measured by the dHvA effect through the following relation

$$x_{2D}=\frac{a^2\sqrt{3}}{4\pi^2 n}\sum_i A_{Fi} \qquad \text{(IV.13)}$$

For $C_{24}K$, n is equal to 2, the sum of the dHvA frequencies is 2856 T. The charge per carbon atom, x_{2D}, is then 0.0362 according to Eq. (IV.13). Thus, the charge f_k, transferred from each potassium atom to 24 carbon atoms, is found to be 0.87.

From Blinowski's model, the charge transfer for stage-2 GIC can be calculated with eq. (II.4):

$$x_{2D}=\frac{(E_F/r_0)^2}{(\pi/\sqrt{3})}=\frac{f}{1}$$

For $C_{24}K$, E_F and γ_0 are found to be 0.5 and 1.12 eV, respectively. Thus, x_{2D} is 0.0367 according to eq. (II.4), and f_k is about 0.88. This result is in very good agreement with the experimental value.

Other experiments, the optical reflectance (Eklung et al, 1986; Doll et al, 1987), the optical transmission (Zhang and Eklung, 1987), the Knight shift of the ^{13}C NMR (Conard et al, 1980), and the specific heat (Mizutani et al, 1978), all derived a complete intercalate ionization ($f_k = 1$) for $C_{24}K$. The present work is consistent with these experiments and suggests that the potassium s-band lies almost totally above the Fermi level in $C_{24}K$.

IV.2.3 Conclusions for $C_{24}K$

The dHvA measurements with the magnetic field direction parallel to the c axis show two dominant frequencies, 286 and 2570 T, in $C_{24}K$. One frequency, 2570 T, is reported for the first time. The predictions of Blinowski's theoretical model for a stage-2 GIC are in agreement with the experimental data when the band parameters, γ_0 and γ_1, are chosen as 1.12 eV and 0.39 eV respectively. The Fermi energy in $C_{24}K$, determined from the dHvA frequencies by using Blinowski's model, is 0.5 eV.

The theoretical calculation for the energy bands of $C_{24}K$ by Yang and Eklund predicts two dHvA frequencies but the values of the frequencies do not agree with the dHvA data very well.

The charge transfer per potassium atom is determined from both the dHvA measurements and Blinowski's model. The value, $f_k \sim 0.88$, suggests that the potassium s-band is above the Fermi level in $C_{24}K$.

CHAPTER V

ACCEPTOR-TYPE GIC

During the intercalation process, if electrons are transferred from graphite, the intercalate is called an acceptor and the graphite intercalation compound is classified as an acceptor-type GIC.

The present chapter concentrates on the study of the electronic properties of the acceptor-type stage-2 $BiCl_3$-GIC, the stage-3 $HgCl_2$-GIC and the stage-3 SbF_5-GIC by dHvA experiments. The Blinowski band models for stage-2 and stage-3 GIC were used to analyze the dHvA data.

The band structure of Blinowski's models for GICs is two-dimensional. Actually, all rigid band models of the electronic structure for GIC have the fundamental assumption that the interaction between carbon atoms separated by an intercalate layer is zero, and the electronic structure of GICs is two-dimensional (2D). This assumption can be justified by the experiment of the angular-dependence of the dHvA effect: for a 2D band structure, the Fermi surface is cylindrical, the angular dependence of the cross-sectional Fermi area, A_θ, which is perpendicular to the magnetic field direction, of a straight cylindrical Fermi surface follows the relation

$$A_\theta = A_0/\cos\theta \qquad (V.1)$$

where A_0 is the cross-sectional area perpendicular to the axis

of the Fermi cylinder, and θ is the angle between the direction of the magnetic field and the axis of the cylinder. According to the proportionality between the Fermi area A and the frequency f, the angular dependence of the dHvA frequencies, f_θ and f_0, corresponding to the areas A_θ and A_0, have the relation

$$f_\theta = f_0/\cos\theta \qquad (V.2)$$

Therefore, if this relation is followed by the dHvA data of the angular dependence, the assumption of the two-dimensionality of the band structure is proven correct.

The measurements of the dHvA effect including angular dependency experiments for stage-2 $BiCl_3$, stage-3 $HgCl_2$ and SbF_5 graphite compounds were performed for the first time and the electronic structures of these acceptor compounds were investigated for each stage as follows.

V.1 Stage-2 $BiCl_3$-GIC

The stage-2 bismuth trichloride ($BiCl_3$) graphite compound is a new "favorite" compound in the group of metal chloride GICs because it can be prepared easily with high staging fidelity (Behrens et al, 1988). In the present work, two samples of stage-2 $BiCl_3$-GIC were prepared and measured. Two dHvA frequencies are expected from Blinowski's model for the

stage-2 compound.

It should be emphasized that the name $BiCl_3$-GIC is really a misnomer because in all cases the prior addition of elemental chlorine is necessary to make the material. This process oxidizes the bismuth from the +3 to the +5 oxidation state which is well known to function as an acceptor of electrons. That is, the chemical identity of the system is more realistically described as a compound of bismuth (V) chloride which is known to be a Lewis acid.

V.1.1 Experimental results

The dHvA oscillations from stage-2 $BiCl_3$-GIC were obtained at 4.2 K. A typical recorder trace of the dHvA oscillation is shown in Fig. V.1. There is essentially a single oscillation frequency before the magnetic field reaches 4.7 T. The second oscillation comes in after 4.8 T and it changed the shape of the dHvA signal with increasing magnetic field. Actually, the second oscillation with a higher dHvA frequency could become stronger and more clearly visible if the magnetic field went beyond 5.4 T. However, the superconducting magnet used here has a maximum field of 5.5 T which limits the measurements of the dHvA signal within 5.4 T. Fig. V.2 shows the Fourier transform spectrum of the dHvA oscillations obtained from the field 4.0 T to 5.4 T at a temperature of 2.1 K. It is very clear to see that there are

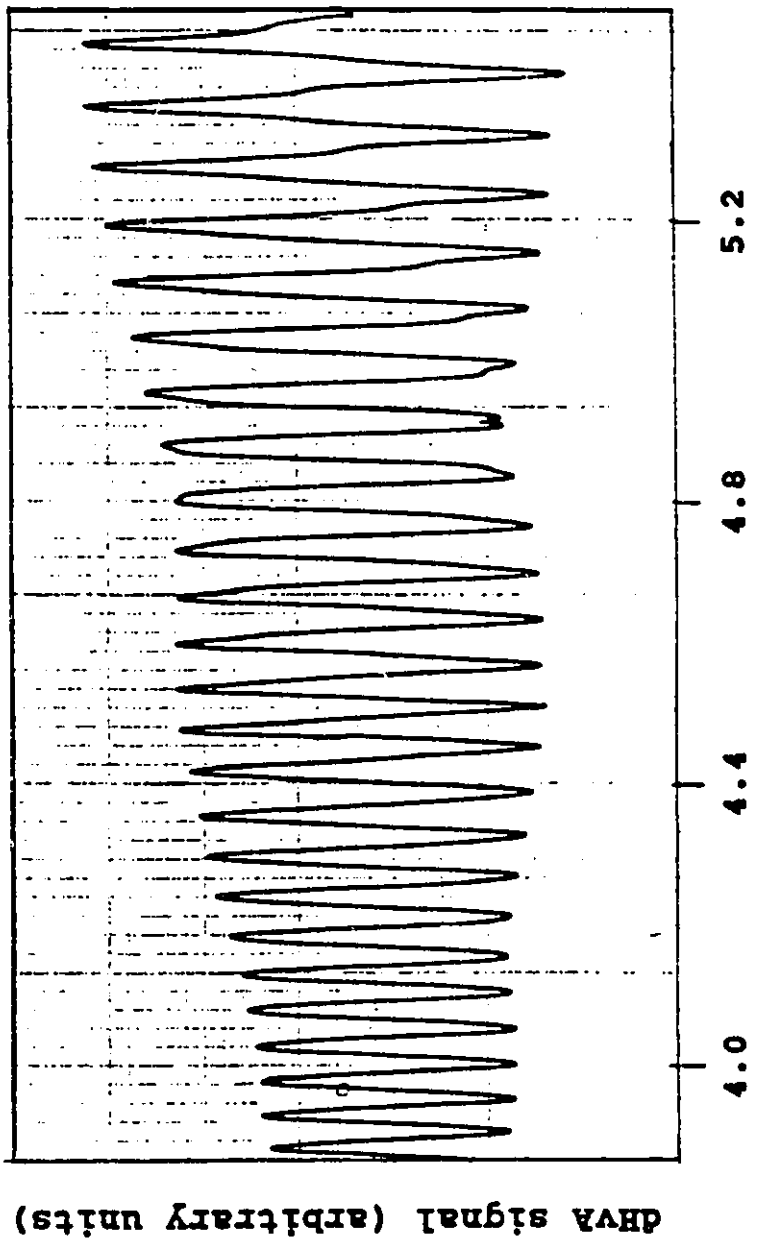

Figure V.1. de Haas-van Alphen oscillations of the stage-2 $BiCl_3$-graphite.

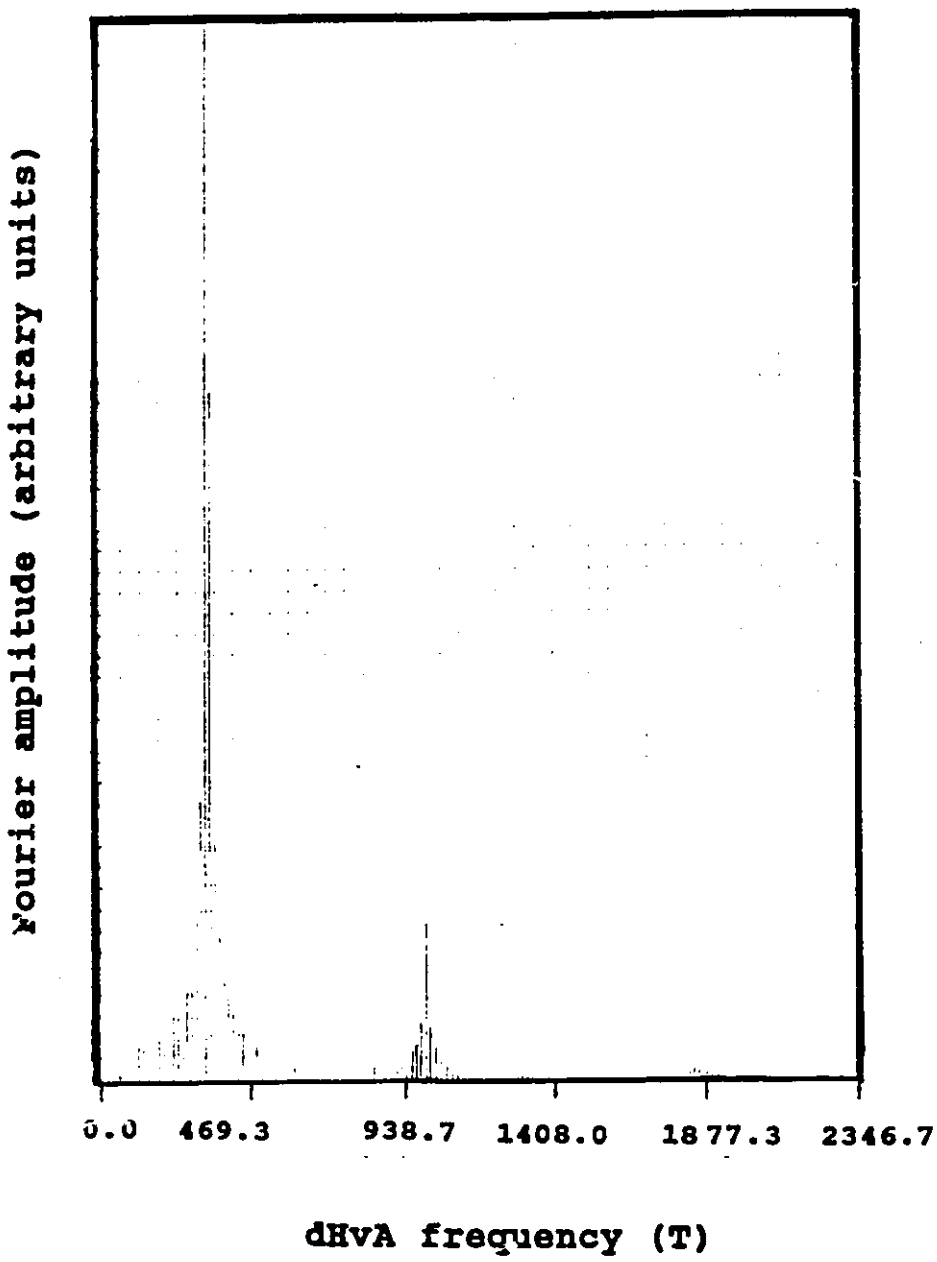

Figure V.2. Fourier transform of the dHvA signal of stage-2 $BiCl_3$-graphite.

two dHvA frequencies as expected. The first one is F_1=327 T and the second is F_2=1012 T. The Fermi areas corresponding to the two frequencies are 0.0312 and 0.0966 $Å^{-2}$, respectively, according to the relation between the Fermi area and the dHvA frequency ($A_F = (2\pi e/\hbar)F$).

The temperature dependence of the dHvA amplitude was measured from 2.1 K to 4.2 K. Fig. V.3 shows the plot of ln(A/T) versus T for both F_1 and F_2. The carrier effective masses corresponding to F_1 and F_2 were obtained from the temperature-dependence. The values are $m_1^* = 0.147\ m_0$ and $m_2^* = 0.265\ m_0$.

All the results were reproducible for different samples, and the experimental data are summarized in Table V.1.

Table V.1

The experimental data for stage-2 $BiCl_3$-GIC.

dHvA Freq. (T)	Fermi area ($Å^{-2}$)	Effec. mass (m_0)
327	0.0312	0.147
1012	0.0966	0.265

The angular dependence of the two dHvA frequencies is shown in Fig. V.4. The solid curves represent the predictions for 2D straight cylinders of the FS given by $f_\theta = f_0/\cos\theta$. The

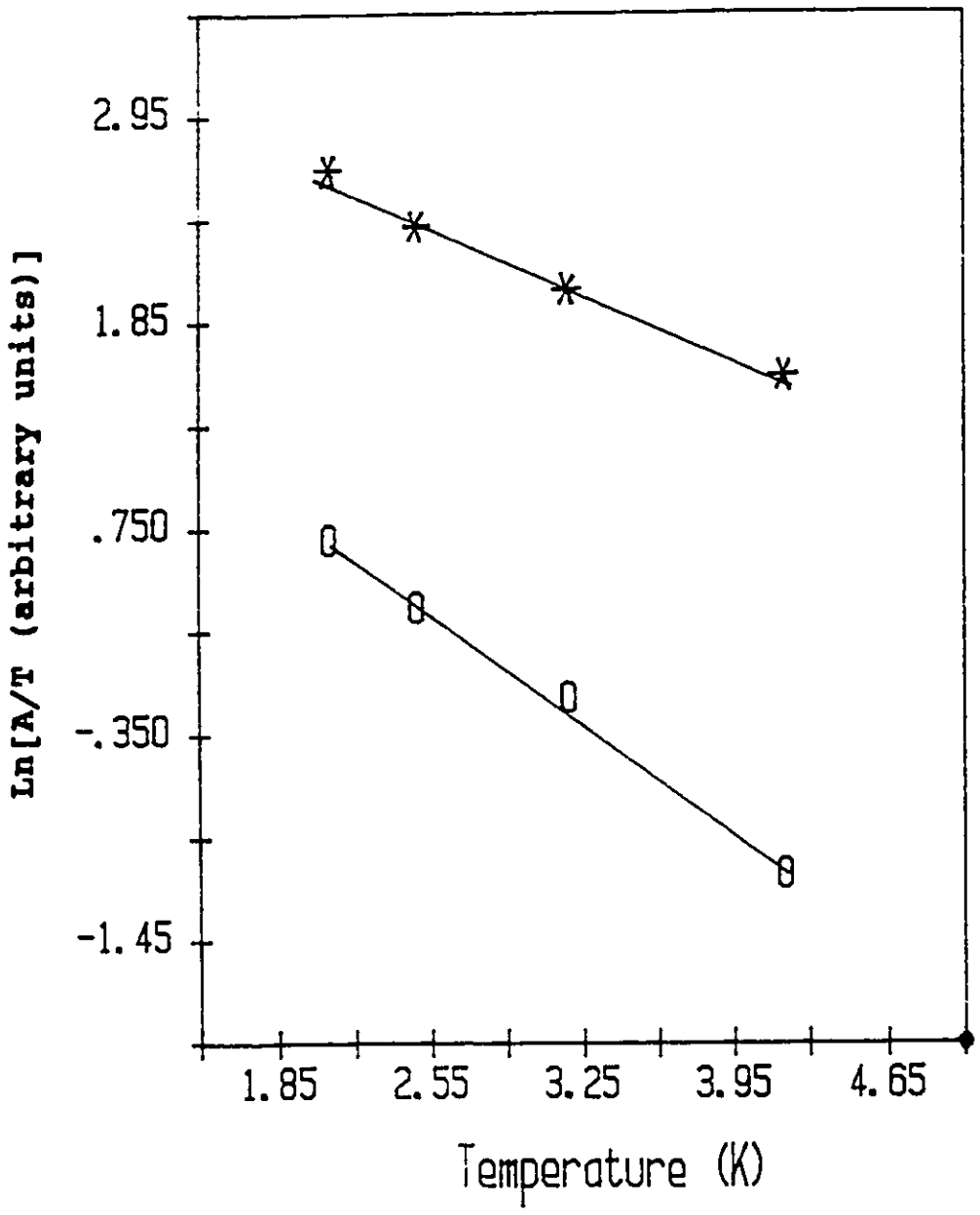

Figure V.3. Temperature dependence of A/T for the first frequency 327 T (*) and the second frequency 1012 T (o), respectively, of stage-2 $BiCl_3$-GIC.

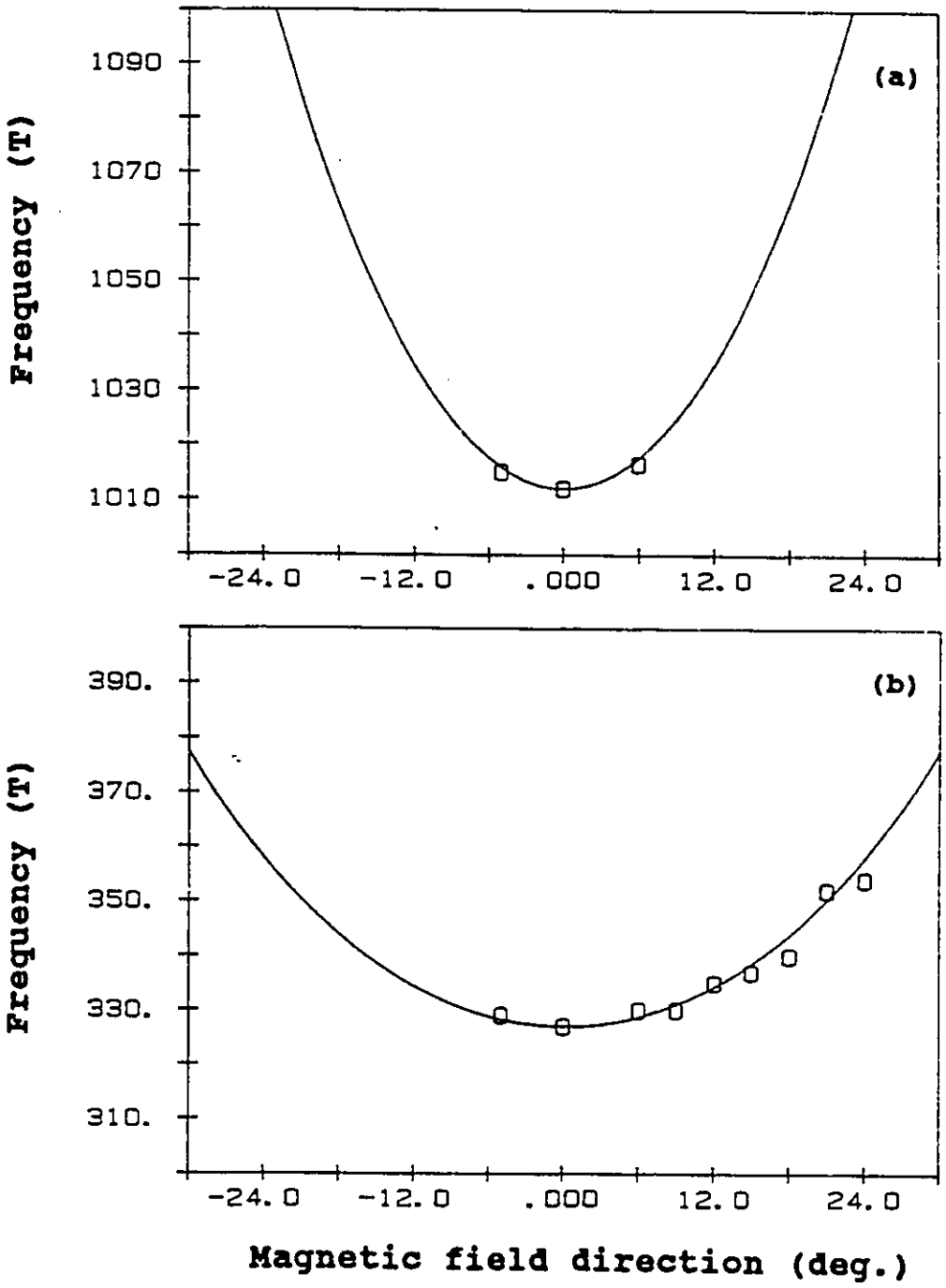

Figure V.4. dHvA frequencies 1012 T (a) and 327 T (b) as a function of magnetic field direction from the c-axis of stage-2 $BiCl_3$-GIC. The solid lines are cylindrical fits.

squares are experimental data. The angular dependence was measured from $\theta = -6^0$ to $\theta = 27^0$. The dHvA frequencies follow a cylindrical behavior very well. This means that the band structure of the stage-2 $BiCl_2$-GIC is quite two-dimensional. The angular range of measurement is however too small to distinguish any differences from a cylinder.

However, the amplitude of the dHvA frequencies decrease with increasing θ, as shown in Fig. V.5 for F_1. The dHvA signal of F_1 disappeared after $\theta=27^0$. The second frequency F_2 was weaker than F_1 and disappeared when the angle exceeded 9^0.

V.1.2 Calculation and discussion

Because the angular dependence of the dHvA frequencies are consistent with cylindrical behavior of the FS, the prediction of the two dimensionality of Blinowski's model is confirmed experimentally. Therefore, one can now examine whether the theoretical bands are in agreement with the experimental data by comparing the dHvA frequencies, the Fermi areas, the cyclotron masses, and the charge transfer coefficients.

V.1.2.1 Band structure

For stage-2 acceptor compounds, two valence bands are given as

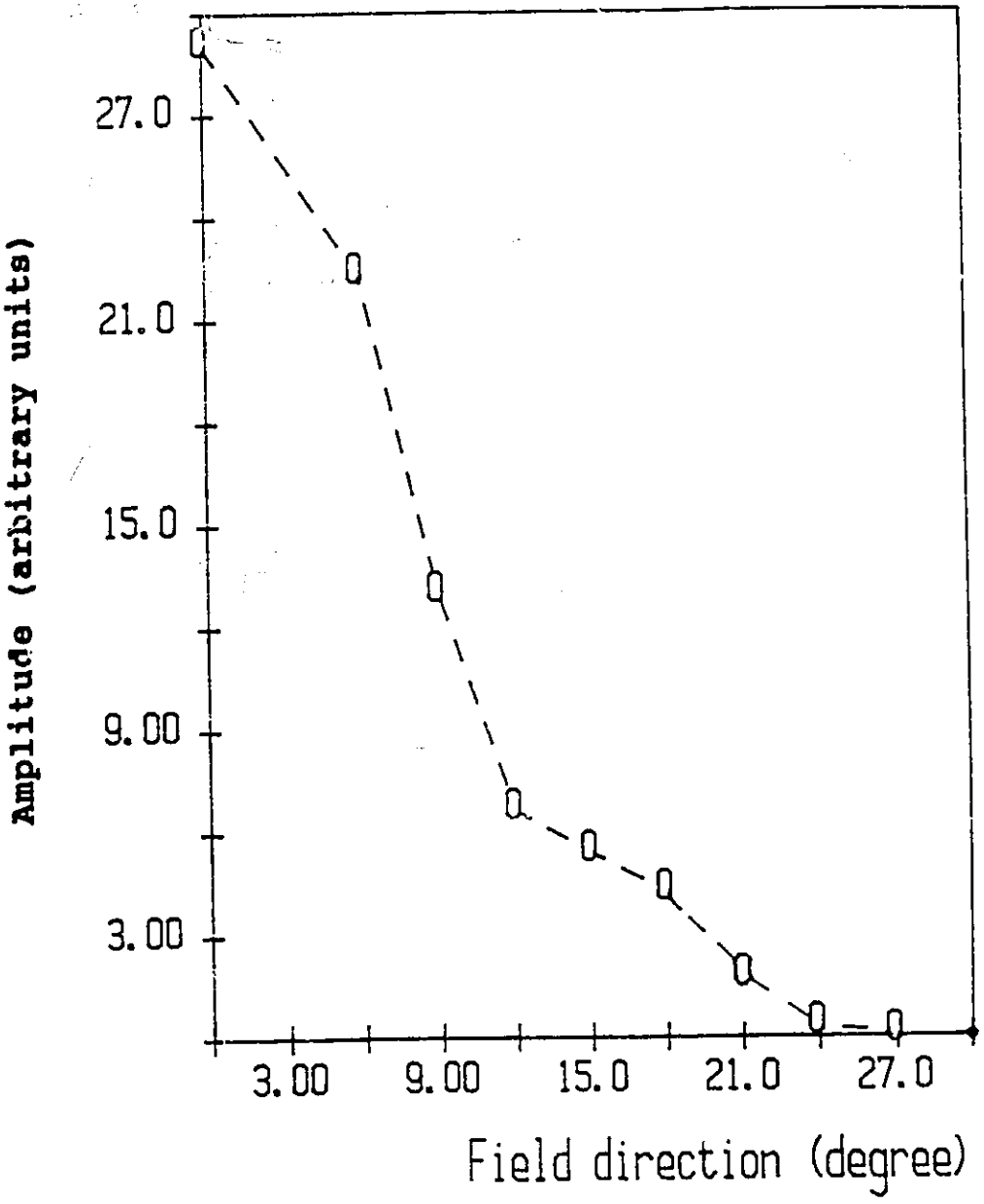

Figure V.5. The dHvA amplitude as a function of the angle between the magnetic field and c-axis of the stage-2 $BiCl_3$-GIC. The dashed line is drawn as a guide to the eye.

$$E_1^V = -(\sqrt{\gamma_1^2 + 3\gamma_0^2 a^2 k^2} - \gamma_1)/2 \qquad \text{(V.3a)}$$

$$E_2^V = -(\sqrt{\gamma_1^2 + 3\gamma_0^2 a^2 k^2} + \gamma_1)/2 \qquad \text{(V.3b)}$$

the Fermi areas of the bands are given by

$$A_{F1} = \frac{4\pi}{3\gamma_0^2 a^2}(E^2 - E\gamma_1) \qquad \text{(V.4a)}$$

$$A_{F2} = -\frac{4\pi}{3\gamma_0^2 a^2}(E^2 + E\gamma_1) \qquad \text{(V.4b)}$$

To determine the theoretical Fermi surface cross sectional areas or dHvA frequencies, the band parameters (γ_0, γ_1) have to be assumed first, then the Fermi energy is adjusted to fit the sum
of the experimental Fermi areas by

$$E_F = \sqrt{\frac{3}{8\pi}}\gamma_0 a\sqrt{A_{F1} + A_{F2}} \qquad \text{(V.5)}$$

The E_F is then used to calculate the theoretical Fermi areas. If the theoretical values fail to fit the experimental data, the assumed band parameters (γ_0, γ_1) are changed until the agreement between the theory and experiment is achieved. For

stage-2 $BiCl_3$-GIC, if one choses any other values of γ_0 and γ_1 than 2.4 and 0.38 respectively, the model does not agree with the experimental Fermi areas very well. The Fermi energy is -0.73 eV and the theoretical Fermi areas are 0.0307 and 0.0974 $Å^{-2}$, respectively, for γ_0 = 2.4 and γ_1 = 0.38 eV for the stage-2 $BiCl_3$-GIC. The comparison of the calculated Fermi areas with the experimental data is shown in Table V.2.

To obtain the theoretical cyclotron masses, the Fermi areas which depend on energy are differentiated according to the definition

$$m_c = \frac{\hbar^2}{2\pi}\frac{\partial A}{\partial E}$$

where A is area and E is energy. The cyclotron masses for a stage-2 acceptor-GIC are given by

$$m_{c1} = \frac{\hbar^2}{2\pi}\frac{4\pi}{3\gamma_0^2 a^2}(-2E_F - \gamma_1) \qquad \text{(V.6a)}$$

$$m_{c1} = \frac{\hbar^2}{2\pi}\frac{4\pi}{3\gamma_0^2 a^2}(-2E_F + \gamma_1) \qquad \text{(V.6b)}$$

Because the band parameters, γ_0 and γ_1, and the Fermi energy are already fixed, the two theoretical cyclotron masses are directly calculated by using γ_0 = 2.4, γ_1 = 0.38 and E_F= -0.73 eV. The calculated values of m_{c1} = 0.149 m_0 and m_{c2} = 0.254 m_0

are also compared with the experimental data in Table V.2. The comparison of the cyclotron masses is more important than that of the Fermi areas, because the band parameters (γ_0, γ_1) are determined from the Fermi areas but fixed for the cyclotron masses.

For the two-dimensional Fermi structure of stage-2 $BiCl_3$-GIC, the experimental charge transfer per carbon atom is calculated directly from the sum of the dHvA frequencies, as shown by eq. (IV.13). It is 0.017 according to the relation. The theoretical prediction of the charge transfer in stage-2 compound is related to the Fermi energy E_F and band parameter γ_0, as expressed by eq. (II.4). It is found to be 0.017 according to the equation. This value is exactly the same as the experimental result.

All the results from both the experiment and theory are summarized in Table V.2.

Table V.2

Comparison of the experimental data with Blinowski's model for the stage-2 $BiCl_3$-GIC.

Freq. (T)		Area ($Å^{-2}$)		Mass (m_0)		Charge trans. per Carbon	
Exp.	Cal.	Exp.	Cal.	Exp.	Cal.	Exp.	Cal.
327	322	0.0312	0.0307	0.147	0.149	0.017	0.017
1012	1020	0.0966	0.0974	0.265	0.254		

One can see that the theoretical predictions for the Fermi areas and dHvA frequencies are within 2% of the experimental values, and the cyclotron masses are within 4%. This agreement between theory and experiment is good for the stage-2 $BiCl_3$-GIC.

Fig. V.6 shows the energy bands for this compound with γ_0=2.4 and γ_1 =0.38 eV. The top of the two valence bands are unoccupied because some electrons are transferred to the acceptor intercalate species. The carriers are holes for the acceptor compound and the Fermi energy is negative with the value of -0.73 eV, as shown by the broken line.

V.1.2.2 Comparison of experimental results for three stage-2 acceptor compounds

In addition to the comparison of the experimental results with the theoretical predictions, the validity of the theoretical model can also be tested by analyzing the data of other related GIC's. For instance, the electronic structure of the stage-2 acceptor-type BF_4 and $SbCl_5$-GIC was also reasonably described by the Blinowski model (Zaleski et al, 1985, 1987). The band parameters which are suitable for stage-2 BF_4^- and $SbCl_5$-GIC were the same as the ones for stage-2 $BiCl_3$-GIC (γ_0=2.4 eV and γ_1=0.38 eV). This means that the three graphite compounds have the same energy bands as shown in Fig. V.6. The only difference is the charge transfer and the effects caused

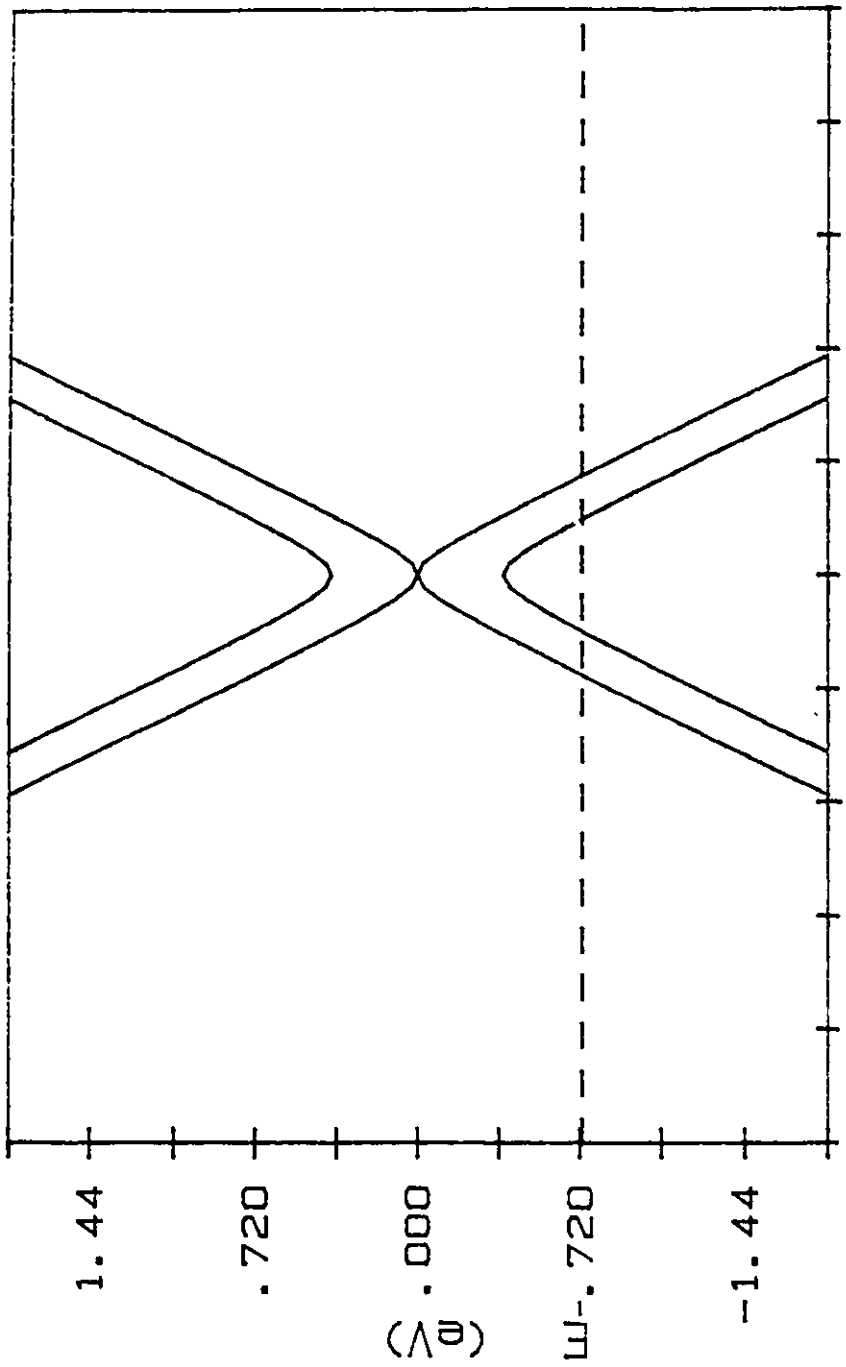

Figure V.6. The band structure of stage-2 $BiCl_3$-GIC with the band parameters γ_0=2.4 eV and γ_1=0.38 eV. The dashed line is the Fermi level of -0.73 eV.

by the charge transfer, because a different acceptor intercalant has a different ability to gain electrons. Therefore, if one of them has a higher charge transfer per carbon atom, the absolute value of the Fermi energy will also be higher because the concentration of holes is higher and the top of valence bands is larger for the same bands. Also, the Fermi areas around the Fermi level will be larger as well according to the band structure.

Table V.3 shows the comparison of the experimental data of the charge transfer, Fermi energy, and Fermi area for these compounds.

Table V.3

Comparison of the data for stage-2 BF_4^-, $SbCl_5$ and $BiCl_3$-GICs.

		BF_4^-	$SbCl_5$	$BiCl_3$
Repeat d-spacing (Å)	I_c	11.13	12.72	13.00
Band parameters (eV)	γ_0	2.4	2.4	2.4
	γ_1	0.38	0.38	0.38
Charge transfer/Carbon (e^+)	f/l	0.0241	0.0204	0.0170
Fermi energy (eV)	E_F	-0.87	-0.80	-0.73
Fermi areas ($Å^{-2}$)	A_1	0.0499	0.0403	0.0312
	A_2	0.1315	0.1136	0.0966

From Table V.3, one can see that the magnitude of the charge transfer per carbon for these compounds is in the sequence of BF_4^-, $SbCl_5$ and $BiCl_3$. As expected, the absolute values of Fermi energy and the Fermi areas are also in the same sequence of magnitude for these compounds. This means that there is no contradiction of the experimental data among these compounds vs. the band structure. Therefore, the theoretical model which describes the band structure is reasonable.

V.1.3 Conclusions for stage-2 $BiCl_3$

The measurements of the dHvA effect were performed on stage-2 $BiCl_3$ - GIC for the first time. Two dHvA frequencies were obtained from the experiment and were interpreted in terms of the electronic structure of the Blinowski model.

The two dimensionality of the band structure predicted by the model was consistent with the angular dependence of the dHvA frequencies. The band parameters (γ_0, γ_1) were fixed when the theoretical predictions for the Fermi areas are in agreement with the experimental data. The Fermi energy was determined from the experimental Fermi areas by using the band model for this compound.

The validity of the model was checked by the comparison of the frequencies, cyclotron masses, and charge transfer. The

theoretical predictions for dHvA frequencies and cyclotron masses are in agreement with the measured results. The charge transfer calculated from the model is exactly same as the experimental value.

In addition, the reasonableness of the model was also checked by analyzing the change of the experimental data of charge transfer per carbon, Fermi energy and Fermi areas among three stage-2 acceptor compounds, which have the same band structure described by the model.The fact that the higher the charge transfer per carbon atom, the higher the absolute value of the Fermi energy, and the larger the Fermi areas among these compounds is consistent with the calculation and predictions of the model.

V.2 Stage-3 $HgCl_2$-GIC and SbF_5-GIC

Stage-3 compounds are somehow different from stage-1 and stage-2 compounds. The graphite layers limited by intercalated layers in stage-1 or stage-2 compounds are equivalent and the same excess charge is accumulated on each graphite layer. However, the layers in stage-3 compounds are no longer equivalent, the internal graphite layer is different from the external graphite layers which are close to the intercalated layers.

This situation is considered by the Blinowski model (described in Chapter II) and the electrostatic effect is

presented by a new band parameter δ, which gives the electrostatic potential energy difference between external and internal graphite layers. From the band structure of Blinowski's model, three dHvA frequencies are expected for the stage-3 acceptor compounds.

V.2.1 Experimental results and analysis

Two samples of stage-3 $HgCl_2$ compounds were measured. Fig. V.7 shows the frequency spectrum. Three groups of dHvA frequencies were obtained. Each group consists of two frequencies which are separated by about 40 T. The dominant frequencies in the three groups are F_1=121, F_2=523, and F_3=664 T. The temperature dependence of the dHvA amplitude of the dominant frequencies was measured from 1.6 K to 4.2 K to determine the cyclotron masses. Fig. V.8 shows the plot of ln(A/T) vs. T for F_2. The results are $m_1^* = 0.084\ m_0$ and $m_2^* = 0.165\ m_0$. It is difficult to determine m_3^* because the dHvA signal of the frequency F_3 only appeared at very low temperature. The charge transfer per carbon for the stage-3 $HgCl_2$-GIC is 0.0111 from the sum of the experimental frequencies according to eq. (IV.13).

Stage-3 SbF_5-GIC is not stable in air. The dHvA measurements were done twice. Fig. V.9 shows the Fourier transform spectrum of the dHvA oscillations. There are also three groups of dHvA frequencies for the stage-3 compound. The

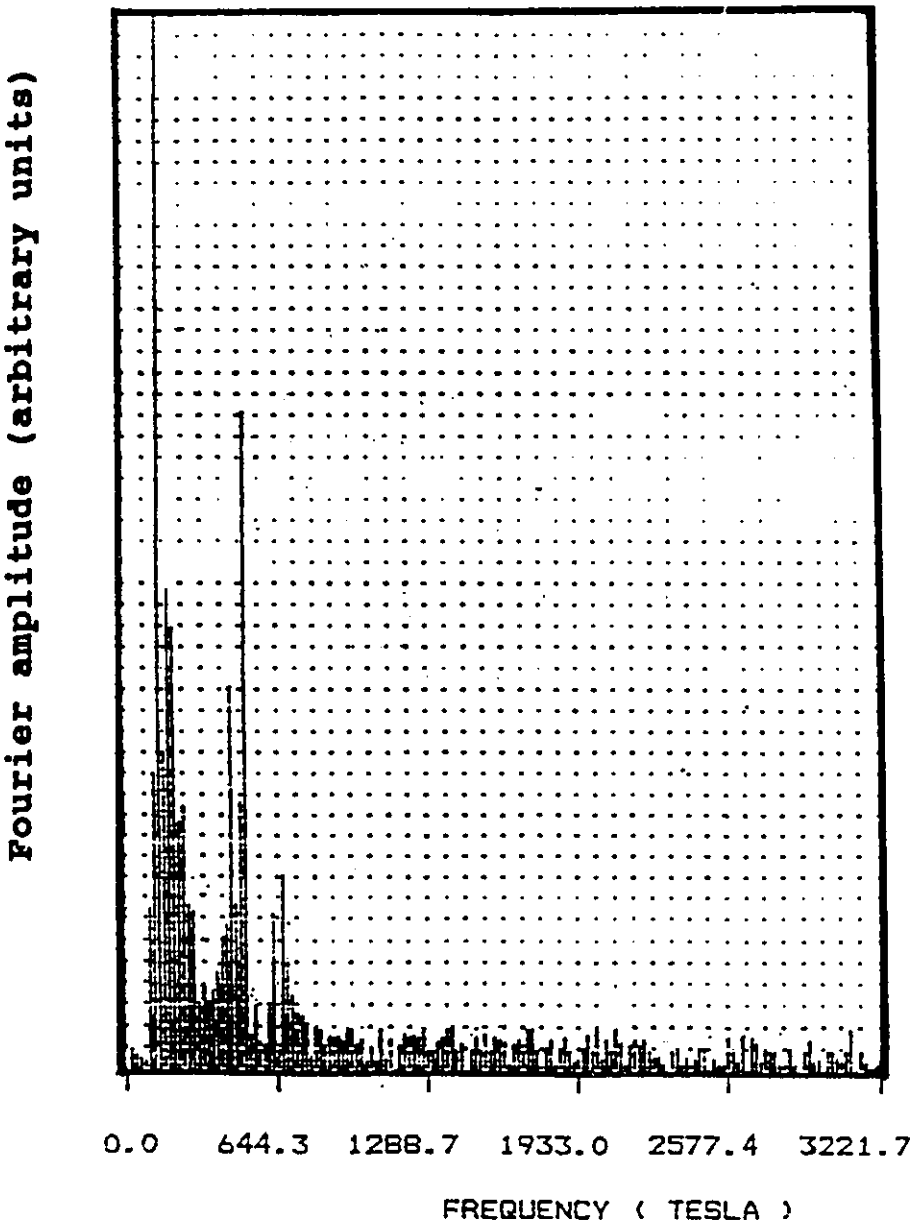

Figure V.7. de Haas-van Alphen spectrum of the stage-3 $HgCl_2$-GIC.

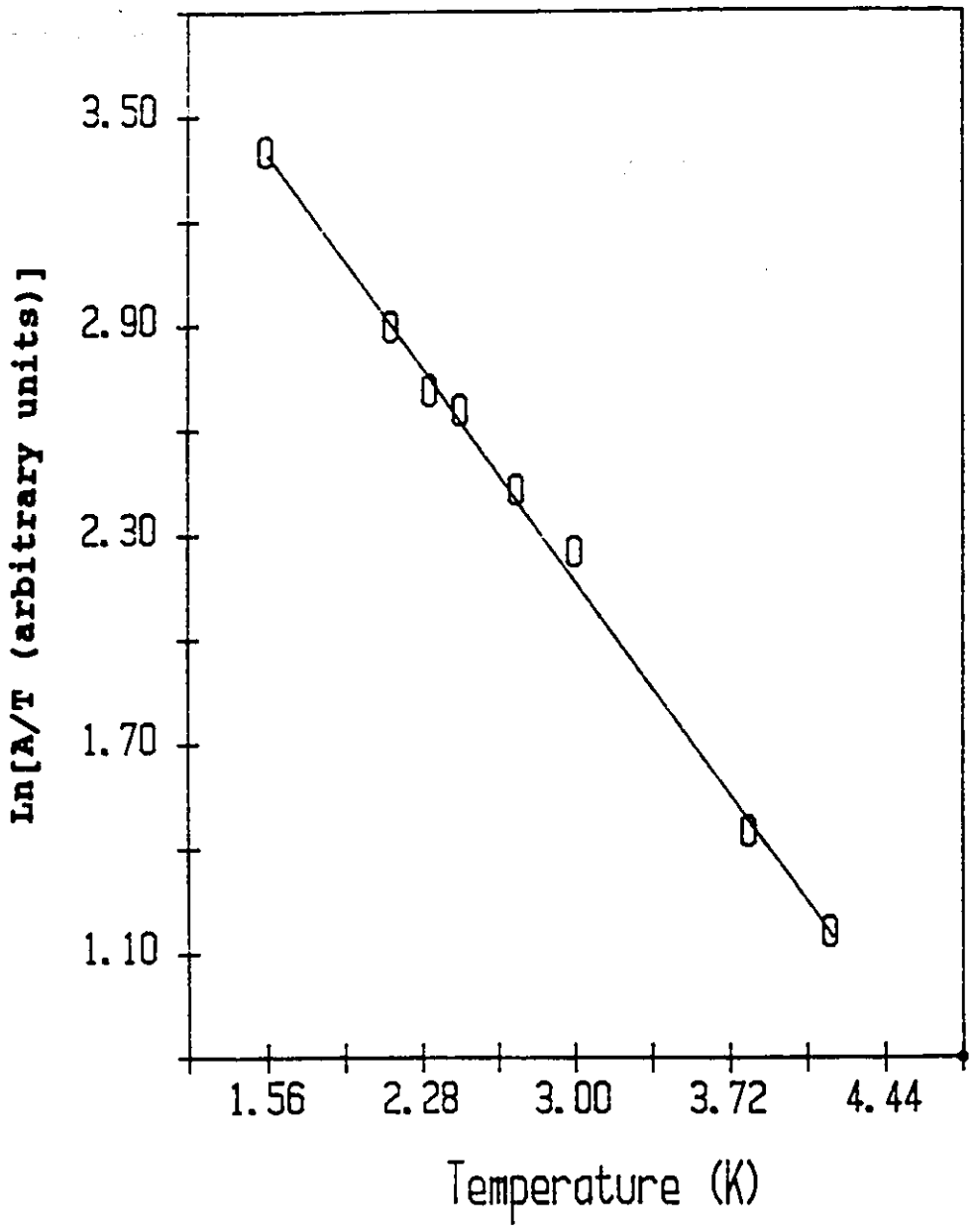

Figure V.8. Temperature dependence of the second dominant frequency 523 T of stage-3 $HgCl_2$-GIC.

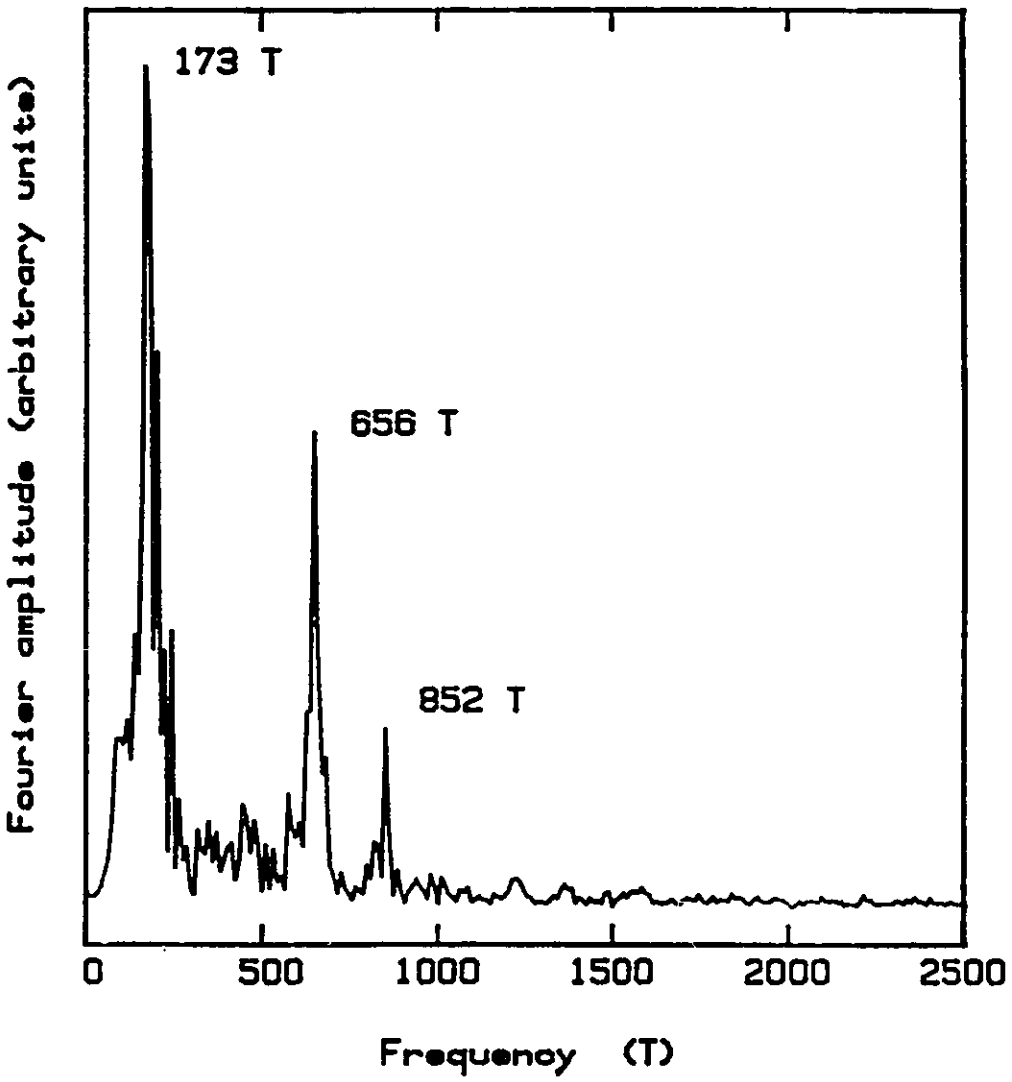

Figure V.9. de Haas-van Aphen spectrum of the stage-3 SbF_5-GIC.

three dominant frequencies are 172, 656, and 852 T. The effective masses corresponding to the three dominant frequencies are $m_1^* = 0.109\ m_0$, $m_2^* = 0.184\ m_0$, and $m_3^* = 0.226\ m_0$, determined from the temperature dependence measurements from 1.6 K to 4.1 K. Fig. V.10 shows the temperature dependence of the first dominant frequency. The charge transfer per carbon atom determined from the sum of the dominant frequencies is 0.0142 for the stage-3 SbF_5 compound. All the measurements were repeated two month later and reproducible results were obtained.

The experimental data for both stage-3 $HgCl_2$ and SbF_5-GIC are summarized in Table V.4

Table V.4

The experimental data for stage-3 $HgCl_2$ and SbF_5-GIC

Compound	dHvA Freq. (T)	Fermi area($Å^{-2}$)	Effective mass (m_0)	Charge trans./C.
$HgCl_2$	121	0.0115	0.084	0.0111
	523	0.0500	0.165	
	664	0.0634	---	
SbF_5	172	0.0164	0.109	0.0142
	656	0.0626	0.184	
	852	0.0813	0.226	

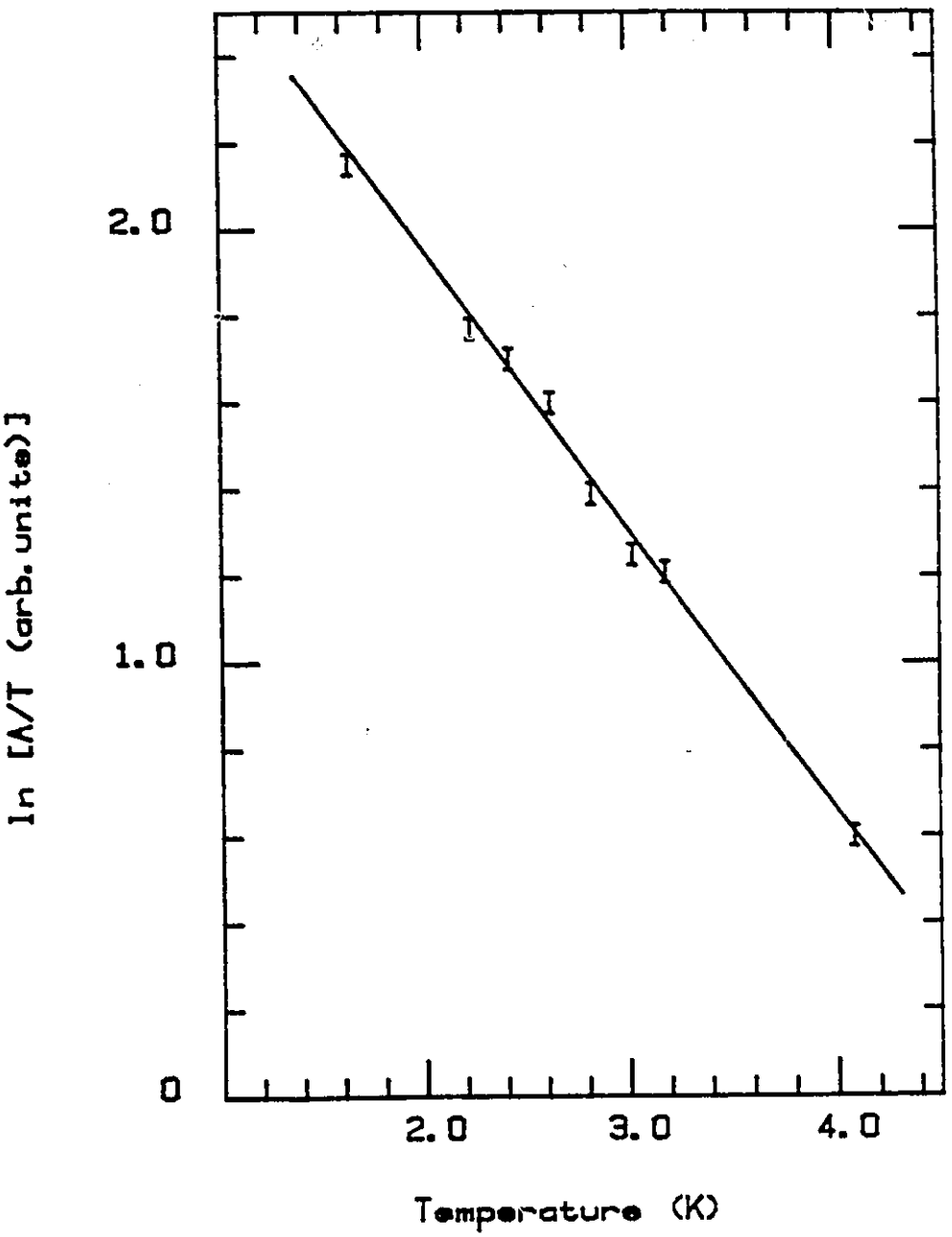

Figure V.10. Temperature dependence of A/T where A is the amplitude of the 172 T dHvA oscillation of stage-3 SbF_5-GIC.

In order to investigate the actual shape of the Fermi surface for the stage-3 compounds, the angular dependence of the dHvA frequencies was measured from $\theta = 0^0$ to $\theta = 60^0$ for SbF_5-GIC. Fig.V.11 shows the plot of the dominant dHvA frequency in the first group as a function of the angle θ. The full curve represents the prediction for a straight cylinder of the Fermi surface. The stars are the experimental data. From Fig. V.11 one can see that the dHvA frequency does follow a cylindrical behavior for angles up to about 40^0. For larger angles, there are deviations from the cylindrical fit.

This measurement of angular dependence was also repeated two month later and the same behavior was obtained.
The present measurement of the angular dependence only went to $\theta = 60^0$. The amplitude of the dHvA frequency decreases with θ and the dHvA signal disappeared after $\theta = 60^0$. This limited the angular-dependence measurements of the frequencies to the region of $\theta < 60^0$.

The basic cylindrical behavior of the angular dependence of the dHvA frequencies means that the Fermi surface of the stage-3 compound is basically two-dimensional. However, the observed frequency has a negative deviation from the cylindrical prediction at high angles which indicates that the cross-sectional area of the Fermi surface is gradually decreasing when the wave vector k_z is close to the top of the BZ. That is, the Fermi surface is not a perfect straight cylinder as Blinowski's model predicted. This is because the

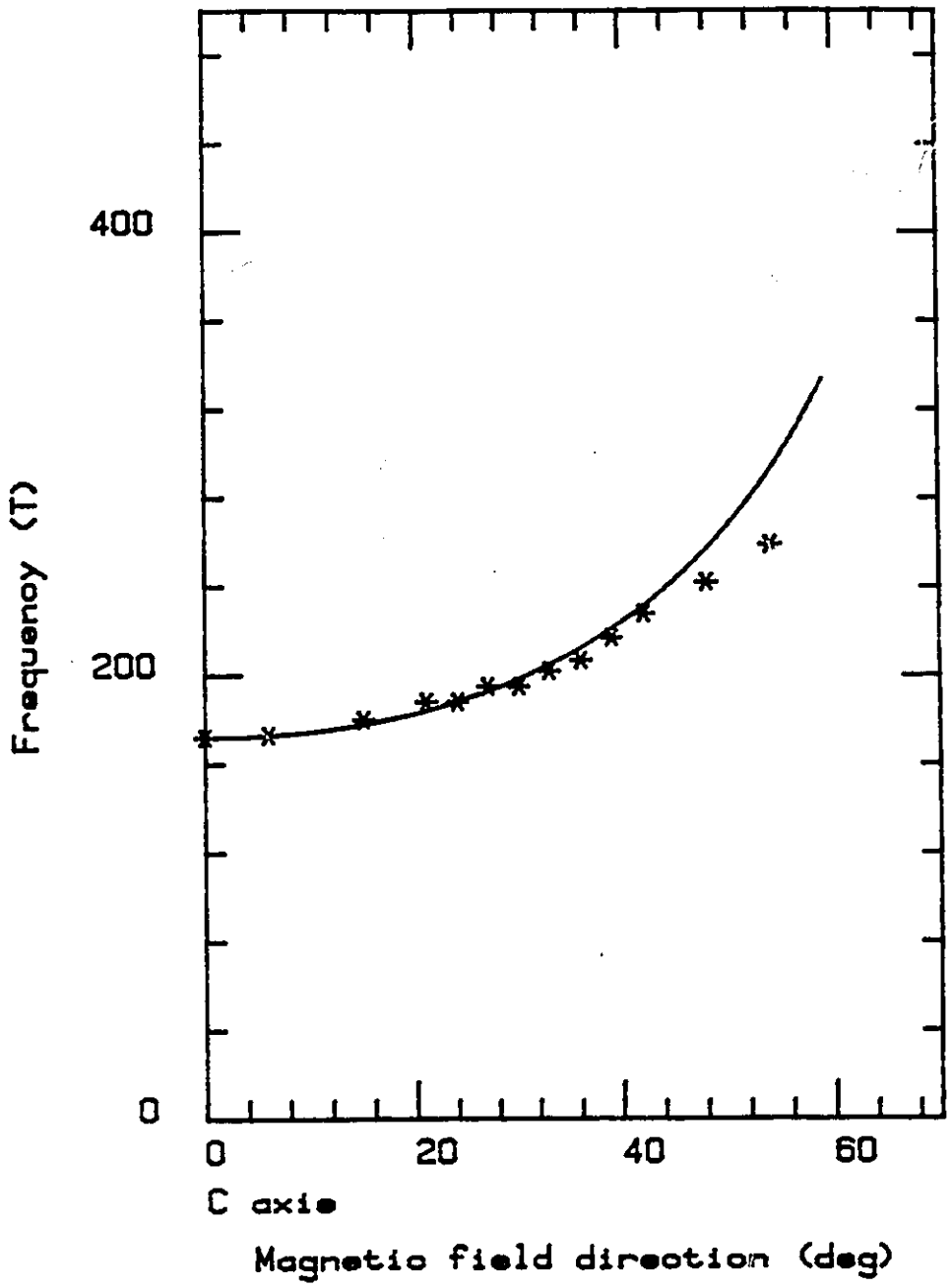

Figure V.11. dHvA frequency of the first dominant oscillation as a function of magnetic field direction from the c-axis of stage-3 SbF_5-GIC. The full curve is for a cylindrical Fermi surface.

model assumes that there are no interactions between the subsystems of three graphite layers limited by intercalated layers for stage-3 compounds. In fact, there exists a small interaction between the subsystems along the c direction. Thus, the electronic energy bands might not be totally two dimensional and some dispersion along the k_z direction could exist. Therefore, the Fermi surface may not be a perfect straight cylinder.

In addition, the three groups of dHvA frequencies obtained from the dHvA measurements show that the band structure is not as simple as the theory describes. Otherwise, it would give three individual dHvA frequencies for stage-3 compounds rather than the observed split frequencies. The reason why the real situation has some deviation from the theory is that the Blinowski model assumes that the potential energy fluctuations produced within the graphite subsystem by the charged acceptor intercalated monolayer can be neglected. This assumption is reasonable if the intercalated monolayers are basically homogeneous in distribution. But in fact, there exist highly inhomogeneous structures in graphite intercalation compounds. For instance, Levi-setti et al. (1985) reported direct imaging of intercalant islands using a focused ion-beam microprobe, Thomas et al. (1980) observed a discontinuity in the intercalant layers, and Hwang et al. (1984) observed Sb-rich islands of lateral dimension 500-1000 Å in $SbCl_5$-intercalated graphite. All these observed results

show that intercalate monolayers exhibit multiphase-multidomain structure. Because the properties of the chemistry and physics of the intercalant layers directly affect the graphite-graphite or graphite-intercalant interactions, the inhomogeneities or discontinuities, particularly the domains of intercalate monolayers, can play a critical role of perturbation to these interactions and therefore affect the band structure of the GIC. Thus, the splitting of the frequencies can result from these perturbations of the highly inhomogeneous structure.

Furthermore, the splitting of the frequencies can also be related directly to the undulation of the Fermi surface along the k_z direction. That is, the undulation of the Fermi surface could be another possible reason for the splitting of the frequencies. This is because the existence of the undulation of the Fermi surface can result in several similar extremal cross-sectional areas which can present several similar dHvA frequencies in one group. The experimental deviation of the Fermi surface from a straight cylinder shown in Fig. V.11 means that there exist at least two extremal cross-sectional areas located at the maximum and the minimum of the Fermi surface if the deviation is always negative at higher angles. The actual shape of the Fermi surface could be more complicated than the description of a cylindrical Fermi surface with two similar extremal cross-sectional areas because the experimental deviation from a straight cylindrical

Fermi surface could be changed from negative to positive with increasing angle. Therefore, the existence of the undulation of the Fermi surface with more than two extremal cross-sectional areas is possible.

V.2.2 Discussion

No matter how complicated the reasons for the undulation of the Fermi surface and the splitting of the dHvA frequencies, the important things from the experimental results are that the behavior of the Fermi surface is basically cylindrical instead of spherical, and that there are three dHvA frequency groups instead of two or four groups for the stage-3 compounds. The cylindrical behavior of the Fermi surface corresponds to the two dimensionality of the theoretical bands and the three dHvA frequency groups correspond to the three individual frequencies expected from the theoretical model. The detailed discussion of the energy bands and the charge distribution of the stage-3 compounds are as follows.

V.2.2.1 The energy bands

For a stage-3 compound Blinowski's model predicts that there are three valence bands whose energies are given by

$$E_1=\delta-|X|, \tag{V.7a}$$

$$E_2=-\{\delta^2+\gamma_1^2+|X|^2-[\gamma_1^4+(4\delta^2+2\gamma_1^2)\,|X|^2]^{1/2}\}^{1/2} \tag{V.7b}$$

$$E_3=-\{\delta^2+\gamma_1^2+|X|^2+[\gamma_1^4+(4\delta^2+2\gamma_1^2)\,|X|^2]^{1/2}\}^{1/2} \tag{V.7c}$$

The Fermi areas of the bands are derived from eq. (V.7) and expressed as

$$A_1=(E-\delta)^2\frac{\pi}{(\sqrt{3}\gamma_0 a/2)^2} \tag{V.8a}$$

$$A_2=\{E^2+\delta^2+[4E^2\delta^2+2\gamma_1^2(E^2-\delta^2)]^{1/2}\}\frac{\pi}{(\sqrt{3}\gamma_0 a/2)^2} \tag{V.8b}$$

$$A_3=\{E^2+\delta^2-[4E^2\delta^2+2\gamma_1^2(E^2-\delta^2)]^{1/2}\}\frac{\pi}{(\sqrt{3}\gamma_0 a/2)^2} \tag{V.8c}$$

The area dependence on energy is differentiated to obtain the cyclotron mass. The cyclotron masses are given by

$$m_{c1}=\frac{\hbar^2}{(\sqrt{3}\gamma_0 a/2)^2}(E-\delta) \tag{V.9a}$$

$$m_{c2}=\frac{\hbar^2}{(\sqrt{3}\gamma_0 a/2)^2}E\left[1+\frac{2\delta^2+\gamma_1^2}{[4E^2\delta^2+2\gamma_1^2(E^2-\delta^2)]^{1/2}}\right] \tag{V.9b}$$

$$m_{c3}=\frac{\hbar^2}{(\sqrt{3}\gamma_0 a/2)^2}E\left[1-\frac{2\delta^2+\gamma_1^2}{[4E^2\delta^2+2\gamma_1^2(E^2-\delta^2)]^{1/2}}\right] \qquad \text{(V.9c)}$$

All the parameters in eqs. (V.7-V.9) have been previously explained in Chapter II. The procedure used for calculating the theoretical data is as follows.

From eq. (V.8), the Fermi areas of the three bands are calculated as a function of energy for various values of the band parameters, γ_0, γ_1, and δ. The value of the Fermi energy is determined at the energy point which makes the theoretical areas agree with the experimental data for one set of the band parameters. For the $HgCl_2$ compound, the choices of γ_0=3.0, γ_1=0.31, and δ=0.13 eV as well as the value of E_F = -0.69 eV make the theoretical Fermi areas in good agreement with the experimental data. For the SbF_5 compound, the choices are γ_0=2.8, γ_1=0.31 and δ=0.13 eV and the value of E_F is -0.73 eV. The Fermi energy and the band parameters are then used to calculate the cyclotron masses according to eq. (V.9).

The comparison of all the experimental data to the model is shown in Table V.5. The cyclotron masses are especially important in the comparison because they are not used to determine the band structure.

Table V.5

The comparison of the experimental data of stage-3 $HgCl_2$ and SbF_5 with Blinowski's model.

Compounds	Frequency (T)		Area ($Å^{-2}$)		Mass (m_0)	
	Exp.	Cal.	Exp.	Cal.	Exp.	Cal.
$HgCl_2$	121	118	0.0115	0.0113	0.084	0.081
	523	542	0.0500	0.0517	0.165	0.153
	664	677	0.0634	0.0646	---	0.177
SbF_5	172	168	0.0164	0.0163	0.109	0.101
	656	684	0.0626	0.0651	0.184	0.184
	852	849	0.0813	0.0814	0.2[illegible]	0.212

From Table V.5 one can see that the calculated frequencies and Fermi areas agree very well (less than 4%) with the measured ones, and the calculated cyclotron masses are within 7% from the observed ones for both stage-3 compounds.

The energy bands for the stage-3 $HgCl_2$ and SbF_5 compounds are shown in Fig. V.12 and Fig. V.13, respectively. Each of them has three conduction bands and three valence bands. There is little overlap between the valence and conduction bands. The Fermi energies are negative with the values of -0.69 eV for $HgCl_2$ and -0.73 eV for SbF_5, as shown by the broken lines.

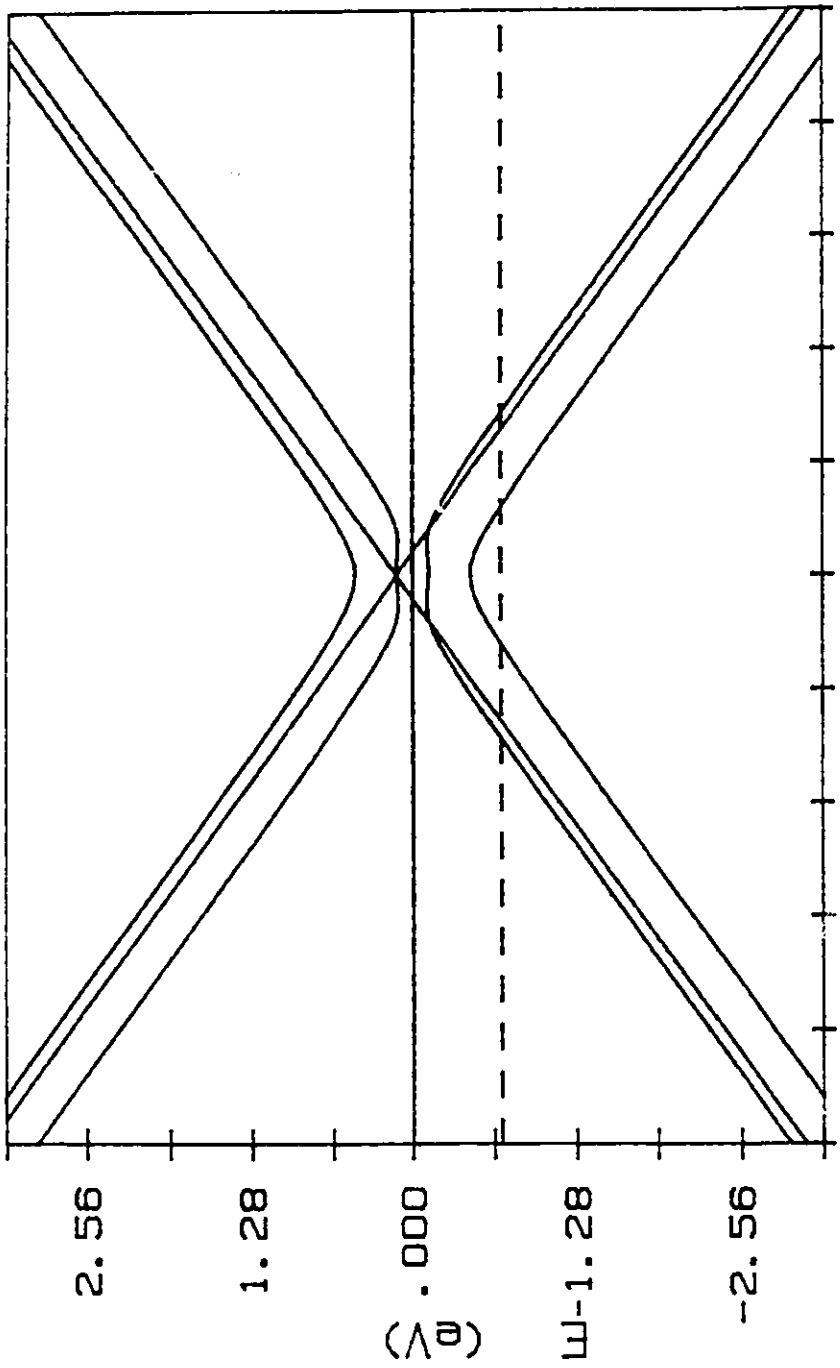

Figure V.12. The band structure of stage-3 $HgCl_2$-GIC with the band parameters δ=0.13 eV, γ_o=3.0 eV and γ_1=0.31 eV. The dashed line is the Fermi level of -0.69 eV.

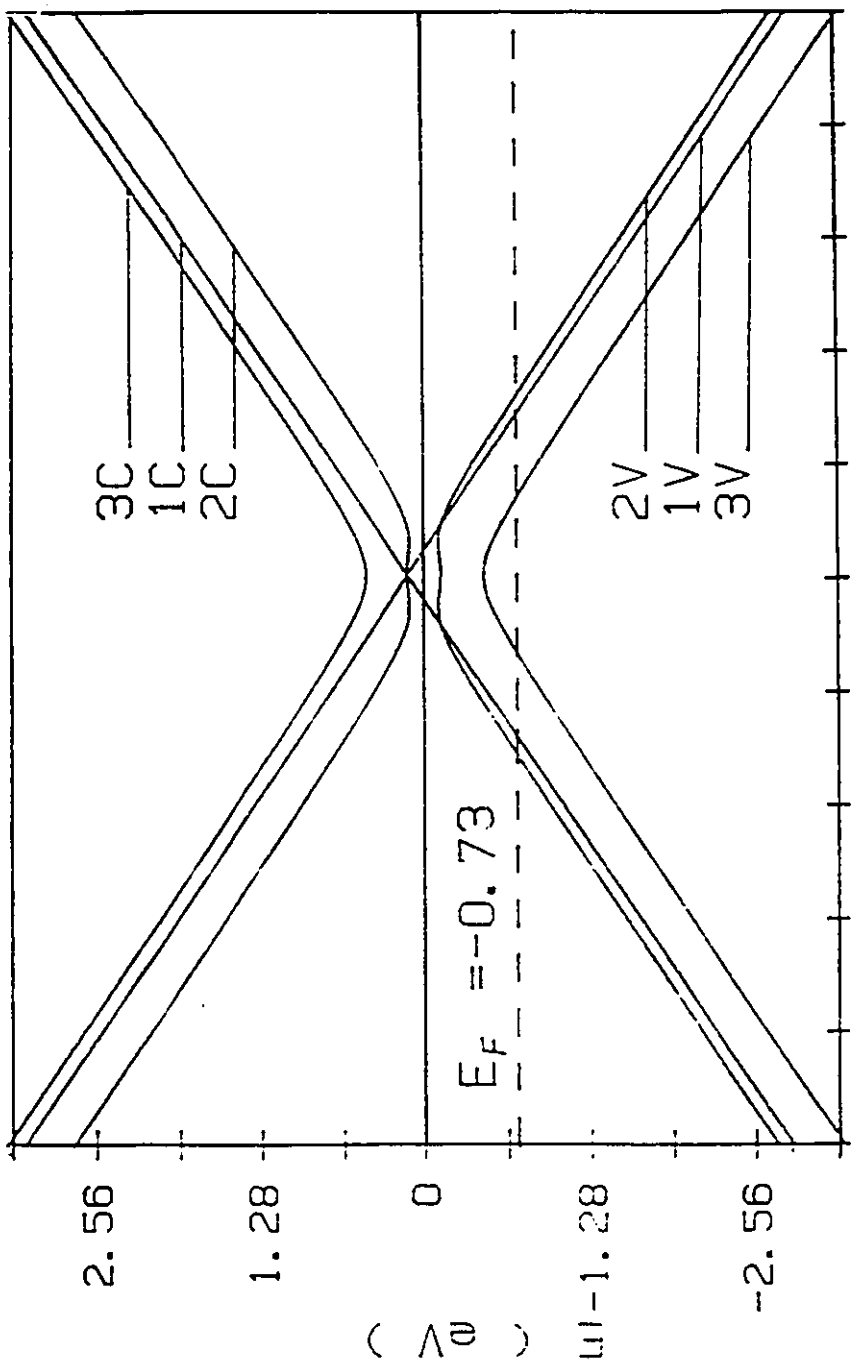

Figure V.13. The band structure of stage-3 SbF_5-GIC with the band parameters δ=0.13 eV, γ_o=2.8 eV and γ_1=0.31 eV.

V. 2.2.2 The charge distribution

The charge distribution along the c-axis has two extremal models for GIC with $n \geq 3$. One is the uniform charge distribution model (Dresselhaus et al 1977) which has a value of 1/3 for the fraction of the excess charge accumulated on the internal layer in stage-3 compounds. Another one is the metallic sandwich model (Batallan et al, 1978) which gives the value of zero to the fraction. Here, Blinowski's model relates the fraction (Z) with the band parameter (δ) and the charge transfer per carbon atom (f/l) by

$$2\delta = 0.1 + (f/l)(57.6Z - 2.7) \text{ eV} \qquad \text{(V.10)}$$

The charge transfer per carbon atom (f/l) is 0.0111 for $HgCl_2$ and 0.0142 for SbF_5. Then with δ=0.13 eV for both compounds, the fraction Z of the excess charge accumulated on the internal graphite layer for the stage-3 compounds are 0.297 for $HgCl_2$ and 0.242 for SbF_5. These values of Z are neither zero nor one third (1/3). Therefore, the charge distribution along the c axis of the samples is neither a metallic sandwich nor a uniform charge distribution. In addition, these values of Z being larger than zero and smaller than 1/3 means that there is a deficiency of charge on the internal graphite layer relative to the layer next to the

intercalant. This situation could result from an effective screening effect of the external graphite layers which are adjacent to the intercalate layers.

V.2.2.3 Data comparison of stage-3 acceptor compounds

In order to check the reasonableness of the band parameters from the model and the experimental results from the measurements, the data for three stage-3 acceptor compounds, $HgCl_2$, $SbCl_5$ (Wang et al, 1988) and SbF_5 are compared in Table V.6. All of the three compounds were described by the Blinowski model very well individually. Therefore, the difference of the data between the three compounds should be explained self-consistently by the model if it is really valid.

Table V.6

The comparison of the data for stage-3 $HgCl_2$, $SbCl_5$ and SbF_5-GICs.

		$HgCl_2$	$SbCl_5$	SbF_5
Repeat d-spacing (Å)	I	16.40	16.02	15.05
Band parameters (eV)	γ_0	3.0	2.8	2.8
	γ_1	0.31	0.31	0.31
	δ	0.13	0.13	0.13
Fermi energy (eV)	E_F	-0.69	-0.71	-0.73
dHvA Frequency (T)	F_1	121	152	172
	F_2	523	654	656
	F_3	664	811	852
Charge transfer/carbon (e^+)	f/l	0.0111	0.0137	0.0142
Fractional charge on internal layer	Z	0.297	0.250	0.242

From Table V.6, one can see that the value of the band parameter γ_0 for stage-3 $HgCl_2$ is higher than the one for stage-3 $SbCl_5$ and SbF_5. However, the dHvA frequencies from $HgCl_2$ compound are lower than the ones of the other two compounds, that is, the Fermi areas around the Fermi level in $HgCl_2$ compound are smaller. Therefore, the values of γ_0 are reasonable because the difference between them is consistent with the theoretical model which predicts a lower value of γ_0 for larger Fermi area.

The band parameters (γ_0, γ_1 and δ) for stage-3 SbF_5 are same as the ones for stage-3 $SbCl_5$. This is in agreement with the fact that the three dHvA frequencies for each compound are very close and there is no big difference between them. Otherwise, the band parameters, at least γ_0, should be different according to the model. In addition, one can see that between the two compounds, the higher the charge transfer per carbon atom, the lower the Fermi level and the larger the Fermi areas. This fact is also consistent with the theoretical predictions discussed in Sec. V.1.2 for the graphite compounds which have same band structure.

The value of the fractional charge on the internal graphite layer for the three compounds is decreasing with the increasing charge transfer per carbon. This is because the more the charge transfer per carbon the stronger the screening effect of the external graphite layers, and therefore, the less the fractional charge on the internal layer.

From the comparison of the data above, one can see that there is no contradiction of the data between the stage-3 compounds, and the differences of the data between them can be reasonably explained by the Blinowski model.

V.2.3 Conclusions for stage-3 $HgCl_2$ and SbF_5-GIC

The electronic properties of stage-3 $HgCl_2$ and SbF_5 were investigated by the dHvA experiments for the first time. Both of the two compounds show three groups of dHvA frequencies. The three dominant frequencies from each compound are identical with the basic graphite bands predicted by Blinowski's model.

The splitting of the frequencies could be attributed to two reasons. The first is the existence of a highly inhomogeneous structure in intercalated monolayers which produce a perturbation affecting the interactions of graphite-graphite or graphite-intercalant. The second is the undulation of the Fermi surface along the k_z-direction which result in more than one extremal cross sectional area and therefore several similar dHvA frequencies.

The two dimensionality of Blinowski's band model is basically proved by the angular-dependence of the dHvA frequency from SbF_5. But the deviation of the experimental data from the straight cylindrical Fermi surface at high angles indicates that the real electronic structure is not

perfectly two dimensional and there could be some interactions between the graphite layers which are separated by the intercalated layers along the c directions. In addition, this deviation also indicates the existence of an undulation of the Fermi surface with at least two extremal cross-sectional areas which is one of the possible reasons for the splitting of the dHvA frequencies.

The charge transfer coefficient per carbon atom for the two compounds is determined from the observed sum of their dHvA frequencies. The charge distribution along the c-axis of the samples are associated with the charge transfer coefficients and another band parameter δ according to the model. The results of the fractional charge distribution for both compounds show that there is a deficiency of charge in the internal graphite layer relative to the layers next to the intercalant. This is between the uniform charge distribution model and the metallic sandwich model. This situation could result from the screening effect of the external graphite layers which are adjacent to the intercalate layers.

The theoretical predictions of the dHvA frequencies and the cyclotron masses from Blinowski's model for the two compounds are in agreement with the experimental results. The comparison of the data for three stage-3 acceptor compounds described by the theory show that there is no contradiction between these data, and the difference among them can be reasonably explained by the model.

CHAPTER VI

SUMMARY AND CONCLUSION

The purpose of this work was to study the Fermi surfaces and the electronic properties of donor-type C_8K and $C_{24}K$, acceptor-type $BiCl_3$, $HgCl_2$ and SbF_5 graphite intercalation compounds. The work involved sample preparation, characterization, measurements of de Haas-van Alphen effect, and analyzing and calculating the band structures.

All the samples in the presented work were prepared by a two-zone method and highly oriented pyrolytic graphite was used as the starting material. The stage index of the samples was determined with (001) x-ray diffraction measurement using a powder diffractometer and CuK_α radiation, and by the weight uptake from intercalation. The samples chosen for the dHvA study were well staged with pure stage index. The $BiCl_3$-GIC and $HgCl_2$-GIC were stable in air while C_8K, $C_{24}K$ and SbF_5-GIC were not. Therefore, great attention was given to each step of the sample handling.

The dHvA measurements were performed with the low frequency field modulation technique. A set of detecting coils with high sensitivity was made specially for the dHvA measurements of the presented samples. Samples were cooled slowly from room temperature to liquid nitrogen temperature, and all the measurements were done with the temperature below

4.2 K. The dHvA measurements include the distribution of the dHvA frequencies, the angular dependence of the frequencies, and the temperature dependence of the amplitude of the frequencies with the magnetic field parallel to the c-axis of the samples. All of the dHvA experimental results for both the donor-type and acceptor-type compounds studied in the present work are summarized in Table VI.1

The dHvA measurements of donor-type GICs caused much more experimental difficulties than acceptor-type GICs. The experiments for both C_8K and $C_{24}K$ were carefully performed and repeated.

There are two dHvA frequencies in C_8K. The first frequency is close to the one reported previously, and the second one is reported for the first time. The angular dependence of the dHvA frequency shows that there exist both three-dimensional and two dimensional Fermi surfaces in C_8K. The Fermi surface which corresponds to the first frequency is quite spherical and the Fermi surface which corresponds to the second frequency is cylindrical. The charge transfer per potassium atom is measured directly by the dHvA frequencies. It is very close to unity. The almost complete charge transfer implies that the potassium s-band is almost empty and the three-dimensional Fermi surface does not arise from the potassium s-band. By comparing the experimental results with the prediction of each theoretical model for C_8K, the model proposed by Tatar and Rabii is supported completely by the

Table VI.1

The experimental results obtained from the present work for C_8K, $C_{24}K$, $BiCl_3$-GIC, $HgCl_2$-GIC, and SbF_5-GIC.

	Compound	n	I_c(Å)	F (T)	m^* (m_0)	FS	f_c (f_k)	Z
D	C_8K	1	5.35	3126 4250	0.86 0.92	3D 2D	0.121 (0.97)	--
	$C_{24}K$	2	8.67	286 2570			0.0367 (0.88)	--
A	$C_{17}BiCl_3$	2	13.06	327 1012	0.147 0.265	2D	0.017	--
	$C_{17}HgCl_2$	3	16.40	121 523 664	0.084 0.165		0.0111	0.297
	$C_{27}SbF_5$	3	15.10	172 656 852	0.109 0.184 0.226	2D	0.0142	0.242

D: donor-type
A: Acceptor-type
n: stage index
I_c: d-space
F: dHvA frequency
m^*: effective mass
FS: Fermi surface
3D: three dimensional
2D: two dimensional
f_c: charge transfer per carbon
f_k: charge transfer per potassium
Z: fractional charge on internal graphite layer

experiment and the revised model of Ohno, Nakao and Kamimura is basically supported. But the difference between the two models, that is whether the character of the three dimensional Fermi surface is an interlayer band or a graphite π band, can not be clarified by the dHvA effect.

The dHvA spectrum of stage-2 $C_{24}K$ is different from the results of Shubnikov-de-Haas measurement reported previously. There are two dominant dHvA frequencies in the spectrum, the lower one is the same as one of the SdH frequencies, the higher one is obtained for the first time. The two dominant dHvA frequencies were interpreted in terms of the basic graphite band. The predictions of Blinowski's theoretical model are in agreement with the experimental data while the theoretical calculation by Yang and Eklud do not agree with the dHvA data very well. The charge transfer per potassium atom is determined from both the dHvA experiments and Blinowski's model. It is about 0.88. This value suggests that the potassium s-band is above the Fermi level in this compound.

The measurements of the dHvA effect for all of the three acceptor-type compounds, stage-2 $BiCl_3$-GIC, stage-3 $HgCl_2$-GIC, and stage-3 SbF_5-GIC were performed for the first time. Two dHvA frequencies were obtained for the stage-2 compound, and three groups of dHvA frequencies were obtained for each of the stage-3 compounds.

The Blinowski theoretical models for stage-2 and stage-3

graphite intercalation compounds were used to analyze the dHvA data. The two fundamental frequencies in the stage-2 compounds and the three dominant frequencies in each of the stage-3 compounds were identified with the basic graphite bands of stage-2 GIC and stage-3 GIC, respectively. The theoretical predictions for the dHvA frequencies and the cyclotron masses for these compounds are in agreement with the measured results. It is within 4% for the stage-2 $BiCl_3$-GIC, and 7% for the stage-3 $HgCl_2$-GIC and the stage-3 SbF_5-GIC.

The two-dimensionality of the band structures of the Blinowski's band models is proved by the experiments of the angular dependence of the dHvA frequencies from stage-2 $BiCl_3$ and stage-3 SbF_5, which show that the Fermi surfaces in these compounds are basically cylindrical.

The measurements of the angular dependence also show that the dHvA amplitudes decrease when the angle between the direction of the magnetic field and the c-axis of the samples increases and that the maximum angle at which the dHvA signal disappears is stage dependent: it increases with stage index. This phenomenon is considered to result from the electron-carbon and the electron-intercalant scattering which limit the electron orbits with the increasing angle.

The fact that three groups of dHvA frequencies instead of three individual dHvA frequencies were obtained in stage-3 compounds is considered to result from the splitting of the three fundamental frequencies. The splitting of the

frequencies could be attributed to two reasons. The first is the existence of the highly inhomogeneous structure in intercalated momolayers which produce a perturbation affecting the graphite-graphite or graphite-intercalant interactions. The second is the modulation of the Fermi surface along the k_z-direction which results in more than one extremal cross-sectional area and therefore several similar dHvA frequencies.

The charge transfer coefficients per carbon atom for the acceptor-type compounds are directly determined from the observed sums of their dHvA frequencies, respectively. It is found that the acceptor compounds have lower charge transfer than the donor compounds.

The charge distribution along the c-axis of the stage-3 samples is associated with the charge transfer coefficient per carbon atom. The results of the fractional charge distribution of the three graphite layers in the stage-3 compounds show that there is a deficiency of charge in the internal graphite layer relative to the layers next to the intercalant. This is between the uniform charge distribution model and the metallic sandwich model. This situation could result from the screening effect of the external graphite layers which are adjacent to the intercalate layers.

In addition, the comparisons of the dHvA and the band parameters for three stage-2 and three stage-3 acceptor compounds which described by Blinowski's models show that there is no contradiction between these data for each stage,

and the difference among them can be well explained by the theories. Therefore, Blinowski's theoretical band models for stage-2 and stage-3 graphite intercalation compounds are found to be reasonable models. Although there exist some discrepancies between the predictions of the models and the results of dHvA experiments, it is valid to describe the electronic structures of the graphite intercalation compounds with the theories.

REFERENCES

Batallan, F., Bok, J., Rosenman, I. and Melin, J., Phys. Rev. Lett. **41**, 330 (1978).

Behrens, P., Woebs, V., Jopp, K., and Metz, W., Carbon **26**, 641 (1988).

Bender, A.S. and Young, D.A., J. Phys. C **5**, 2163 (1973).

Blinowski, J. and Rigaux, C., Synt. Metals **2**, 297 (1980).

Blinowski, J. and Rigaux, C., J. Physique **41**, 667 (1980).

Blinowski, J., Nguyen, H.H., Rigaux, C., Vieren, J.P., Letoullec, R., Furdin, G., Herold, A and Melin, J., J. Physique **41**, 47 (1980).

Bok, J. Batallan, F. and Rosenman, in Proc. Int. Conf. Application of high Magnetic fields to semicond. Phys., R.A. Strading, ed., Clarendon Press, Ox., U.K., 1978.

Cartier, E., Heinrich, F., Pfluger, P., and Gunthrodt, H.J., Solid St. Comm. **38**, 197 (1980); Phys. Rev. Lett. **46**, 272(1981).

Conard, J., Estrade, H., Lauginie, P., Fuzellier, H., Furdin, G., and Vosse, R., Physica B**99**, 521 (1980).

Cooper, J.D., Woore, J., and Young, D.A., Nature, Lond., **225**, 721 (1970).

DiVincenzo, D. P. and Rabii, S., Phys. Rev. B**25**, 4110 (1982).

Datars, W.R. and Ummat, P.K., J. Phys. C **1**, 5031 (1989).

Doll, G. L., Yang, M. H., and P. C. Eklund, Phys. Rev. B**35**, 9790 (1987).

Dresselhaus, M.S., Physics Today, March, 60 (1984).

Dresselhaus, M.S., Mater. Sci. Eng. B1, 259 (1988).

Dresselhaus, M.S. and Dresselhaus, G., Adv. Phys. **30**, 139 (1981).

Dresselhaus, M.S., Dresselhaus, G., and Fischer, J.E., Phys. Rev. B**15**, 3180 (1977).

Dresselhaus, G. and Leung, S.Y., Solid State Comm. **35**, 819 (1980)

Dresselhaus, G., Leung, S.Y., Shayegan, M., and Chieu, T.C., Synth. Met. **2**, 321 (1980).

Dresselhaus, M.S. and Sugihara, K., in Extended abstract of the first symposium of the Materials Research Society, edited by P.C. Eklund, M.S. Dresselhaus and G. Dresselhaus, (MRS, Pittsburgh, 1984), p. 36

Eklund, P.C., Yang, M.H., and G. L. Doll, in Intercalation in Layered Materials, edited by M.S. Dresselhaus (Plenum, New York, 1986), p. 257.

Ebert, L.B., A. Rev. Mater. Sci. **6**, 181 (1976).

Enoki, T., Yeh, N.C., Chen, S.T. and Dresselhaus, M.S., Phys. Rev. B**33**, 1292 (1986).

Fischer, J.E. and Thompson, T.E., Physics Today, July, 37 (1978).

Fischer, J.E., Phys. Chem. of Mater. with layered structures, Vol. 6, Levy, F., ed., Reidel, Dordrecht, 481 (1979).

Foley, G.M.T., Zeller, C., Falardeau, E.R. and Vogel, F.L., Solid State Comm. **24**, 371 (1977).

Furdin, G., Herold, A., and Melin, J., J. Phys. (Paris) **41**, 47 (1980).

Gubler, U.M., Oelhafen, P., and Gunthrodt, H.J., Solid St. Comm. **44**, 1621 (1982).

Hague, C.F., and Mariot, J.M., Synthetic Metals **23**, 211(1988).

Hannay, N.B., Geballe, T.H., Matthias, B.T., Andres, K., Schnidt, P. and MacNair, D., Phys. Rev. Lett. **14**, 225 (1965).

Hennig, G.R., J. Chem. Phys. **43**, 1202 (1965).

Herinckx, C., Perret, R. and Ruland, W., Carbon **10**, 711 (1972).

Herold, A., Bull. Soc. Chim. France **187**, 999 (1955).

Herold, A., Mater. Sci. Eng. **31**, 1 (1977).

Herold, A., in Phys. Chem. of Mater. LAyered Struc., Vol. **6**, edited by F. Levy (Dordrecht, Reidel), 323, 1979.

Higuchi, K., Suematsu, H., and Tanuma, S., J. Phys. Soc. Jpn. **48**, 1532 (1980).

Higuchi, K., Suematsu, H., and Tanuma, S., Physica, B**99**, 420 (1980).

Holzworth, N.A.W., Phys. Rev. b**21**, 3665 (1980).

Hwang, D.M., Qian, X.W. and Solin, S.A., Phys. Rev. Lett. **53**, 1473 (1984).

Inoshita, T., Nakao, K., and Kamimura, H., J. Phys. Soc. Jpn. **43**, 1237 (1977).

Iye, Y., Takahashi, O. and Tanuma, S., Solid State Comm. **33**, 1071 (1980).

Iye, Y., Takahashi, O., Tanuma, S., Tsuji, K. and Minomura, S., J. Phys. Soc. Japan **51**, 475 (1982).

Johnson, L.G. and Dresselhaus, G., Phys. Rev. b7, 2275 (1973).

Kamimura, H., Physics Today, Dec., 64 (1987).

Kamimura, H., Graphite Intercalation Compounds, Extended Abstracts Mater. Research Soc. Symp., Mater. Res. Soc., Pittsburgh, PA, 1984, p. 36.

Kamimura, H., Annales de Physique Coll. **11**, 39 (1986).

Kamimura, H., Synthetic Metals **23**, 171 (1988).

Koike, Y., Tanuma, S.-I., Suematsu, H., and Higuchi, K., J. Phys. Chem. Solids **41**, 1111 (1980).

Koma, A., Miki, K., Suematsu, H., Ohno, T., and Kamimura, H., Phys. Rev. B**34**, 2434 (1986).

Kondow, T., Mizutani, U., and Massalski, T., Mat. Sci. Eng. **31**, 267 (1977).

Lifshitz, I.M. and Kosevich, A.M., Sov. Phys. JETP **2**, 636 (1956).

Levi-Setti, R., Cron, G., Wang, Y.L., PArker, N.W. and Mittleman, R.K., Phys. Rev. Lett. **54**, 2615 (1985).

Loupias, G., Chomilier, J., and Tarbes, J., Synthetic Metals **23**, 205 (1988).

Loupias, G., Rabii, S., Tarbes, J., Nozieres, S., and Tatar, R.C., Phys. Rev. B**41**, 5519 (1990).

Mansour, A., Schnatterly, S.E., and Ritsko, J.J., Phys. Rev. Lett.**58**, 614 (1987).

Marchand, D., Fretigny, C., Lecomte, N., and Lagues, M., Synthetic Metals **23**, 165 (1988).

Markiewicz, R.S., Hart, H.R., Interrante, Kasper, J.S., Solid State Comm. **35**, 513 (1980).

McClure, J.M., Phys. Rev. **108**, 612 (1957); **119**, 606 (1960).

McClure, J.M., Proc. Int. Conf. on Semic. & Narrow gap semic., edited by D.L. Carter and R.T. Bate (New York, Pergamon Press), p.127, (1971).

McRae, E., Billaud, D., Mareche, J.F., Herold, A., Physica B**99**, 489 (1980)

Mizuno, S., Hiramoto, H., and Nakao, K., Solid St. Comm. **63**, 705 (1987).

Mizutani, U., Kondow, T., and Massalski, T.B., Phys. Rev. B**17**, 3165 (1978).

Moore, A.W., in Chem. and Phys. of Carbon, P.L. Walker, Jr., and P.A. Thrower (eds.), Dekker, New York, p. 69, (1973).

Nixon, D.E., and Parry, G.S., J. Phys. D**1**, 291 (1968).

Nixon, D.E., and Parry, G.S., J. Phys. C**2**, 1732 (1969).

Oelhafen, P., Pfluger, P., Hauser, E., and Gunthrodt, H.J., Phys. Rev. Lett. **44**, 197 (1980).

Ohno, T., Nakao, K., and Kamimura, H., J. Phys. Soc. Jpn. **47**, 1125 (1979).

Parry, G.S., 3nd Conf. on Ind. Carbon and Graphite (London: Soc. Ind. Chem.), p. 58 (1971); Mater. Sci. Eng. **31**, 99 (1977).

Posternak, M., Baldereschi, A., Freeman, A.J., Wimmer, E., and Weinert, M., Phys. Rev. Lett. **50**, 761 (1983).

Preil, M.E., and Fischer, J.E., Phys. Rev. Lett. **52**, 1141 (1984).

Ritsko, J.J., and Brucker, C.F., Solid St. Comm. **44**, 889 (1982).

Rosenman, I., Batallan, F., and Furdin, G., Phys. Rev. **B20**, 2373 (1979).

Rudorff, W., Adv. Inorg. Chem. Radiochem. **1**, 225 (1959).

Rudoff, W., and Schulze, E., Z. anorg. allgem. Chem. **277**, 156 (1954).

Saito, R., and Kamimura, H., Synth. Met. **12**, 295 (1985).

Schafhautl, C., J. Prakt Chem. **21**, 129(1841).

Schleede, A., Wellman, M., Z. Phys. Chem. **18**, 1 (1932).

Shayegan, M., Dresselhaus, M.S. and Dresselhaus, G., Phys. Rev. **B25**, 4157 (1982).

Shoenberg, D., Magnetic Oscillations in Metals, (University Press, Cambridge), 1984.

Simon, C., Batallan, F., Rosenman, I., Fuzellier, H., Phys. Rev. **B23**, 2836 (1981).

Slonezewski, J.C. and Weiss, P.R., Phys. Rev. **109**, 272 (1958).

Soule, D.E., McClure, J.W., and Smith, L.B., Phys. Rev. A **134**, 453, (1964).

Spain, I.L., Mater. Sci. Eng., **31**, 183 (1977).

Spain, I.L., in Chem. and Phys. of Carbon, P.L. Walker, Jr., and P.A. Thrower (eds.), Dekker, New York, p. 1, 105, 110 (1973).

Stumpf, E., Mater. Sci. Eng. **31**, 53 (1977).

Suematsu, H., Higuchi, K., and Tanuma, S., J. Phys. Soc. Jpn. **48**, 1541 (1980).

Takahashi, T., Gunasekara, N., Sagawa, T., and Suematsu, H., J. Phys. Soc. Jpn. **55**, 3498 (1986).

Tanuma, S., Higuchi, K., Suematsu, H., and Koike, Y., In Proc. 15th Int. Conf. Low Temp. Phys., J. Phys. (France) Suppl. **39**, C6-1104 (1978).

Tanuma, S., Iye, Y., Takahashi, O., and Koike, Y., Synth. Met. **2**, 341 (1980).

Tanuma, S., Suematsu, H., Higuchi, K., Inada, R., and Onuki, Y., Proc. of Con. on Appl. High Magn. Fields in Semic. Phys., J.F. Ryan, ed., (Oxford, Clarendon Press), p.85, 1978.

Tatar, T.C., and Rabii, S., in Extended abstract of the first symposium of the Materials Research Society, edited by P.C. Eklund, M.S. Dresselhaus and G. Dresselhaus, (MRS, Pittsburgh, 1984), p. 71.

Thomas, J.M., Millward, G.R., Schlegl, R.F. and Boehm, H.P., Mater. Res. Bull. **15**, 671 (1980).

Timp, G., Chieu, T.C., Dresselhaus, P.D. and Dresselhaus, G., Phys. Rev. B**29**, 6940 (1984).

Toy, W.W., Dresselhaus, M.S. and Dresselhaus, G., Phys. Rev. **15**, 4077 (1977).

Ubbelohde, A.R., Proc. Roy. Soc. A327, 289 (1972).

Vogel, F.L., J. Mater. Sci. **12**, 982 (1977).

Wang, G., Ummat, P.K., and Datars, W.R., in Extended abstract of the symposium of the Materials Research Society on Graphite intercalation Compounds, edited by P.C. Eklund, M.S. Dresselhaus and G. Dresselhaus, (MRS, Boston, 1988), p. 217.

Wang, G., Zaleski, H., Ummat, P.K., and Datars, W.R., Phys. Rev. B37, 9029 (1988).

Wang, G., Ummat, P.K., and Datars, W.R., J. Phys.: Condens. Matter 3, 787 (1991).

Wang, G., Datars, W.R., and Ummat, P.K., Phys. Rev. B44, Oct. 15, (1991).

Wang, G., Datars, W.R. and Ummat, P.K., Phys. Rev. B, (in press).

Williamson, S., Foner, S., and Dresselhaus, M.S., Phys. Rev. A140, 1429, (1965).

Woollam, J.A., Phys. Lett. A32, 115 (1970).

Wortmann, G., Goder, F., Penscheid, B., and Kaindl, Synth. Met., **26**, 109 (1988).

Wu, T.C., Vogel, F.L., Pendrys, L.A. and Zeller, C., Mater. Sci. Eng. **47**, 161 (1981).

Yang, M.H., and Eklund, P.C., Phys. Rev. B38, 3505 (1988).

Yosida, Y., Synth Met., **34**, 387 (1989).

Zaleski, H., Ph.D Thesis, McMaster Univ., Unpublished, 1985.

Zaleski, H., Ummat, P.K., and Datars, W.R., J. Phys. C17, 3167 (1984).

Zaleski, H., Ummat, P.K., and Datars, W.R., Solid State Comm. 55, 401 (1985).

Zaleski, H., Ummat, P.K., and Datars, W.R., Synth Met. 11, 183 (1985).

Zaleski, H., Ummat, P.K., and Datars, W.R., Phys. Rev. B35, 2958 (1987).

Zaleski, H., Ummat, P.K., and Datars, W.R., J. Phys. C1, 369(1989).

Zanini, M., and Fischer, J.E., Mat. Sci. Eng. 31, 169 (1977).

Zhang, J.M. and Eklund, P.C., J. Mater. Res. 2, 858 (1987).